Bimolecular chemical reaction in a two-dimensional Navier-Stokes flow

Farid Ait Chaalal

Doctor of Philosophy

Department of Atmospheric and Oceanic Sciences

McGill University

Montréal, Québec, Canada

February, 2012

A thesis submitted to McGill University in partial fulfillment of the requirements for the degree of Doctor of Philosophy

©Farid Ait Chaalal 2012

DEDICATION

"Les articles de fond ne remontent jamais à la surface." *Boris Vian*

À Leila et Kamel

Acknowledgements

In French, my mother tongue.

Tout d'abord, je pense à mes superviseurs Michel Bourqui et Peter Bartello. Je les remercie pour m'avoir laissé libre d'orienter ma recherche dans les directions que je choisissais, de m'avoir fait confiance pour développer mes idées tout en m'encourageant. Je pense en particulier à Michel et à son optimisme légendaire, qui toujours a été d'un grand secours. Au-delà de l'aspect strictement scientifique de la supervision, je lui sais gré de m'avoir aiguillé sur le chemin où s'acquiert la maturité scientifique, où l'on apprend à la fois l'humilité, la confiance en soi, l'indépendance, le doute éclairé. Mes pensées vont aussi à tous ceux qui au cours de ma scolarité m'ont donné le goût du savoir et m'ont encouragé: mon professeur de biologie au collège Canteperdrix de Grasse, dont le nom m'échappe malheureusement, mon professeur de français de seconde au Lycée Stanislas à Paris, M. Beugras, mon professeur de Philosphie de terminale, au lycée Henri IV à Paris, dont le nom m'échappe également, mon professeur de physique en mathématiques spéciales au Lycée Louis-Le-Grand à Paris, M. Olivier.

A l'université McGill, je remercie également chaleureusement Bruno Tremblay, qui m'a donné énormément de liberté en tant qu'assistant d'enseignement et avec qui j'ai eu des discussions scientifiques très enrichissantes. Également, le travail de Michael en tant qu'administrateur du réseau informatique a été plus qu'exceptionnel. Je pense tout spécialement à ceux qui y ont partagé avec moi l'aventure du doctorat, en particulier Barbara et Louis-Philippe.

Sur un plan plus personnel, je pense chaleureusement à mes proches dont l'amitié fut précieuse: mes amis de Paris et d'ailleurs Julien, Pablito, Kordo, Caroline, Joël, Lamis, Laurent, Stouff, Mélanie avec une pensée particulière pour ceux qui ont

partagé la même aventure doctorale: Anne, Sabine, Marie, Antoine, Raphi; et pour ceux dont j'ai fait la connaissance à Montréal: Luc, Daniel, Maxime, Esther, Iman et Rabah.

Je pense á mes grands parents: Louisa, Dalila, Amar et Driss, aujourd'hui décédé mais dont la droiture fut pour moi un exemple. Enfin, je pense à mes parents Leila et Kamel et à tous leurs sacrifices afin que je puisse poursuivre mes souhaits pour réaliser mes rêves d'enfance à l'abri des aléas de la vie. Ils me disent qu'enfant je souhaitais devenir astrophysicien. C'est plus qu'un luxe d'y être presque parvenu.

Contributions of Authors

This project was initiated by Prof. Bartello and Prof. Bourqui to understand the dependence of chemistry on resolution in climate-chemistry models. We started studying a fast bimolecular chemical reaction in a barotropic quasi-geostrophic flow on the β-plane with a Newtonian relaxation toward a barotropically unstable zonal jet. This was a crude parametrization for the polar vortex transport barrier. Farid Ait Chaalal reorientated the research toward the study of a statistically stationary homogeneous and isotropic biperiodic Navier-Stokes flow because it captured some basic scaling laws of the chemistry with resolution as observed using stratospheric reanalysis (*Tan et al.*, 1998; *Wonhas and Vassilicos*, 2002, 2003). This project was presented and approved as Farid Ait Chaalal's thesis proposal (*Ait-Chaalal*, 2008). The numerical model was written by Peter Bartello. Farid Ait Chaalal modified it to include the computation of the concentrations of chemicals involved in a bimolecular reaction (2008). He also implemented the FFTW (*Frigo and Johnson*, 2005) fast Fourier transform during the summer 2009. We started exploring the Lagrangian stretching theory approach at the summer 2008 when an undergraduate trainee in Prof. Bourqui's group (Jason Boubalos) wrote a code to compute finite-size Lyapunov exponents. Farid Ait Chaalal wrote the trajectory code to compute finite-time Lyapunov exponents and other Lagrangian diagnostics in the summer 2010.

The idea for the first paper (chapter 2) was Farid Ait Chaalal's. The theory was developed by Farid Ait Chaalal during the fall 2010 with regular discussions with Prof. Bourqui and Prof. Bartello. The paper was written by Farid Ait Chaalal, edited by Prof. Bourqui and Prof. Bartello and submitted in June 2011 to Physical

Review E. The version included here is the revised version resubmitted in December 2011. It reflects the suggestions and criticisms made on the original manuscript by two anonymous reviewers. One of the them contributed significantly to improve and clarify the theoretical developments. The content of the second paper (chapter 3) was determined by discussions between the three co-authors. It was written by Farid Ait Chaalal during the summer 2011, edited by Prof. Bourqui and submitted in October 2011 to Physical Review E. We are currently working on the revisions. Chapter 4 constitutes the preliminary version of a letter and was written by Farid Ait Chaalal.

Statement of Originality

- Previous theoretical attempts to understand the dependence of chemical production with resolution in Climate-Chemistry models have used an on/off assumption on the chemical fields (*Wonhas and Vassilicos*, 2002, 2003). Our framework is more general.
- We apply local Lagrangian stretching theories (LLST) to the mixing zone of two reactants involved in a bimolecular chemical reaction. LLST, which were developed to study the decay of passive tracers in two-dimensional flows characterized by chaotic Lagrangian trajectories (*Antonsen et al.*, 1996), have already been applied to active tracers, like phytoplankton in the oceans (*Tzella and Haynes*, 2009) or implicitly to the same problem as ours (*Tsang*, 2009). However, applying them to the contact zone between two reactive chemicals is new. Some previous studies had a similar approach, but did not take into account the distribution of stretching rates (*Karolyi and Tél*, 2007), which is actually the whole point of LLST.
- We use a solution of the barotropic two-dimensional Navier-Stokes equation, which is dynamically consistent, as opposed to flows used in the literature to verify the predictions of LLST. These are prescribed kinematics flows and are basically the renewing sine flow inherited from the chaotic map proposed by *Pierrehumbert* (1994).
- In the introduction, we propose reviews of chaotic advection in the stratosphere and of local Lagrangian stretching theories for passive tracers, which are not available in the literature to our knowledge.

Abstract

This thesis studies an infinitely fast bimolecular chemical reaction in a two-dimensional Navier-Stokes flow using a local Lagrangian stretching theory approach. Our flow, large scale and characterized by chaotic Lagrangian trajectories, is an idealized framework for stirring and mixing in the wintertime midlatitude deep stratosphere (WMDS). The dynamics of the WMDS are indeed non-local with chaotic advection thought to occur. The reactants are initially segregated and separated by a one-dimensional contact line. Because the chemical reaction is instantaneous, this problem simplifies to the study of a passive tracer defined as the difference between the reactants. We investigate the effect of the reactants diffusion on the their concentration in order to understand the effect of spatial resolution on similar stratospheric reactions in Climate-Chemistry models.

In chapter 1 we review (a) chaotic advection for mixing of chemicals in the WMDS, (b) previous numerical and theoretical works dealing with the issue of horizontal resolution in Climate-Chemistry models in the WMDS, (c) local Lagrangian straining theories applied to the passive tracer problem in large scale flows, like chaotic advection or the Batchelor regime of turbulence.

Chapter 2 and chapter 3 focus on the initial regime of the reaction where the contact line between the reactants, independent of the diffusion, is a material line only function of the dynamical properties of the flow. In Chapter 2, we theoretically show that, over an ensemble of realizations of a statistically stationary flow with chaotic trajectories, the ensemble averages of the contact line length, of the reactants gradients along it and of the time derivative of the domain average reactants concentration can be predicted knowing the diffusion and the statistics of the Lagrangian stretching properties (LSP) of the flow. In chapter 3, we adopt the same

approach to express the probability density function of the tracer gradients along the contact line and of the tracers as a function of the LSP and of diffusion. In both chapters, the theoretical results are tested with an ensemble of direct numerical simulations (DNS) of the two-dimensional Navier-Stokes flow using a pseudospectral model.

Chapter 4 discusses the long-term decay of a passive tracer fluctuation in our dynamically consistent flow, emphasizing on the differences with kinematics flow that are generally used in the literature.

Abrégé

L'objet de cette thèse est l'étude d'une reaction chimique bimoléculaire infiniment rapide dans un fluide doublement périodique et solution des équations de Navier-Stokes en deux dimensions. Ce fluide définit un cadre idéalisé pour le touillage et le mélange dans la stratosphère l'hiver et aux latitudes tempérées. La dynamique y est en effet non locale et l'état actuel des connaissances suggère que l'advection chaotique y prend place. Ce travail utilise une approche locale et lagrangienne de la dilatation des particules de fluides. Les réactifs sont initialisés dans deux parties différentes du domaine et sont séparés par une ligne de contact de dimension un. Nous examinons l'effet de la diffusion des réactifs sur l'avancement de la réaction, afin de comprendre la dépendence de réactions chimiques similaires dans la stratosphère à la résolution horizontale des modèles numériques du climat couplant dynamique et chimie.

Le premier chapitre constitue une revue de littérature (a) de l'advection chaotique d'espèces chimiques dans la stratosphère (b) de précédents travaux concernant l'effet de la resolution horizontale des modelèles couplant chimie et climat sur la chimie de la stratosphère l'hiver aux latitudes moyennes (c) des théories locales et Lagrangiennes de la dilatation des particules de fluides pour expliquer la phénoménologie d'un traceur passif dans un fluide grande échelle, par exemple charactérisé par une advection chaotique ou dans le régime turbulent de Batchelor.

Les deux chapitres suivant concernent le régime initial de la réaction, où la ligne de contact entre les réactifs, ne dépendant pas de la diffusion, est une ligne materielle fonction uniquement des propriétés dynamiques du fluide. Nous montrons, de manière théorique, que sur un ensemble de réalisations du fluide statistiquement stationnaires avec trajectoires chaotiques, la moyenne de la longueur de la ligne de

contact, des gradients des réactifs le long de cette ligne et de la dérivée temporelle des concentrations moyennes des réactifs sur le domaine peuvent être prédites à partir de la diffusion et des propriétés lagrangiennes de dilatation des particules de fluides (PLD). Les PLD sont constituées des exposants de Lyapunov à temps fini et de deux temps équivalents pouvant être calculés sur une trajectoire à partir de l'évolution de l'exposant de Lyapunov. L'inverse de l'exposant de Lyapunov définit sur une trajectoire le temps caractéristique de dilatation d'une particule de fluide au temps t, alors que les temps équivalents le mesurent respectivement dans le passé récent avant t et aux moments initiaux de la trajectoire. Les résultas théoriques sont éprouvés à l'aide de simulations numériques avec un modèle pseudo-spectral du fluide solution des équations de Navier-Stokes en dimension deux.

Le quatriéme chapitre s'intéresse au déclin d'un traceur passif dans ce même fluide. Nous mettons l'accent sur les différences avec le déclin dans des fluides cinématiques largement décrits dans la littérature. Comprendre la dépendence de ce déclin avec la diffusion s'applique directement à une réaction infiniement rapide.

Table of Contents

List of Figures

CHAPTER 1
Introduction

Preamble

Chlorofluorocarbons (CFCs) released by human activities have depleted the ozone layer in the stratosphere. With the banning of most of the CFCs by the Montréal Protocol in 1987, and the actual decrease of CFC concentrations in the atmosphere that started a few years later, stratospheric ozone is expected to recover. However, climate change is affecting stratospheric dynamics (e.g. *Winter and Bourqui* (2010)) and it is not clear how this will interact with ozone recovery (e.g *Son et al.* (2008)). Chemistry and dynamics are coupled in the stratosphere (*Andrews et al.* (1987)) and an accurate representation of chemistry seems necessary to build relevant Climate-Chemistry models (e.g. *Waugh et al.* (2009)) and understand this complex issue.

Chemical reactions occur at the molecular level, which is several tens of orders of magnitude smaller than typical length scales of atmospheric flows. Hopefully, molecular diffusion and turbulent eddy diffusivity make possible an accurate representation of chemistry in numerical models if length scales of a few kilometers are resolved. However, this is still out of reach of current Climate-Chemistry models, whose typical horizontal resolutions are one or two orders of magnitude larger. In particular, in the stratosphere, chemical tracers exhibit filamentary structures whose width is of the order of 10^0 km or 10^1 km. In section 1.2 we will discuss some previous works dealing with the dependence of chemistry on model resolution.

The stratosphere is characterized by a strong static stability which constrains, together with Earth's rotation, transport and mixing on two-dimensional surfaces of

constant potential temperature (the isentropes). Stratospheric flows on isentropes are large scale, in the sense that they exhibit large-scale coherent structure like the polar vortex and planetary waves. Nevertheless, trajectories of fluid parcels are chaotic: trajectories initially close diverge exponentially in time. A direct consequence is that chemical tracers fields exhibit the filamentary structures we have just mentioned and that these filaments develop exponentially fast. The emergence of chaotic trajectories in large-scale smooth flows is known as chaotic advection and can occur in very simple non-turbulent flows. One can think of the structures that can be observed at the surface of coffee when cream is gently dropped in it. Chaotic advection will be defined more rigorously in section 1.1 and its applicability to stratospheric mixing will be discussed in the same section.

The object of this thesis is to quantify the errors of current models in representing some aspects of stratospheric chemistry because of their coarse resolution. This is done in the framework of a two-dimensional flow with chaotic trajectories which is a solution of the two-dimensional barotropic Navier-Stokes equation, an idealized framework for quasi two-dimensional advection in the stratosphere. The effect of resolution will be captured by varying the diffusion of the reactants. We will focus on a bimolecular reaction $A + B \longrightarrow C$ between two reactants that do not overlap initially. This study is both numerical and theoretical. The theoretical development will make the use of local Lagrangian stretching theories (LLST) to understand the dynamics of the contact zone where A and B mix under the action of the diffusion and react. LLST were developed to describe passive tracer phenomenology in chaotic advection or in the Batchelor regime of turbulence, characterized by a scalar diffusivity much smaller than viscosity. We will refer to these kinds of flows as "large-scale". LLST are based on the decomposition of the tracer field in elementary elements on

scales much smaller than the flow scale. Each element is followed on Lagrangian trajectories and the statistical and spectral properties of the field are recovered through an ensemble average on the stretching histories. In section 1.3, we will review LLST for the passive scalar problem.

1.1 Chaotic advection and mixing in the stratosphere

1.1.1 Chaotic advection in geophysical fluids

Welander noted in 1955 (*Welander*, 1955) the analogy between the structure of large-scale tracers in the atmosphere[1] and in a lamellar two-dimensional flow in a buthanol film over water (figure 1–1). In both case, filaments develop, their extension reaching the scale corresponding to the large eddies, and then they fold. Welander's work is really a precursor of both chaotic advection and of its application to geophysical flows because it emphasizes the analogy between the stirring of tracers in two systems of totally different scales, one lamellar and one turbulent. In 1948, Eckart, working on mixing in the oceans, proposed a clear distinction between stirring and mixing (*Eckart*, 1948): advection, a purely mechanical process, was responsible for the former through the formation of filaments, whilst diffusion, a molecular process, was responsible for the latter at times sufficiently large to have permitted straining to increase the gradients in the direction perpendicular to the filaments. This description of stirring and mixing is sometimes named the Eckart paradigm in the literature.

Chaotic advection, sometimes called chaotic mixing, was introduced in 1984 by *Aref* (1984). This paper gave some visibility in the fluid dynamics community to previous works by *Arnóld* (1966) and *Hénon* (1966), two mathematicians who

[1] Large-scale filamentary structures in the atmosphere were conjectured as early as 1937 by Rossby (*Rossby*, 1938) for mixing of moisture with dry air in the upper troposphere.

pioneered the study of dynamical systems in the fifties and the sixties. The idea is that for incompressible two-dimensional flows, the two coordinates (X, Y) of a fluid parcel trajectory can be interpreted as the two coordinates of a trajectory in the phase space of a dynamical system. A two-dimensional dynamical system is necessarily non-chaotic. However, the time dependence of the flow introduces a third degree of liberty, which makes possible chaotic trajectories, even if the flow is very regular[1] . It follows that chaotic advection is often described as the emergence of irregular and highly sensitive trajectories on their initial conditions in flows very regular both in time and space (see *Ottino* (1989) for an early review). Chaotic advection has been shown to occur in flows exhibiting a closed streamline containing a stagnation point, where the velocity of the flow is equal to 0 (*Aref*, 1984; *Chien et al.*, 1986). Chaotic advection was mainly studied, both theoretically and experimentally, in non-turbulent laminar flows (*Aref*, 1984; *Chien et al.*, 1986; *Ottino et al.*, 1988), for example in boxes where the flow is generated by moving walls (*Chien et al.*, 1986). For a recent review of chaotic advection, one can refer to *Wiggins and Ottino* (2004).

After the connection between advection in time-dependent two-dimensional incompressible flows and chaos in dynamical systems was shown to be fruitful numerous mathematical tools developed for dynamical systems were applied to fluids (*Chien et al.*, 1986; *Wiggins*, 1988; *Ottino et al.*, 1988; *Ottino*, 1989). In particular, some aspects of the Lyapunov theory are particularly useful to describe stirring in chaotic advection. Given the chaotic nature of the trajectories, two initially infinitely close

[1] The coordinates (X, Y) are actually the generalized momentum and coordinate of a Hamiltonian system, the Hamiltonian being the stream function $\psi(x, y, t)$. In particular, given the non-autonomous nature of the system, there are just enough degrees of freedom to allow chaotic orbits, even when ψ is a very smooth function of space and time. The time dependence of the Hamiltonian is a necessary but not a sufficient condition to obtain chaotic orbits.

Figure 1–1: Deformation of a fluid element as observed by Welander (*Welander*, 1955) in a film of buthanol over water. The size of the tank is $50 \times 30 \times 30$ cm. The flow is lamellar and the tank is rotating to keep the motion two dimensional.

trajectories separate exponentially, at a time dependent rate given by the finite-time Lyapunov exponent (FTLE).

In geophysical flows, the study of chaotic advection was pioneered by Pierrehumbert who noted in the early nineties that large-scale eddies in a large-scale background current could play the rôle of closed orbits (*Pierrehumbert*, 1991a). Chaotic advection in the context of atmospheric dynamics is not fully defined yet, and its relevance will be discussed. It might seem surprising to find it in flows as complex as the atmosphere or the ocean. However planetary rotation and stratification inhibits 3D turbulence on large scales, resulting in almost two dimensional incompressible flows on isentropes, as suggested by quasi-geostrophic wave and turbulence theory (*Charney*, 1971; *Rhines*, 1975, 1979; *Hoskins et al.*, 1985). The impossibility of vortex stretching, and the resulting enstrophy conservation constraint, prevents any direct local energy cascade, the cornerstone of three-dimensional turbulence, but

rather favors the apparition of large-scale coherent structures (e.g. *Boer and Shepherd* (1983)) with an enstrophy cascade towards smaller scales. This phenomenology is often cited to explain why the wave analysis of the atmosphere is so efficient, despite the linearization of equations of motion that could be thought *a priori* highly non linear given the tremendous Reynolds number. It is worth noting that the applicability of quasi-geostrophic theories for geophysical flows and the reasons for the success of linear and weakly non linear theoretical models are still a matter of debate (e.g. *Schneider* (2004); *Schneider and Walker* (2006) in the troposphere). A directly related issue is our poor understanding of the atmospheric energy spectrum (*Bartello* (2010) and references therein, see also *Bacmeister et al.* (1996) for the stratospheric spectrum), which is not predicted by the quasi-geostrophic theory of turbulence.

Nevertheless, planetary waves, and their weakly non-linear interactions with the mean flow, in particular Rossby-wave critical layers at mid-latitudes in the deep winter stratosphere (the surf zone, see 1.2.2), were cited to produce chaotic advection (*Ngan and Shepherd*, 1997a, 1999a,b). Chaotic advection by modulated traveling waves was first described by *Knobloch and Weiss* (1987). In the context of atmospheric dynamics, more realistic setups were studied by *Pierrehumbert* (1991a) for traveling Rossby waves, and by *del Castillo-Negrete and Morrison* (1993) for traveling Rossby waves in a shear flow. These works paved the way for studies of chaotic advection on isentropes in the troposphere (*Pierrehumbert*, 1991b; *Pierrehumbert and Yang*, 1993), and in the stratosphere (*Pierrehumbert* (1991b); *Ngan and Shepherd* (1999a,b), see section 1.2.3).

1.1.2 Large-scale stirring and mixing in the stratosphere

Filamentary structure of tracers

The emergence of tracer filaments growing exponentially in the stratosphere was shown by *Waugh and Plumb* (1994) in stratospheric reanalysis, and by *Norton* (1994)

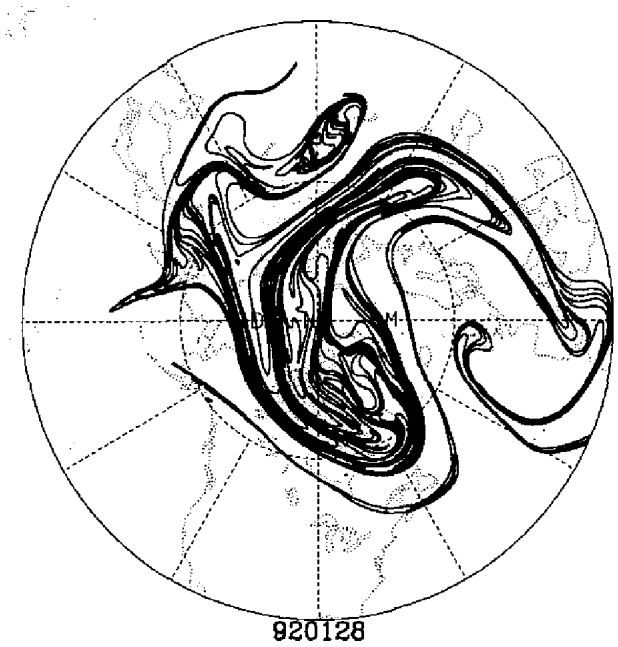

Figure 1–2: Contour advection with surgery (from *Waugh and Plumb* (1994)) in the stratosphere on the 450 K isentrope in January 1992 in the Northern Hemisphere (altitude around 20 km). The contours are circular at the initial time and the advection is run during two weeks. The length of the contours grows exponentially.

in a shallow water model for stratospheric flows. They both used contour advection with surgery algorithms (CAS). These structures were confirmed by airborne observational campaigns (*Waugh et al.*, 1994, 1997a). An example of structures obtained by CAS is shown on figure 1–2. One can notice the analogy with the structures of figure 1–1.

Following the picture drawn by Eckart, the role of molecular diffusion in the stratosphere is played by three dimensional features (probably like breaking of gravity waves) which become paramount at scales smaller than a few tens of kilometers in the extratropical stratosphere. *Haynes and Anglade* (1997) argued that this horizontal diffusivity κ_e parametrizing these small scale processes can be written:

$$\kappa_e \approx \alpha^2 \kappa_v. \tag{1.1}$$

The parameter α, the aspect ratio between typical horizontal and the vertical tracer scales, can be estimated from the ratio between the BruntVäïsälä frequency and the Coriolis parameter, and is of the order of 250 in the lower deep extratropical stratosphere (altitude $\approx 20\,\mathrm{km}$). The vertical diffusivity κ_v parametrizes small scale vertical mixing processes. Equation (1.1) can be understood intuitively noting that the filaments are, in three dimensions, sheets that intersect the isentropes. Estimations of κ_v from aircraft measurements campaigns in the lower deep extratropical stratosphere range from $0.01\,\mathrm{m}^2/\mathrm{s}$ to $0.1\,\mathrm{m}^2/\mathrm{s}$ (*Balluch and Haynes*, 1997; *Legras et al.*, 2005). It follows that κ_e is of the order of $10^3\,\mathrm{m}^2/\mathrm{s}$ to $10^4\,\mathrm{m}^2/\mathrm{s}$ (see also *Waugh et al.* (1997b)). Estimating typical strain rates at 0.2 day^{-1} in the stratosphere (e.g. *Balluch and Haynes* (1997)), the corresponding diffusive cutoff is of the order of a few tens of kilometers. This gives the typical width of the filaments, which is in accordance with observations (*Waugh et al.*, 1994, 1997a). An accurate representation of chemistry in Climate-Chemistry models would need to represent accurately these length scales.

Moreover, scalar tracer variance spectra for ozone O_3 and nitrous oxide NO_2 calculated from aircraft measurements campaigns suggest a k^{-2} spectrum (*Strahan and Mahlman*, 1994; *Bacmeister et al.*, 1996) at scales ranging from a few tens to a few hundreds of kilometers, with k the horizontal wavenumber. This spectrum is significantly different from the Batchelor k^{-1} spectrum, which was interpreted as the signature of filaments with sharp edges ejected from the polar vortex (*Ngan and Shepherd*, 1997b). This idea was developed in a theoretical random strain based study (*Haynes and Vanneste*, 2004) to predict the kink in the variance spectrum from k^{-1} at the largest scales to k^{-2} at smaller scales.

The stratospheric surf zone

The vertical profile of temperature in the atmosphere can be understood heuristically with radiative arguments. Shortwave radiation is absorbed by the surface of Earth, which heats the atmosphere from below (long wave radiation, sensible and latent heat), and by ozone in the middle atmosphere situated between 20 km and 80 km. As a consequence the average atmospheric temperature profile exhibits two local maxima, one at the surface, and one in the middle atmosphere, at around 50 km. The high altitude maximum defines the upper limit of the stratosphere or stratopause. The minimum in-between, at an average of 12 km altitude, separates the troposphere, where convective and baroclinic effects produce weather, and the stratosphere characterized by a positive vertical temperature gradient. This is the thermal definition of the tropopause. Figure 1–3 shows the average temperature profile of the atmosphere. The height of the tropopause can be roughly estimated, especially in tropical regions, from the altitude where convective processes in the troposphere are blocked by radiative heating in the stratosphere and ranges from 18km near the equator to 8km over the polar regions. However, the processes controlling the height of the tropopause in extratropics are not fully understood yet (e.g. *Schneider* (2004) for the role of baroclinic eddies, and references therein). In this introduction, we are discussing the deep stratosphere, situated above 20km, and where stratospheric and tropospheric exchanges are not essential.

An important aspect of the stratosphere is its high stability implied by positive vertical temperature gradients. Hence, as suggested by its name, the stratosphere is highly stratified, constraining transport of potential vorticity on two-dimensional isentropic surfaces evolving slowly compared to the advective processes, also much faster than diabatic processes.

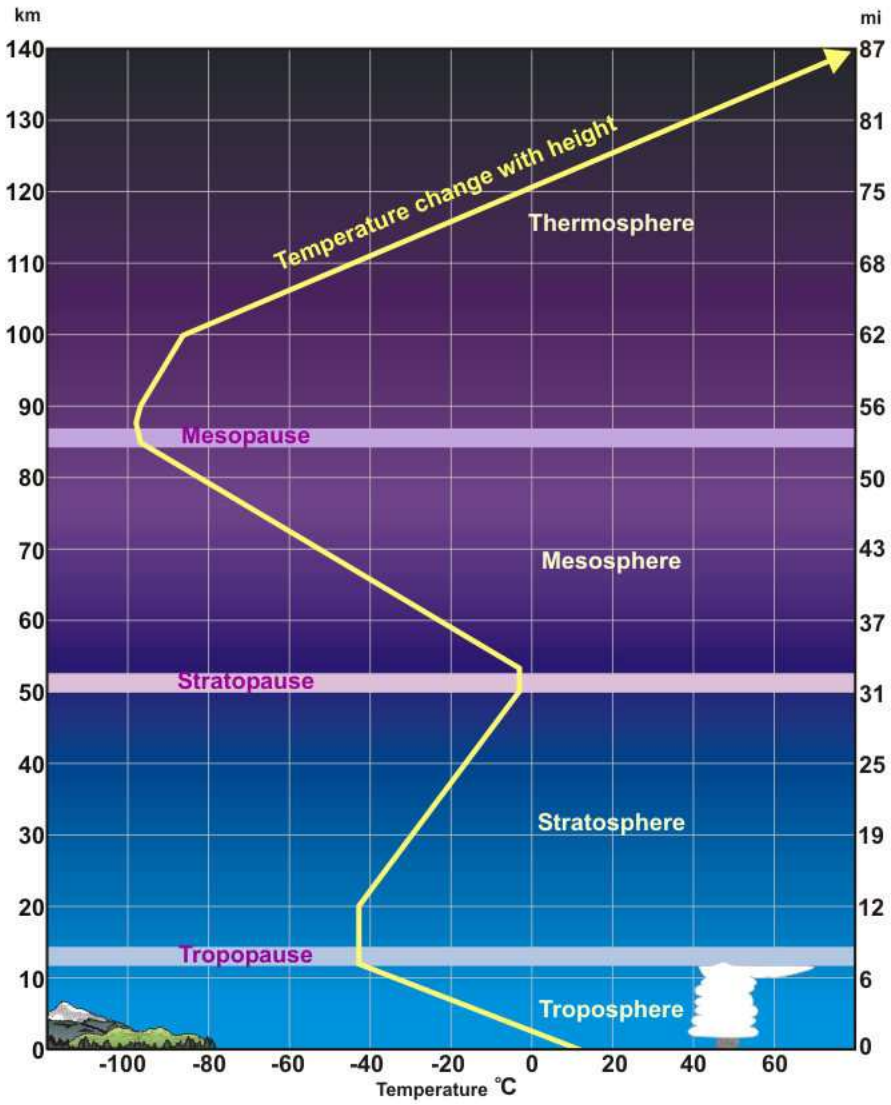

Figure 1–3: Average atmosphere temperature profile. From *NOAA* (2011).

A central phenomenon in stratospheric dynamics is the breaking of upward synoptic and planetary Rossby waves excited by baroclinic activity in the extratropical troposphere and by topographic or thermal effects at the surface of Earth (only planetary waves reach the deep stratosphere). This breaking deposits momentum which is the main driving force for the slow diabatic overturning Brewer-Dobson circulation, the Coriolis torque balancing the down gradient meridional eddy vorticity flux in terms of residual circulation to maintain the zonal flow (e.g. *Andrews et al.* (1987)). This circulation, particularly strong in the winter hemisphere, consists of large-scale ascent in the tropical stratosphere, northward transport at midlatitudes and large-scale descent over the pole. The Brewer-Dobson circulation is pictured in figure 1–4. The deposition of momentum also forces the flow on the isentropes and is a source of potential enstrophy cascading to smaller scales. This cascade is thought to be responsible for the details of quasi two-dimensional transport and stirring of tracers, like chemicals (e.g. *Vallis* (2006)). Here, we focus on the wintertime northern hemisphere stratosphere, where the planetary wave activity is particularly important, because of a favorable moderate background eastward flow (*Charney et al.*, 1961) and the intense wave activity originating from the troposphere.

From the analysis of potential vorticity maps on isentropes, McIntyre and Palmer (*McIntyre and Palmer*, 1983, 1984) showed in the early eighties that the theory developed a few years before for weakly non-linear critical layers of Rossby waves propagating in a shear flow (*Stewartson*, 1977; *Warn and Warn*, 1978)[1] could explain the deposition of momentum by planetary waves in the stratosphere. The basic idea

[1] This theoretical model is known as the Stewartson-Warn-Warn (SWW) solution of Rossby-wave critical-layer theory.

is that the solution of the linearized quasi-geostrophic equations for zonally propagating Rossby waves in a background shear flow accelerating with the meridional coordinate is singular when the background flow velocity matches the phase speed of the wave (Rayleigh-Kuo equation). Nonlinearities have to be taken into account to obtain a physical solution. Figure 1–5 shows the streamfunction for the critical layer as derived by *Warn and Warn* (1978), and known as the Kelvin cat's eye, and the advection of vorticity contours within the eye (*Killworth and McIntyre*, 1985). We note the similarity of this structure with the Kelvin-Helmholtz instability, where stratification has a stabilization effect playing the same rôle as the gradient of planetary vorticity in the case of Rossby-wave critical layers. Within the cat's eye, material contours can be irreversibly deformed: the Rossby waves are breaking, momentum is deposited, which can accelerate the mean zonal flow, and potential enstrophy is cascading irreversibly towards small scales. For a comprehensive discussion and theoretical description of Rossby-wave critical layers, one can refer to *Killworth and McIntyre* (1985) and *Haynes* (1985). The zone of the stratosphere characterized by strong large-scale stirring associated with a planetary-scale critical layer and a residual polarward circulation extends from 10 hPa to 100 hPa (15 km to 35 km) at midlatitudes (60° to 20° latitude) and is called the 'surf zone' since the seminal work of McIntyre and Palmer (*McIntyre and Palmer*, 1983, 1984). It is shown on figure 1–4.

An other central feature of the stratosphere is the winter time polar vortex, consisting of a planetary scale high-latitude coherent cyclonic structure centered on polar regions (*Waugh and Polvani* (2010) for a review). It acts as a transport barrier between high and mid-latitudes. This vortex is reversibly distorted and displaced by the propagation of planetary waves, and irreversibly by the deposition of momentum at its outer edge in the critical layer. It was argued that irreversible distortions

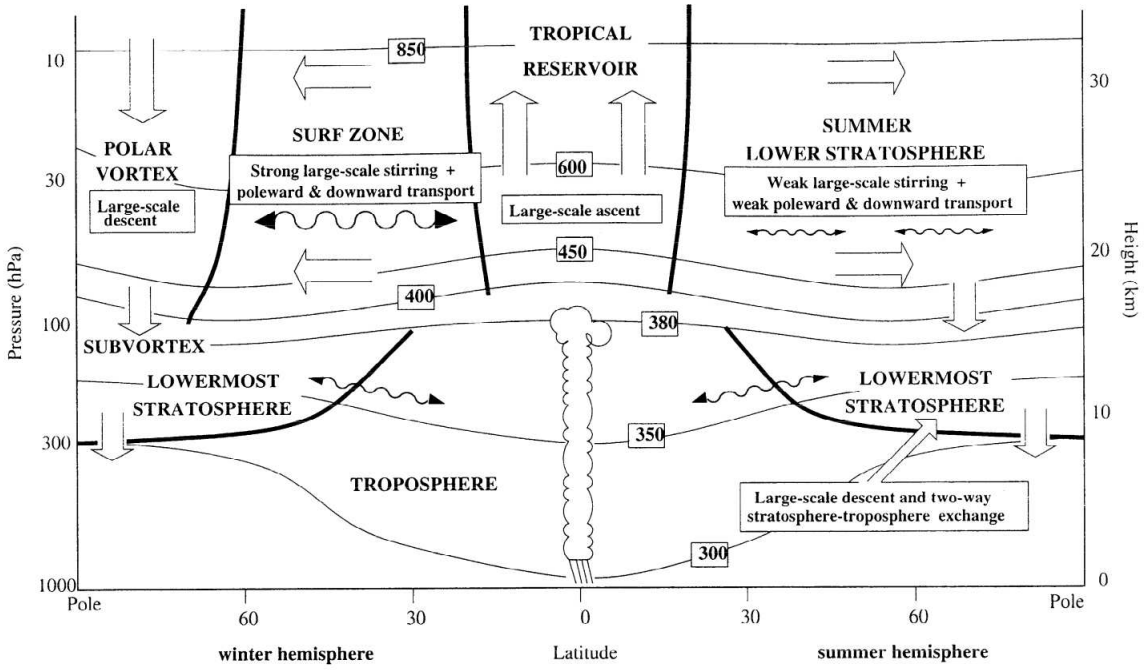

Figure 1–4: Zonal mean dynamics of the stratosphere from *Haynes and Shuckburgh* (2000). The isolines from 300 to 850 indicates the potential temperature of the isentropes in Kelvin.

cause the ejection of high potential vorticity filaments in the surf zone sharpening the edge of the polar vortex, in terms of potential vorticity, and strengthening the transport barrier and the zonal flow around the vortex (*Juckes and McIntyre*, 1987; *Polvani and Plumb*, 1992). A simplified model for this process based on the shallow water equations with a radiative relaxation was proposed by (*Juckes*, 1989) [1] . This phenomenology was confirmed and made more precise using idealized models based on the stratified quasigesotrophic equations (*Waugh and Dritschel*, 1999) and the primitive equations (*Polvani and Saravanan*, 2000), showing in particular the vertical structure of the upward propagating Rossby waves and of the critical layers.

[1] This might be a manifestation of a more general process, known as vortex stripping (*Legras et al.*, 2001)

Polar vortex erosion has important consequences for the mixing of chemical tracers because it is associated with the ejection of polar vortex air in the surf zone. Similar phenomena have been described at the subtropical edge of the surf zone, also characterized by a transport barrier but weaker than the polar vortex: the tropical pipe (*Polvani et al.*, 1995; *Chen*, 1996).

1.1.3 Chaotic advection in the surf zone

As explained in section 1.1.2, it has been shown that tracers in the stratosphere, in particular in the surf zone, exhibit filamentary structures that develop exponentially fast. This suggests that chaotic advection may be relevant to describe transport and stirring in the stratospheric surf zone (e.g. *Waugh and Plumb* (1994)). Later on, more rigorous and systematic studies have shown the probable validity of chaotic advection (*Ngan and Shepherd*, 1999a,b). In the following paragraphs, we present briefly what led to these results.

The first studies of chaotic advection in a context potentially applicable to the stratosphere were performed by *Knobloch and Weiss* (1987) and *Weiss and Knobloch* (1989), even though the former is a model for a lamellar two-dimensional fluid consisting of a layer of methanol above water (similar to the system studied in 1955 by Welander *Welander* (1955) and discussed above in 1.1.1) and the latter a model for weakly non-linear Rayleigh-Bénard convection. They showed that chaotic advection could be obtained with a stationary wave perturbed by a traveling wave of weak amplitude. Building on these studies, a model for the superposition of Rossby waves was studied by *Pierrehumbert* (1991a) before it was made more realistic by *del Castillo-Negrete and Morrison* (1993), who added a background shear. However, as noted by *Pierrehumbert* (1991b) and *Ngan and Shepherd* (1997a), these models are not dynamically consistent in the sense that they are purely kinematic and do not conserve vorticity, the dynamical consistency being recovered only in the simple

and irrelevant case of homogenized vorticity. However, the SWW solution stipulates that the vorticity behaves like a passive tracer at leading order in the critical layer, which has been argued to justify a wave superposition with a background cat's eye structure to build an idealized kynematic model for chaotic advection in the stratospheric surf zone (*Ngan and Shepherd*, 1997a). The streamlines defining the edge of the cat's eye (the separatix) forms a closed orbit, a characteristic feature of many systems with chaotic advection (see figure 1–5, left panel. The stagnation points are in $(x = \pm\pi, y = 0)$).

The central picture of these studies (*Knobloch and Weiss*, 1987; *Weiss and Knobloch*, 1989; *Pierrehumbert*, 1991a; *del Castillo-Negrete and Morrison*, 1993; *Ngan and Shepherd*, 1997a) consists of large-scale stationary background flows (and consequently integrable, i.e necessarily non chaotic) that are perturbed by a weak time-dependent pattern, for example a traveling wave, to produce chaotic advection. The addition of the weak pattern preserves some invariant curves (forming Kolmogorov-Arnold-Moser, or KAM, tori), chaotic islands growing between some of them, especially in the vicinity of hyperbolic points. The size of the chaotic islands grows with the strength of the perturbation. The surviving barriers of transport in these simple, dynamically inconsistent flows, were cited to explain stratospheric barriers of transport (the vortex and the tropical pipe), since the cat's eye structure is planetary scale in the stratosphere (see figure 1–6). However it is not clear how taking into account the dynamical consistency changes the nature of chaotic advection, or even allows it. *Brown and Samelson* (1994) showed that a two dimensional flow perfectly conserving vorticity is necessarily non chaotic when the vorticity gradient never vanishes. However, real systems do not conserve vorticity perfectly. In particular, one can think that viscosity is particularly important, playing a non-trivial rôle

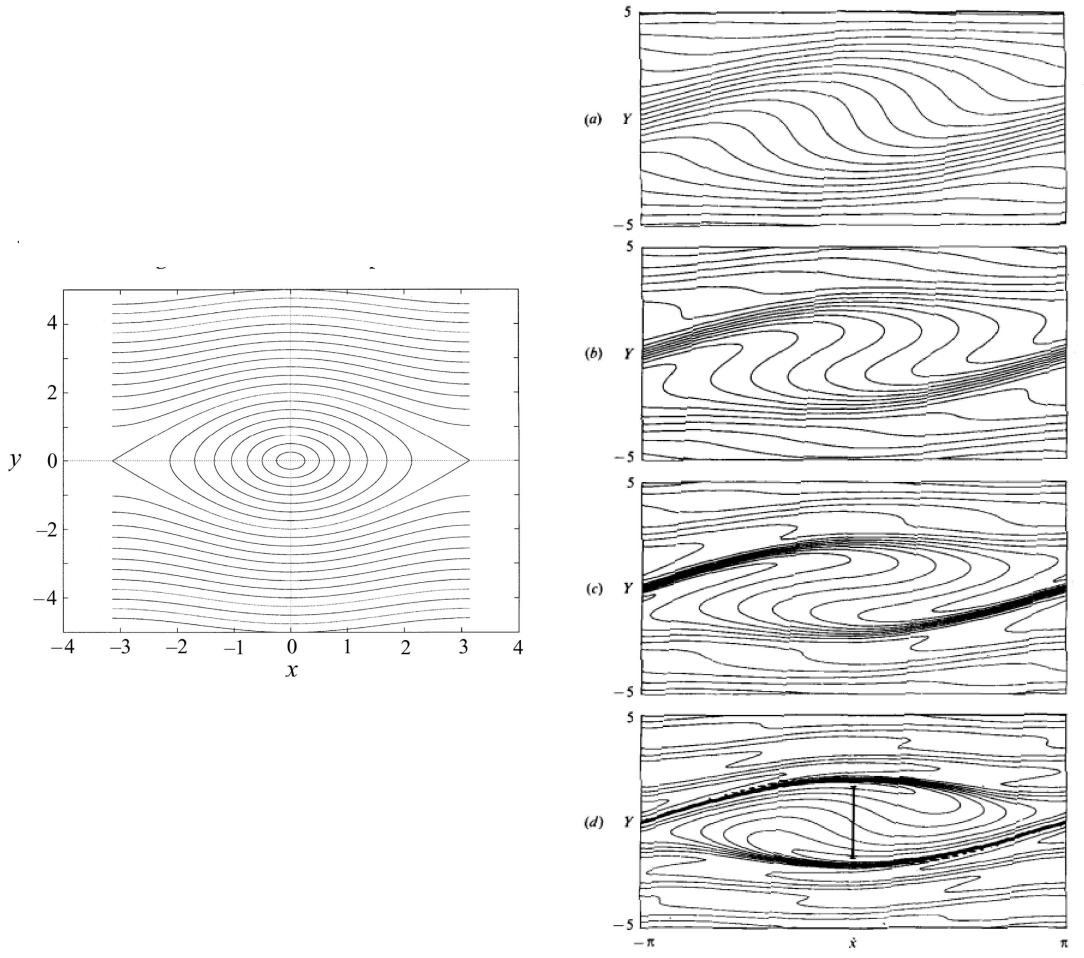

Figure 1–5: On the left is shown the SWW solution for weakly nonlinear Rossby waves critical layers (Kelvin Cat's eye), from *Ngan and Shepherd* (1997a). With x the zonal coordinate and Y a rescaled meridional coordinate, the streamfunction is given by $-\frac{1}{2}Y^2 + \cos x$. Formally this is the equivalent of the phase space of a simple pendulum without friction with the angle in x and the acceleration in y. On the right is shown the advection of potential vorticity as predicted by the SWW theory (from *Killworth and McIntyre* (1985)). The potential vorticity is a passive tracer at the leading order (however one can note the rotation of the cat's eye).

as in theories of turbulence. For a discussion on the effect of dynamical consistency on chaotic advection, one can refer to *Haynes et al.* (2007).

Chaotic advection in the stratosphere was studied more systematically by *Ngan and Shepherd* (1999a,b). It was shown that a cat's eye structure for the advection of a passive tracer was observed in both a simple shallow water model for stratospheric flow and in a middle atmosphere general circulation model (figure 1–6). Also, the parcel trajectories were shown to be chaotic within the cat's eye. With the additional observation that Lagrangian correlation time were smaller than Eulerian correlation times, they argued that the critical layer was the analog of the time dependent heteroclinic structure in simple dynamical models of chaotic advection. Verifying this statement would require explicit calculations of the manifolds, which is unfortunately very complicated (references in *Ngan and Shepherd* (1999a)).

We have presented how chaotic advection could explain stratospheric stirring and mixing in the surf zone. However, as noted recently by *Shepherd* (2007), there is no general theoretical approach to horizontal mixing in the stratosphere. In particular, eventhough the "effective diffusivity" approach might not be physically relevant to describe mixing in the stratosphere because of its inconsistency with the Eckart paradigm (*Pierrehumbert*, 1991b; *Pierrehumbert and Yang*, 1993), it is particularly useful and accurate to describe latitudinal transport barriers (*Nakamura*, 1996; *Haynes and Shuckburgh*, 2000). It was argued that the effective diffusivity is more relevant to describe the details of mixing in geophysical flows, in particular detecting barriers of transport, than tools developed for dynamical systems (FTLE in particular) by *Shuckburgh and Haynes* (2003). However, there is no theory to support these claims to our knowledge.

We tried to justify the large-scale nature of the stratospheric surf zone with chaotic advection. However, other results that do not necessarily imply chaotic

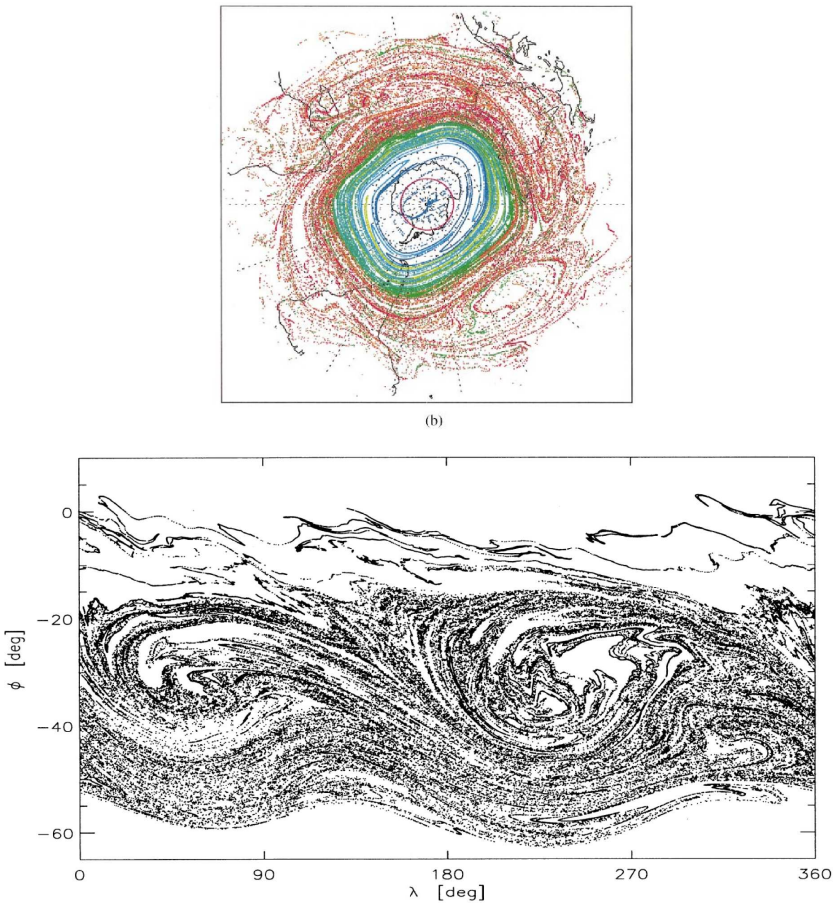

Figure 1–6: On the top are shown the results of trajectory calculations on the $450\,K$ isentrope (20 km) during one month in the northern hemisphere winter (*Shepherd*, 2000). At the bottom, it is the same but on the $1000\,K$ isentrope corresponding to the upper stratosphere (*Ngan and Shepherd*, 1999a). The winds are calculated with the Canadian Middle Atmosphere Model (CMAM). The cat's eye structures are clearly visible. There are four at $450\,K$ and two at $1000\,K$. This reduction is due to the fact that only the largest scale waves reach the upper stratosphere. The transport barriers (polar vortex and tropical pipe) are clearly visible.

advection show that atmospheric flows are large scale. In particular, the steep non-local energy spectrum of the stratosphere simulated in middle atmosphere models (*Koshyk et al.*, 1999; *Koshyk and Hamilton*, 2001) [1] suggests that small-scale stirring is determined by the largest scales of the flow. This is consistent with *Bartello* (2000), where it is shown that truncated coarse resolution winds reproduce fairly well the small scale structure of the tracer in simulations of a barotropic $\beta-$plane turbulent flow. Chaotic advection can be seen as an abstract, theoretical and elegant framework that could explain this phenomenology. However, even though numerous study strongly suggest that chaotic advection is occurring in the stratosphere, there is no definitive proof of it.

1.2 The issue of resolution in Climate-Chemistry models

1.2.1 Ozone chemistry in the polar vortex and the surf zone

The total ozone quantity in the stratosphere has shrunk since the seventies. This decrease goes with an annual sharp decrease of stratospheric ozone in spring over polar regions. The southern hemisphere is particularly affected, the "ozone hole" above Antarctica having extended very significantly over the past few decades. The culprits are chlorofluorocarbons (CFCs) that had been widely used as refrigerants, solvents, foam packaging and for many other purposes before their partial banning by the Montréal protocol in 1987. Its signature was an impressively fast reaction from the international community to a problem whose importance was stressed only two years before by the scientific community in a paper published in Nature (*Farman et al.*, 1985). For a comprehensive description of ozone chemistry in the stratosphere, see *Andrews et al.* (1987); *Solomon* (1999). CFCs that reach the stratosphere are

[1] We not that this was claimed to be an additional evidence of chaotic advection in the stratosphere by *Shepherd et al.* (2000).

photoloyzed to give chlorine atoms (henceforth for CFC-12):

$$CCl_2F_2 + h\nu \longrightarrow CClF_2 + Cl \tag{1.2}$$

Chlorine atoms are partly responsible for ozone depletion through a catalytic cycle involving ClO radicals (*Andrews et al.*, 1987):

$$Cl + O_3 \longrightarrow ClO + O_2 \tag{1.3a}$$

$$ClO + O \longrightarrow Cl + O_2 \tag{1.3b}$$

$$\text{———} \tag{1.3c}$$

$$O_3 + O \longrightarrow 2O_2(\text{net}). \tag{1.3d}$$

As seen in (1.3), Cl is a catalyst and a small amount can destroy a large amount of ozone. However, the activated chlorine monoxide ClO can be deactivated, for example by methane CH_4 or NO_2 (more generally NO_x) and be converted into reservoirs of relatively inert compounds, respectively chlorine nitrate ($ClONO_2$) and hydrogen chloride (HCl).

Polar ozone hole chemistry involves heterogeneous processes on polar stratospheric clouds, which condense under particularly cold conditions (they are very common in the wintertime southern hemisphere stratosphere but are much more rare in the wintertime northern hemisphere stratosphere, with a strong interannual variability). NO_2 is tied up to these clouds and is not available to react with active chlorine compounds to form inert compounds. In addition, the inactive compounds $ClONO_2$ and HCl react on these clouds to form the active compound Cl_2 and HNO_3 (HNO_3 precipitates). As a result, air inside the polar vortex contains high quantities of active chlorine (in particular in the form of the dimer ClOClO). These high quantities are maintained by the polar vortex transport barrier. In the spring, when the sun returns, the activated chlorine will destroy ozone. The mechanism involved

was described by Molina and Molina (*Molina and Molina*, 1987). MJ Molina was awarded the Nobel prize of chemistry in 1995 for his work on stratospheric chemistry and ozone depletion. His mechanism yields:

$$2(\mathrm{Cl} + \mathrm{O_3} \longrightarrow \mathrm{ClO} + \mathrm{O_2}) \tag{1.4a}$$

$$\mathrm{ClO} + \mathrm{ClO} \longrightarrow \mathrm{ClOClO} \tag{1.4b}$$

$$\mathrm{ClOClO} + h\nu \longrightarrow \mathrm{Cl} + \mathrm{OClO} \tag{1.4c}$$

$$\mathrm{OClO} \longrightarrow \mathrm{Cl} + \mathrm{O_2} \tag{1.4d}$$

$$\text{———} \tag{1.4e}$$

$$2\mathrm{O_3} + h\nu \longrightarrow 3\mathrm{O_2}(net) \tag{1.4f}$$

In this discussion, we have omitted the role of bromine BrO, which is thought to have important effects on the ozone chemistry, with Br being even more reactive (e.g. *Salawitch et al.* (2005)).

1.2.2 Numerical and theoretical results

The effect of small scale stirring and mixing on ozone chemistry in the polar vortex was investigated in the wintertime northern hemisphere by *Edouard et al.* (1996). They advected active chemicals with stratospheric reanalysis at different horizontal resolutions. They suggested a significant dependence of spring total ozone depletion with horizontal resolution, ranging from 64.5% at 200 km to 21.6% at 15 km. However, *Searle et al.* (1998a,b) questioned this result, showing only a weak dependence in their own similar simulations and attributing it to the complete activation of chlorine at all resolutions.

The picture in the surf zone is fundamentally different. We have explained in 1.1.2 that chemical tracers originating from both the tropical pipe and the polar vortex, are stirred through chaotic advection in a planetary scale surf zone, located

at mid-latitudes in the deep stratosphere. Transport, stirring and mixing processes can be described by the Eckart paradigm down to a scale of a few tens of kilometers, determined by cross-isentropic three-dimensional processes. The width and life time of the filaments were observed to be very sensitive to the model resolution by *Searle et al.* (1998a). The effect of resolution, captured by an effective resolution determined by the model horizontal tracer diffusion, was studied in the context of the surf zone ozone depletion by *Tan et al.* (1998), during a northern hemisphere winter. Mixing effects are expected to be more important in the northern hemisphere than in the southern hemisphere since the vortex is more perturbed irreversibly by breaking Rossby waves propagating from the troposphere. Ozone concentration in the surf zone can be affected several different ways potentially dependent on resolution: dilution of ClOClO, mixing of polar air rich in O_3 with midlatitude air, destruction of the active form of chlorine by locally produced NO_x through photolysis of HNO_3 or by NO_x coming from low latitudes, where the production is particularly important because of the intense insulation south of the surf zone. *Tan et al.* (1998) argued, using box models, that the deactivation of ClO by low-latitude NO_x alone determined the ozone concentration in the surf zone to a very good approximation. Thus, they studied the effect of diffusion on the total concentration of $ClONO_2$, product of the deactivation of ClO by NO_2:

$$ClO + NO_2 \longrightarrow ClONO_2. \tag{1.5}$$

The chemicals were advected by reanalysis of the stratosphere on the $475K$ isentrope and different initial conditions were investigated, changing the location of the center of the area of the polar activated air and the distance between this area and the NO_2-rich low latitude air (the two reactants are segregated and do not initially overlap). The chemical reaction (1.5) is very fast compared to advective

and diffusive processes and is consequently diffusively limited. They showed that the concentration of $ClONO_2$ scales like $\kappa^{-p(t)}$, where κ is the tracer diffusion and $p(t)$ a negative increasing function depending on the initial conditions, over a time span of a few weeks. This problem was addressed by *Wonhas and Vassilicos* (2002, 2003) from a theoretical point of view. They proposed that $p(t)$ is equal to $-1+\frac{D(t)}{2}$ with $D(t)$ the box counting fractal dimension of the interface between chemicals reacting instantaneously and assumed to be on/off at any time. If the spectrum of the variance of a passive scalar (here defined as the difference between the reactants) is proportional to $k^{\alpha(t)}$, then coefficient $\alpha(t)$ can be linked to $D(t)$ because the fields are on/off (*Vassilicos and Hunt*, 1991). The concentration of the reactants, and consequently of the product, can be directly calculated from the variance thanks to the on/off assumption for the tracer fields. This reasoning leads to $p(t) = -1+\frac{D(t)}{2}$.

1.3 Local Lagrangian stretching theories (LLST)

1.3.1 Background

Lagrangian stretching theories were developed to describe the phenomenology of passive tracers in large-scale flows. To develop on the Eckart paradigm let's consider the advection diffusion of a tracer $\phi(\mathbf{x}, t)$ in a large-scale, smooth, closed two-dimensional flow $\mathbf{u}$. We consider a globally chaotic system without KAM surfaces. The equation for ϕ is the classical advection-diffusion equation:

$$\frac{\partial \phi}{\partial t} + \mathbf{u} \cdot \nabla \phi = \kappa \nabla^2 \phi. \tag{1.6}$$

This equation is linear in ϕ - which does not mean it is simple - because we are dealing with a passive tracer that does not affect the flow. As a consequence we can assume, without loss of generality, that the ensemble average $\langle \phi \rangle$ is equal to 0 at all times. If the variance $\langle \phi^2 \rangle$ is equal to 0, we can say that the tracer is perfectly mixed. Hence, it is natural to define the variance as a measure of mixing. integrating and

averaging (1.6), the equation obeyed by $\langle\phi^2\rangle$ is:

$$\frac{d\langle\phi^2\rangle}{dt} = -2\kappa\langle|\nabla\phi|^2\rangle. \tag{1.7}$$

Without any flow ($\mathbf{u} = 0$), the decay of $\langle\phi^2\rangle$ is determined by diffusion. In this case, a dimensional analysis of (1.6) shows that the time scale of the exponential decay of $\langle\phi^2\rangle$ is $T_\kappa = \frac{L^2}{\kappa}$, with L the initial typical scale of variation of ϕ, and converges to infinity as $\kappa \to 0$. Calculating T_κ for sugar in tea, we would find that it would be difficult to drink a cup of sweet tea before a couple of months. The mixing can be enhanced by transport and turbulence, for example using a spoon. In the case of a cup of tea, three-dimensional turbulence is involved and the right evaluation of the mixing time scale is obtained with turbulent eddy diffusivity. In the lower stratosphere, horizontal diffusivity was estimated at $\kappa_e = 10^3\,\mathrm{m}^2/\mathrm{s}$ ((*Waugh et al.*, 1997b) and discussion below (1.1) in section 1.1.2). An estimate of T_{κ_e} on a scale of 1000 km gives one millennium, which is of course not consistent with the mixing time scales in the stratosphere. Mixing is accelerated by stirring induced by chaotic advection: the dynamical action of the flow is "hidden" in the gradient operator of equation (1.7). If we consider a small circle of tracer, it will be stretched into an elongated ellipsoid of length $\propto e^{\lambda t}$ (for a very simplified description, we assume here a uniform stretching rate without taking into account the vorticity and the reorientation of the strain axis on a Lagrangian trajectory). Because of incompressibility, its width decreases like $e^{-\lambda t}$ as long as diffusion can be neglected and then saturates at a length that scales like $\sqrt{\frac{\kappa}{\lambda}}$, where that advective and diffusive terms in (1.6) become of the same order. A dimensional analysis of (1.7) suggests that the variance $\langle\phi^2\rangle$ decays exponentially at rate 2λ independent of the diffusion.

This picture is over-simplified but gives an intuitive insight into the mechanism for the decay of tracer fluctuations. An exponential decay, independent of diffusion

in the limit of an infinitely small diffusion, of the variance of a passive tracer has been observed in both numerical simulations of two-dimensional chaotic advection in renewing flow consisting of alternating sinusoidal shear flows in each direction of space every half-time period $\frac{T}{2}$ (*Pierrehumbert*, 1994; *Antonsen et al.*, 1996; *Pierrehumbert*, 2000; *Sukhatme and Pierrehumbert*, 2002; *Fereday and Haynes*, 2004; *Haynes and Vanneste*, 2005; *Tsang*, 2009) and experiments in electromagnetically-driven two-dimensional flows (*Rothstein et al.*, 1999; *Voth et al.*, 2003). Some of these flows were rigorously periodic while others where characterized by a random uniformly distributed phase in the sinusoidal flow renewed every T. The random phase can produce flows with chaotic orbits almost everywhere, destroying KAM. When barriers of transport are present, the mixing rate converges to 0 in the limit of an infinitely small diffusion (e.g *Pikovsky and Popovych* (2003)) and the theory we are presenting is not applicable.

An important feature observed in this kind of flow is the Pierrehumbert strange eigenmode, sometimes associated with the exponential decay of the variance (the exponential decay is a necessary condition for the strange eigenmode, but is not sufficient, as suggested by *Sukhatme and Pierrehumbert* (2002)), and observed at very long times. It was first described by Pierrehumbert (*Pierrehumbert*, 1994). It means that the tracer field $\phi(\mathbf{x}, t)$ can be written:

$$\phi(\mathbf{x}, t) = e^{-\gamma t}\hat{\phi}(\mathbf{x}, t), \tag{1.8}$$

where γ is the variance exponential decay and is often called mixing rate. The function $\hat{\phi}(\mathbf{x}, t)$ is statistically stationary and can be described as a structure of packed filaments that fill the whole domain (*Pierrehumbert and Yang*, 1993; *Sukhatme and Pierrehumbert*, 2002). The striation thickness of these filaments correspond to the diffusive cutoff and diffusion is responsible for the fluctuation decay. In particular

(1.8) implies the self-similarity of the probability density function of ϕ and of its variance spectra, when ϕ is rescaled with $e^{-\gamma t}$. The decay rate of the β-order moment $\langle|\phi|^\beta\rangle$ is a linear function of β. This eigenmode is called strange because it is not a true eigenmode of the advection diffusion operator $\mathcal{AD} \equiv \kappa\nabla^2 - \mathbf{u}\cdot\nabla$. In the case of a non chaotic stationary flow, such a time independent eigenmode exists for $\kappa \neq 0$ and corresponds to the smallest eigenvalue of the spectrum of eigenvalues of the operator $\mathcal{AD}$ (see *Katō* (1995); *Childress and Gilbert* (1995) for the mathematical details). In the case of chaotic $T-$periodic flows, such an eigenmode exists and corresponds to the smallest Floquet exponent. It was observed in both numerical simulations (*Sukhatme and Pierrehumbert*, 2002) and experiments of magnetically-driven, two-dimensional flows (*Rothstein et al.*, 1999; *Voth et al.*, 2003). This approach based on diagonalizing a linear operator was extended to δ-correlated (Kraichnan limit) non-periodic flows and renewing flows by *Haynes and Vanneste* (2005) for the operator acting on the the second order cumulant $\Gamma(\mathbf{x}, \mathbf{r}, \mathbf{t}) \equiv \langle\phi(\mathbf{x}+\mathbf{r})\phi(\mathbf{x})\rangle$ (brackets are for an ensemble average). This work will be discussed later in section 1.3.4.

A more traditional approach in fluid dynamics would use an effective diffusivity to predict the exponential decay (see *Majda and Kramer* (1999) for a review about homogenization theories). However, as stated earlier, (*Pierrehumbert*, 1991b) suggested that this approach is not relevant to two dimensional chaotic advection when the eddy length scale is not small compared to the the scale of the tracer. Relating the mixing rate, as well as the statistical and spectral properties of the tracer field, to the stretching properties of the flow has inspired numerous studies over the past decades in the general frameworks of chaotic advection or Batchelor regime turbulence. In both cases, there is a separation between the flow and the finite scalar scales. This approach was pioneered by *Kraichnan* (1974) for a stochastic δ-correlated irrotational model of turbulence (sometimes named the Kraichnan-Kazantsev model)

and exploits the separation of scales to linearize the velocity gradient, on the tracer finite scale, in the comoving frame with a Lagrangian parcel. Hence, the behavior of the tracer field depends on the ensemble average of products of the instantaneous velocity-gradient tensor, each product corresponding to a Lagrangian parcel, seen from a mathematical point of view as the product of random matrices (see 1.19 below) . This defines the big picture for random strain theories and LLST (see the review *Falkovich et al.* (2001) for the passive scalar problem).

Irrotational flows in the Kraichnan limit were first studied (velocity gradients $\delta-$correlated in time defines this limit, as in *Kraichnan* (1974)), before arbitrary correlations for more general tensors were considered (*Chertkov et al.*, 1995; *Balkovsky and Fouxon*, 1999; *Son*, 1999). These papers are exclusively theoretical and do not provide any validation with numerical simulations or experiments. Similar approaches, usually called "local Lagrangian stretching theories" in the literature, do not make any assumption about the form or the statistics of the velocity gradient tensors (except for incompressibility). Their starting point is also the separation of scale between the velocity and the tracer finite scales, which allows the differentiation of the velocity gradient at the tracers' finite scale and thus the use of finite-time Lyapunov exponents (FTLE) which can be defined from the multiplication of the local velocity gradients along the trajectory (see 1.3.2 below). LLST predict the statistical and spectral properties of the scalar field from the FTLE pdf, as predicted by the large deviation theory (see 1.3.2 below). These theories are local and Lagrangian because they consist of the ensemble averaging of individual Lagrangian parcels small in comparison to the large-scale flow. In particular, the flow has to be ergodic for these theories to have any chance to describe the decay of the total variance (KAM are ruled out, as mentioned earlier). An intuitive definition of ergodicity is that the

behavior of quantities averaged in space is the same as quantities averaged in time. Basically almost all locations in the phase space can be visited by almost any orbit.

The distinction we are suggesting between "random strain theories" and "local Lagrangian stretching theories" is pretty artificial and is only justified by the common use, not always consistent, of these two terms in the literature. Both are actually local and Lagrangian. The former is probably more theoretical, while the latter is more directly related to direct numerical simulations or experiments. However, the former builds upon statistical arguments (in particular large-deviation theory) based on a random strain approach to describe the distribution of the Lyapunov exponents. The fundamental importance of the product of ordered random matrices (*Kraichnan*, 1974; *Crisanti et al.*, 1994; *Chertkov et al.*, 1995; *Falkovich et al.*, 2001) makes an additional, essential and direct relationship between the study of complex flows and the ergodic theory of dynamical systems (*Eckmann and Ruelle* (1985) for an early review, part III. in particular).

The starting point of Lagrangian stretching theories (*Kraichnan*, 1974; *Monin and Yaglom*, 1975) is writing the advection-diffusion equation (1.6) in the co-moving frame with a Lagrangian trajectory $\mathbf{X}$ solution of

$$\frac{d\mathbf{X}}{dt} = \mathbf{u}(\mathbf{X}(t), t), \tag{1.9}$$

where $\mathbf{u}(\mathbf{X}(t), t)$ is the Eulerian velocity field along the trajectory. We introduce the coordinate $\mathbf{r} = \mathbf{x} - \mathbf{X}$ corresponding to the co-moving frame. Writing the concentration field $\chi(\mathbf{r}, t) \equiv \phi(\mathbf{x}, t)$, we can show using (1.6) and (1.9) that:

$$\frac{\partial \chi}{\partial t} + [\mathbf{u}(\mathbf{X} + \mathbf{r}, t) - \mathbf{u}(\mathbf{X}, t)] \cdot \nabla \chi = \kappa \nabla^2 \chi \tag{1.10}$$

We have assumed that the finite scales of the flow are smooth. Writing $[\mathbf{u}(\mathbf{X}+\mathbf{r},t)-\mathbf{u}(\mathbf{X},t)]$ in (1.10) at first order in $\mathbf{r}$, we get:

$$\frac{\partial\chi}{\partial t}+\mathbf{r}\cdot\nabla\mathbf{u}(\mathbf{X},t)\cdot\nabla\chi=\kappa\nabla^2\chi. \tag{1.11}$$

1.3.2 Lyapunov exponents

Here we define Lyapunov exponents and vectors and present some of their asymptotic and statistical properties in an ergodic two-dimensional flow. Most of the results we will present have been shown for dimensions $d \geq 2$. However, our objective is not a rigorous and comprehensive mathematical description of the Lyapunov theory, but to introduce local Lagrangian stretching theories for incompressible two-dimensional flows ($d = 2$).

Definition

Lyapunov exponents characterize in dynamical systems the rate of growth of initially infinitely close trajectories in the phase space. Noting the analogy with the phase space of a dynamical system (*Aref*, 1984), we can also define Lyapunov exponents in the flow of a fluid. If we consider two trajectories $\mathbf{X}$ and $\mathbf{X}+\delta\mathbf{X}$ originating in $\mathbf{x}$ and $\mathbf{x}+\delta\mathbf{x}$ at time $t=0$, we define the maximum finite-time Lyapunov exponent as follows:

$$\lambda(\mathbf{x},t)=\frac{1}{t}\max_{\delta\mathbf{x}}\lim_{|\delta\mathbf{x}|\to 0}\Big\{\ln\frac{|\delta\mathbf{X}|}{|\delta\mathbf{x}|}\Big\}\ . \tag{1.12}$$

The maximum is calculated over all possible orientations of $\delta\mathbf{x}$. As a consequence the distance $|\delta\mathbf{X}|$ will be equal to $|\delta\mathbf{x}|e^{t\lambda(\mathbf{x},t)}$ when the orientation of $\delta\mathbf{x}$ corresponds to this maximum growth.

Because of the scale separation between the scalar and the velocity, it is possible to linearize the velocity to obtain the ordinary differential equation obeyed by $\delta\mathbf{X}$:

$$\frac{d\delta\mathbf{X}}{dt}=\mathbf{S}(\mathbf{X}(t),t)\delta\mathbf{X}. \tag{1.13}$$

The tensor $\mathbf{S} \equiv \nabla \mathbf{u}(\mathbf{X}, t)$ is the velocity gradient tensor evaluated along the trajectory. If the flow is incompressible we have $\mathrm{tr}(\mathbf{S}) = 0$. The solution of (1.13) can be written using a resolvent matrix (or metric tensor) $\mathbf{M}$ solution of:

$$\frac{d\mathbf{M}}{dt} = \mathbf{S}(\mathbf{X}, t)\mathbf{M} \tag{1.14a}$$

$$\text{with } \mathbf{M}(t = 0) = \mathbf{Id} \ . \tag{1.14b}$$

The square of the modulus of $\delta\mathbf{X}$ is

$$|\delta\mathbf{X}|^2 = \delta\mathbf{x}^T\mathbf{M}^T\mathbf{M}\delta\mathbf{x}. \tag{1.15}$$

This expression links the Lyapunov exponents to the eigenvalues of the positive symmetric matrix $\mathbf{M}^T\mathbf{M}$ (which can be diagonalized in a orthonormal basis of $\mathbb{R}^2$ from the spectral theorem). Let $\boldsymbol{\psi}_+(t)$ and $\boldsymbol{\psi}_-(t)$ be the two eigenvectors, with $\Lambda_+(t)$ and $\Lambda_-(t)$ the associated eigenvalues. A direct consequence of $\mathrm{tr}(\mathbf{S}) = 0$ and $\det(\mathbf{M}(t = 0)) = 1$ is $\det(\mathbf{M}) = 1$, which implies $\det(\mathbf{M}^T\mathbf{M}) = \Lambda_+\Lambda_- = 1$. Here we will deal with the case of $\Lambda_+ > 1 > \Lambda_- = \frac{1}{\Lambda_+} > 0$, for which the trajectory $\mathbf{X}$ has a chaotic behavior. If $\delta\mathbf{x}$ is aligned with $\boldsymbol{\psi}_+(t)$, then $|\delta\mathbf{X}|^2 = \Lambda_+|\delta\mathbf{x}|^2$ and the finite-time Lyapunov exponent is $\lambda(t) = \frac{1}{2t}\ln\Lambda_+$. If $\delta\mathbf{x}$ is aligned with Λ_-, then we have $|\delta\mathbf{X}| = \Lambda_-^{\frac{1}{2}}|\delta\mathbf{x}| = e^{-\lambda(t)t}|\delta\mathbf{x}|$. With $\alpha(t)$ the initial orientation of $\delta\mathbf{x}$ with $\boldsymbol{\psi}_+(t)$, (1.15) gives:

$$|\delta\mathbf{X}|^2 = |\delta\mathbf{x}|^2 \left[e^{2\lambda t}\cos^2\alpha + e^{-2\lambda t}\sin^2\alpha\right]^{\frac{1}{2}} . \tag{1.16}$$

The component of $\delta\mathbf{x}$ aligned with $\boldsymbol{\psi}_+(t)$ will be stretched at a rate given by the Lyapunov exponent λ, while the component normal to it will shrink at the same rate.

The FTLE can also characterize the growth rate of a wavenumber $\mathbf{k}$ associated with a small "wave packet" of the tracer ϕ advected on a chaotic orbit. The dimension of the packet has to be much smaller than the typical scale of variation of the velocity $\mathbf{u}$ in order to be able to differentiate the velocity tensor gradient $\mathbf{S}$. Writing this "wave

packet" in the form $\chi(\mathbf{r},t) \equiv \widetilde{\chi}(t)e^{\mathbf{k}(t)\cdot\mathbf{r}}$ and putting it in the linearized advection-diffusion equation in the comoving frame (1.11), we obtain:

$$\frac{d\mathbf{k}}{dt} + \mathbf{S}^T.\mathbf{k} = 0 \tag{1.17a}$$

$$\frac{d\widetilde{\chi}}{dt} = \kappa \left|\mathbf{k}\right|^2 \widetilde{\chi}. \tag{1.17b}$$

The equation of evolution of the wavenumber is obtained by *Antonsen et al.* (1996) using scalar concentration conservation along a trajectory in the inviscid limit. The same argument is used by *Lapeyre* (2002) to show that (1.17a) is also the equation for the evolution of a tracer gradient advected along a chaotic orbit in the same limit. Noting the analogy between (1.13) and (1.17a), the solution of (1.17a) is:

$$\left|\mathbf{k}\right|^2 = \left|\mathbf{k}_0\right|^2 \left[e^{2\lambda t}\cos^2\alpha + e^{-2\lambda t}\sin^2\alpha\right]^{\frac{1}{2}}, \tag{1.18}$$

with $\mathbf{k}_0$ the initial wavenumber on the trajectory.

The solution of (1.14) can be expressed with $\mathbf{S}(t)$ using a time ordered exponential $\mathcal{T}$:

$$\mathbf{M}(t) = \mathcal{T}\exp\left(\int_0^t \mathbf{S}(u)du\right) \equiv \lim_{n\to\infty}\left[e^{\frac{t}{n}\mathbf{S}(t)}e^{\frac{t}{n}\mathbf{S}\left(t(1-\frac{1}{n})\right)}\ldots e^{\frac{t}{n}\mathbf{S}(0)}\right] \tag{1.19}$$

The order of the matrices matters because, except in one dimension, they do not commute in general. The infinite-time behavior of this time-ordered exponential is non-trivial. The convergence of the finite-time Lyapunov vectors λ and of the singular vector $\boldsymbol{\psi}_+$ has been shown by Osseledec (*Oseledec*, 1968) for ergodic dynamical systems. This result is known as the multiplicative ergodic theorem of Osseledec. It states that, almost everywhere, in the absence of KAM surfaces:

- the eigenvalues of $\left(\mathbf{M}^T\mathbf{M}\right)^{\frac{1}{2t}}$, i.e $e^{\lambda(t)}$ and $e^{-\lambda(t)}$, converge to e^{λ_∞} and $e^{-\lambda_\infty}$, where λ_∞ is the infinite-time Lyapunov exponent,
- the infinite-time Lyapunov exponent λ_∞ is independent of the orbit $\mathbf{X}$,

- the orthonormal basis $(\boldsymbol{\psi}_+, \boldsymbol{\psi}_-)$ of eigenvectors of $\mathbf{M}^T\mathbf{M}$ converge to an orthonormal basis of Lyapunov vectors $(\boldsymbol{\Psi}_+, \boldsymbol{\Psi}_-)$ that depend on $\mathbf{X}$. These are rigorously the forward Lyapunov vectors. The backward Lyapunov vectors can be defined similarly considering a backward integration in time. We will only deal with the forward vectors and we will simply refer to them as the Lyapunov vectors.

More recent studies have shown that the finite-time Lyapunov exponents converge slowly in time, typically in $\mathcal{O}(\frac{1}{\sqrt{t}})$. This has been obtained by *Goldhirsch et al.* (1987) in ergodic dynamical systems and by *Tang and Boozer* (1996) for an advection operator. It has been verified numerically in two-dimensional turbulence by *Lapeyre* (2002). The infinite-time Lyapunov exponent λ_∞ is in general smaller than the mean strain in incompressible flows because of the reorientation of the instantaneous strain axis and the effect of vorticity. (e.g *Chertkov et al.* (1995)). The convergence of the Lyapunov vectors is much faster, typically exponential in time (*Goldhirsch et al.*, 1987).

Probability density function

If we consider the resolvent matrix in one dimension, it becomes a scalar $m(t)$ that can be related directly to the history of the scalar stretching $\mathbf{S} \equiv s(t)$ along the chaotic orbit. It's logarithm can be written

$$\ln m(t) = \int_0^t s(u)du = \lambda(t)t \tag{1.20}$$

for times much larger than the correlation time $t_{corr} \equiv \frac{\int_0^\infty \langle s(u)s(0)\rangle du}{\langle s^2\rangle}$. We assume that $\Sigma \equiv \ln m(t)$ behaves as a random variable equal to the sum of $N \propto \frac{t}{t_{corr}}$ independent equally distributed random variables (the instantaneous strain) of variance $\langle s^2\rangle - \langle s\rangle^2$ in order to apply the law of large numbers and the central limit theorem (CLT). We obtain that the distribution of $\frac{1}{t_{corr}}\frac{\Sigma}{N}$ (i.e the Lyapunov exponent) converges to a

distribution that can be approximated by a Gaussian of variance $\frac{\langle s^2\rangle-\langle s\rangle^2}{t}$ and mean $\lambda_0 \equiv \langle s\rangle$ for deviation of λ from its mean scaling like $\mathcal{O}(\sqrt{\frac{\langle s^2\rangle-\langle s\rangle^2}{t}})$. However, we are interested in large deviations of the FTLE from their average: for example (1.16) and (1.18) involve exponentials of Lyapunov exponents, and the ensemble average of $|\delta\mathbf{x}|$ or $|\mathbf{k}|$ may be dominated by very rare events located out of the range where the CLT is valid. We will see that (small) rare events are also crucial in the LLST predictions for the long-time decay of the variance, of its spectrum and of the higher order moments in section 1.3.3.

The tails of the FTLE pdf are predicted by the large deviation theory (see paragraph 8.6.4 in *Frisch* (1996) and references therein, see also *Falkovich et al.* (2001)):

$$P_\lambda(t,\lambda) = \sqrt{\frac{tG''(\lambda_0)}{2\pi}}\exp(-tG(\lambda)), \tag{1.21}$$

The function G measures the rate of exponential decrease of the probability in the tail of the distribution as $t \to \infty$ and is called the rate or Cramèr function. Also G is a concave function with $G(\lambda_0) = G'(\lambda_0) = 0$. A Taylor expansion of G at the second order in λ_0 gives in (1.21) the CLT.

In the case of 2×2 matrices, the picture is much more complicated. *Chertkov et al.* (1995) showed that a CLT was valid for the FTLE distribution. In addition, the large deviation result (1.21) was used to describe the distribution of Lyapunov exponents resulting from the time-ordered exponential of random matrices (1.19) before Balkovsky and Fouxon (*Balkovsky and Fouxon*, 1999) proposed a derivation of this result for an arbitrary dimension. Note that in that case, the mean and variance of the Lyapunov exponent cannot be related directly to the tangent matrix $\mathbf{S}$, as for $d = 1$. *Chertkov et al.* (1995) proposed an expression for λ_0 as a function of the mean of the absolute value of strain S, of the mean of the absolute value of

the vorticity Ω and of the Lagrangian correlation time τ_c:

$$\lambda_0 \equiv \langle\lambda\rangle = S \tanh \frac{S\tau_c}{1+\Omega\tau_c} \tag{1.22}$$

They derived this expression from the time ordered exponential (1.19) only for a few asymptotic cases. Because of the reorientation of the instantaneous strain axis and because of the vorticity, we must have $\lambda_0 < S$ for an incompressible flow. In particular in the limit of $S\tau_c \ll 1$ and $\Omega\tau_c \ll 1$, for example when the tangent matrix $\mathbf{S}$ decorrelates much faster than the typical strain time scale, the mean Lyapunov exponent goes to 0. The same limit is observed when vorticity dominates over strain.

1.3.3 Passive tracer fluctuations decay

Variance

In this section, we present some important results of the Lagrangian stretching theories. The main argument uses a WKB (Wentzel, Kramers and Brillouin) approach and was initially developed in a 1995 paper by Antonsen (*Antonsen et al.*, 1996). However we will include some ideas from following papers (*Balkovsky and Fouxon*, 1999; *Sukhatme and Pierrehumbert*, 2002; *Fereday and Haynes*, 2004; *Tsang et al.*, 2005) to elucidate some aspects of the seminal paper.

The results of LLST we are interested in deal with the decay of the variance of passive tracers. We note $\mathbf{k}$ the wave vector and $\mathbf{x}$ the space coordinate. The variance spectrum $\widetilde{E}(\mathbf{k},t)$ of $\phi(\mathbf{x},t)$ can be written in terms of the phase action density $N(\mathbf{k},\mathbf{x},t)$:

$$\widetilde{E}(\mathbf{k},t) = \langle N(\mathbf{k},\mathbf{x},t)\rangle \tag{1.23}$$

with

$$N(\mathbf{k},\mathbf{x},t) = \frac{1}{2\pi^2}\int d\mathbf{r} e^{-i\mathbf{k}\cdot\mathbf{r}} \phi\left(\mathbf{x}+\frac{\mathbf{r}}{2}\right)\phi\left(\mathbf{x}-\frac{\mathbf{r}}{2}\right). \tag{1.24}$$

The brackets are for an ensemble average, or equivalently a space average since the flow is assumed statistically homogeneous. Assuming a spectrum that extends to wavenumbers much larger than the wavenumbers associated with the flow and that $N(\mathbf{k}, \mathbf{x}, t)$ varies smoothly in $\mathbf{k}$, *Antonsen et al.* (1996) showed that the action density at a time t can be related to its value at an earlier time (here $t = 0$):

$$N(\mathbf{k}, \mathbf{x}, t) = \int d\mathbf{x}' d\mathbf{k}' N(\mathbf{x}', \mathbf{k}', 0) \delta\left(\mathbf{x} - \mathbf{X}(\mathbf{x}', t)\right) \delta\left(\mathbf{k} - \mathbf{K}(\mathbf{x}', \mathbf{k}', t)\right) e^{-2\kappa \int_0^t |\mathbf{K}|^2} \tag{1.25}$$

The trajectory $\mathbf{X}$ is the solution of (1.9) with the initial condition $\mathbf{X}(\mathbf{t} = \mathbf{0}) = \mathbf{x}'$ and $\mathbf{K}$ is the solution of (1.17a) with $\mathbf{K}(\mathbf{x}', \mathbf{k}', t = 0) = \mathbf{k}'$. The function δ is the Dirac delta function. Basically, (1.25) tells us that the action at a time t in $(\mathbf{k}, \mathbf{x})$ is the action in $(\mathbf{k_0}, \mathbf{x_0})$ at $t = 0$ obtained following an orbit backward in time on the trajectory $\mathbf{X}$ going from $\mathbf{x_0}$ to $\mathbf{x}$ and damped by the viscous term $e^{-2\kappa \int_0^t |\mathbf{K}|^2}$, with $\mathbf{K}$ the corresponding trajectory for the wavenumber.

The spectrum $\widetilde{E}(\mathbf{k}, t)$ is obtained through the average (1.23). We then define the power spectrum $E(k, t)$:

$$E(k, t) = \int \frac{d\mathbf{k}}{(2\pi)^2} \delta(k - |\mathbf{k}|) \widetilde{E}(\mathbf{k}, t) \tag{1.26}$$

Antonsen et al. (1996) split the whole domain into small areas whose dimension l is much larger than the inverse of the wavenumber that characterizes each area and much smaller than the scale of the flow. He replaced the average over the initial phase space in (1.25) by an average on these small areas (here indexed by i) to obtain:

$$E(k, t) = \sum_i \omega_i(t) \delta(k - |\mathbf{k}|). \tag{1.27}$$

The variance ω_i contained in the i^{th} area is damped by the diffusive term introduced in (1.25)

$$\omega_i(t) = \omega_i(t = 0) e^{-2\kappa \int_0^t |\mathbf{k}_i(t)|^2}. \tag{1.28}$$

The wavenumber $\mathbf{k}_i$ following a trajectory is given in (1.18). For times large enough ($t \gg \frac{1}{2\lambda}$), it is dominated by the increasing term:

$$|\mathbf{k}_i(t)| \approx |\cos\alpha|\ e^{\lambda(t)t}. \tag{1.29}$$

Integrating the spectrum $E(k,t)$ over k and replacing the sum over space in (1.27) by an integral over the Lyapunov exponents and the initial orientation α, we obtain the total variance of ϕ:

$$\langle\phi^2\rangle(t) = \langle\phi^2\rangle(t=0) \iint d\lambda d\tau P(t,\lambda,\tau) \int \frac{d\alpha}{2\pi} e^{-2k_0^2\kappa\tau\cos^2\alpha e^{2\lambda(t)}}. \tag{1.30}$$

The time τ is defined as follows:

$$\tau = \frac{\int_0^t e^{2u\lambda(u)}du}{e^{2t\lambda(t)}}. \tag{1.31}$$

It measures the stretching rate in the recent past before t along a Lagrangian trajectory. It was called an equivalent time by *Haynes and Vanneste* (2004) because it is the time that diffusion would take to reduce the local variance from $\omega_i(t=0)$ to $\omega_i(t)$ with the norm of the wavenumber constant and equal to its value at time t. The function $P(t,\lambda,\tau)$ is the time-dependent joint density function of λ and τ. In the sum (1.30), it is assumed that all initial wavenumbers have a modulus k_0. This may seem a huge approximation since the initial spectrum is not a Dirac in general. However as noted by *Tsang et al.* (2005) the orthogonality of individual Fourier components allows for the simple addition of different wavenumber characterizing an element i of the domain, which validates the results in a more general framework. We have chosen to present the calculus done by Antonsen for historical reasons and because it is more easily understood with intuition. However, the derivation proposed by *Haynes and Vanneste* (2004) is more rigorous.

When the angle between the initial wavenumber and the direction normal to the Lyapunov vector α is non-zero the decay of the integrand of (1.30) is super-exponential. This decay has been observed by some authors as a transient (e.g. *Sukhatme and Pierrehumbert* (2002); *Thiffeault* (2003)). In general, for a long enough time, the decay is exponential. LLST provide a theoretical result for the mixing rate because the integral in (1.30) is dominated by waves initially almost orthogonal to the Lyapunov vector. A Taylor expansion of α around $\pm\frac{\pi}{2}$ gives:

$$\langle\phi^2\rangle(t) \propto \kappa^{-\frac{1}{2}} \iint d\lambda\, d\tau\, P(t,\lambda,\tau)\, \tau^{-\frac{1}{2}}\, e^{-\lambda t}. \tag{1.32}$$

It was argued that λ and τ become quickly independent because λ is the result of the average of many random variables, and consequently becomes independent of each as the number of averaged variables goes to infinity. Using the same argument, it has been argued (*Antonsen et al.*, 1996; *Haynes and Vanneste*, 2004) that its pdf P_τ converges to a time independent asymptotic form. Assuming the independence between τ and λ and using the form for the pdf of λ suggested by the large deviation theory, we obtain:

$$\langle\phi^2\rangle(t) \approx \frac{1}{\sqrt{\kappa\langle\tau\rangle}} \int d\lambda e^{-(G(\lambda)+\lambda)t} \sim e^{-\gamma_2^L t} \tag{1.33}$$

The decay rate γ_2^L, using the notation of *Haynes* (2005), is determined estimating the integral in (1.33) with the steepest descent method:

$$\begin{cases} \gamma_2^L = -F(-1) & \text{if} \quad G'(0) < -1 \\ \gamma_2^L = G(0) & \text{if} \quad G'(0) \geq -1 \end{cases}. \tag{1.34}$$

The function F is the Legendre transform of the Cramèr function and contains the same information as G:

$$F(l) = \sup_\lambda \left(l\lambda - G(\lambda)\right). \tag{1.35}$$

The result stated in (1.34) is one of the main results of Lagrangian stretching theories and it has been the subject of many experimental, numerical and theoretical studies.

Variance spectra

The theory developed above also provides the decay of the spectrum. With (1.23), (1.25) and (1.27), we can show, taking as previously the modulus of all the initial wavenumbers equal to k_0:

$$E(k,t) = \int\int d\lambda d\tau P(t,\lambda,\tau) \int \frac{d\alpha}{2\pi} e^{-2k_0^2 \kappa\tau \cos^2\alpha e^{2\lambda(t)}} \delta\left(k - k_0|\cos\alpha| e^{\lambda t}\right). \quad (1.36)$$

Integrating over α with a Taylor expansion around $\pm\frac{\pi}{2}$ and writing $P(t,\lambda,\tau) \propto e^{-tG(\lambda)} P_\tau$, as suggested by the large deviation theory and the independence of τ and λ, we can show from (1.36):

$$E(k,t) \sim e^{-\gamma_2^L t} \int d\tau P_\tau(\tau) e^{-2\kappa k^2 \tau}. \quad (1.37)$$

The decay rate, common to all wavenumbers, is given by (1.34) and the shape of the spectrum can be calculated from the Laplace transform of the pdf of τ. The spectrum is self-similar and scales as $\frac{1}{\sqrt{\kappa}}$. The factorization between the time dependence and the wavenumber dependence, together with the exponential decay of the total variance (1.33), has been interpreted as a manifestation of the Pierrehumbert strange eigenmode (*Antonsen and Ott*, 1991; *Antonsen et al.*, 1996). However, as we shall see, the Pierrehumbert strange eigenmode is not expected to be observed when LLST are valid (*Sukhatme and Pierrehumbert*, 2002; *Fereday and Haynes*, 2004; *Tsang et al.*, 2005).

This spectrum is flat for values of the wavenumber much larger than the diffusive cutoff $\sqrt{\kappa\tau}$, which has been numerically verified in regimes where LLST were shown to be valid (*Fereday and Haynes*, 2004; *Tsang et al.*, 2005). This shape is not in accordance with the k^{-1} Batchelor spectrum. However the Batchelor argument of

a self-similar forward cascade stands when there is a forcing term in (1.6) at low wavenumber (e.g. *Antonsen and Ott* (1991)). It is possible to take into account a large-scale forcing by integrating (1.36) over time, assuming that the variance contained in a wavenumber k at time t is the superposition of spectra resulting from a forcing at the large scale k_0 for all times s such that $t-s$ goes from 0 to ∞ (the idea was introduced by *Antonsen and Ott* (1991) in the case $\kappa = 0$, developed by *Antonsen et al.* (1996); *Yuan et al.* (2000); *Fereday and Haynes* (2004) for a finite diffusion and extended to two-dimensional flows varying in the vertical by *Haynes and Vanneste* (2004)). Doing the corresponding math, and under the hypothesis of independence between λ and τ, we get the spectrum:

$$E(k,t) \sim \frac{1}{k\langle\lambda\rangle} \int d\tau P_\tau(\tau) e^{-2\kappa k^2 \tau}. \tag{1.38}$$

This expression gives the k^{-1} and the viscous correction at large k taking into account the distribution of $\sqrt{\kappa\tau}$, which can be interpreted as the distribution of the diffusive cutoff. This is an alternate method to obtain the Batchelor spectrum. Its advantage to self-similar cascade arguments (*Batchelor*, 1959) or to closures parametrizing the third order moment that inject scalar variance to smaller scales (e.g. eddy-damped quasi normal Markovian closures, *Lesieur and Herring* (1985)) is its direct link to the geometrical structure of the cascade, as captured by FTLE maps.

Higher-order moments

An alternate derivation of the decay of the tracer based on a LLST approach was proposed by *Balkovsky and Fouxon* (1999). Instead of dealing with a superposition of elementary sine solutions, they used elementary Gaussian functions. The idea is based upon the fact that solutions of the advection-diffusion equation in a straining flow is Gaussian for a Dirac initial condition when there is scale separation between the velocity and the scalar. The full solution is given by the superposition of

elongated Gaussian bulbs. Beside providing a more physical interpretation of LLST, this approach predicts the decay γ_β of $\langle|\phi|^\beta\rangle$ for any $\beta \geq 1$ from the distribution of the finite-time Lyapunov exponents (the previous approach only provides $\beta = 2$ since higher order moments involve the interaction of different Fourier modes). An alternate derivation was proposed by *Thiffeault* (2008) without considering explicitly the multiplication of random matrices and assuming that large deviation theory provides the right FTLE pdf. Similar results were obtained by *Son* (1999), deriving a Shrödinger equation for the probability distribution functional of a passive scalar advected by a flow in the Kraichnan limit.

The essential result is that γ_β is an increasing function of β for $\frac{\beta}{2} < -G'(0)$ and then saturates at $\gamma_\beta = G(0)$, the mixing rate being exactly the same as the mixing rate predicted with the Fourier approach (1.34). We note that in the second case considered in (1.34), the saturation is already reached at $\beta = 2$. This saturation can be understood intuitively (*Sukhatme and Pierrehumbert*, 2002; *Thiffeault*, 2008): if we consider a filament of statistically stationary width determined by the balance between advective and diffusive processes, the direct consequence of its exponential lengthening at a rate given by the FTLE λ is that its concentration decays exponentially at a rate $-\lambda$. As a consequence, the decay rate of $\langle|\phi|^\beta\rangle$ is directly related to the ensemble average of $e^{-\beta\lambda t}$, which is dominated by rarer events as β increases (1.21). The decay rate saturates as the dominant events correspond to a stretching going to 0.

1.3.4 LLST challenged

Experiments and numerical simulation

Despite the fact that LLST predict an exponential decay of the tracer variance and a factorization of its spectrum between the spectral and the time dependence, these results being supported by numerical simulations (*Antonsen et al.*, 1996; *Yuan*

et al., 2000; *Fereday and Haynes*, 2004; *Tsang et al.*, 2005), the saturation of γ_β as β increases suggests that LLST do not explain the Pierrehumbert strange eigenmode for which γ_β is necessarily a linear function of β. However, experimental and numerical results dealing with the mixing rate and the tracer pdf suggest that the strange eigenmode is the correct long-time behavior (*Rothstein et al.*, 1999; *Sukhatme and Pierrehumbert*, 2002; *Voth et al.*, 2003; *Fereday and Haynes*, 2004). In addition, the numerical results of *Antonsen et al.* (1996) were questioned because of the difficulty of computing accurately the Cramèr function for small stretching rates and because their simulations were run at a small but finite diffusion κ, with the asymptotic behavior of $\gamma(\kappa)$ totally unknown as $\kappa \to 0$ (*Fereday and Haynes*, 2004).

More specifically, the exponential decay rate was measured to be 10 times smaller than LLST predictions in a two-dimensional magnetically driven large-scale chaotic flow by *Voth et al.* (2003). They showed that the tracer field enters a strange eigenmode and they suggested that the decay of the passive tracer is globally controlled by the large-scale flow, rather than locally, when the system is large scale compared to the velocity correlation length (even though the tracer finite scales can be very small compared to the velocity field). They argued that an effective diffusivity approach was more relevant to describe the decay, which is also expected in the limit of very large domain and tracer length scales compared to the velocity field scale (e.g. homogenization theory and one point closures, *Majda and Kramer* (1999) for a review). Numerical simulations performed by *Sukhatme and Pierrehumbert* (2002) are consistent with the results from *Voth et al.* (2003). However, when initializing the tracer field at small scales compared to the advective flow, they observed an evolving tracer pdf at intermediate time scales, consistent with the LLST as predicted by *Balkovsky and Fouxon* (1999), before the emergence of the strange eigenmode. However they

did not compute the Cramèr function and the distribution of τ to check the theoretical prediction of the mixing rate and the variance spectrum. Furthermore, a global mechanism for predicting the mixing rate was proposed by *Fereday et al.* in a one-dimensional inhomogeneous baker map (because of the one-dimensional character, LLST predicts a super-exponential decay of the variance, as $\alpha = 0$ in (1.30), which is not consistent with the exponential decay observed by *Fereday et al.*). The analysis is based upon the diagonalization of an advection diffusion operator in Fourier space, which makes a direct connection with the approach pioneered 10 years earlier by Pierrehumbert. They showed that the exponential decay can be dominated by the decay of the gravest Fourier modes.

In light of these results, *Fereday and Haynes* (2004) developed an argument to explain the failure of LLST. The domain of influence of a point $\mathbf{x}$ at a time t, i.e. the subset of the domain that determines the scalar concentration in $\mathbf{x}$ at a time t, has an area that can be estimated at an earlier time $t-s$. We note that the solution of (1.11) may be written at a time t as an average of Green's functions $\mathcal{G}(\mathbf{x}, t, \mathbf{l}, s)$ weighted with the field at an earlier time $\chi(\mathbf{l}, s)$. These Green's functions are solution of the same equation (1.11) with the initial condition at time s $\chi(\mathbf{x}, s) = \delta(\mathbf{x} - \mathbf{l})$. We have:

$$\chi(\mathbf{x}, t) = \int d\mathbf{l}\, \chi(\mathbf{l}, s)\, \mathcal{G}(\mathbf{x}, t, \mathbf{l}, s) \tag{1.39}$$

$\mathcal{G}(\mathbf{x}, t, \mathbf{l}, s)$ is also the solution of an advection-diffusion equation, changing the sign of the diffusive term and using the initial condition $\chi(\mathbf{l}, t) = \delta(\mathbf{l}-\mathbf{x})$. As a consequence, going into the past, the domain of influence is initially dominated by diffusion and grows to a circle of radius $\sqrt{\frac{\kappa}{S}}$ (regime I of *Fereday and Haynes* (2004)), estimating the local stretching rate with the mean Eulerian strain S), then it stretches exponentially, its length being equal to $\sqrt{\frac{\kappa}{S}} e^{S(t-s)}$ (regime II of *Fereday and Haynes* (2004)). The typical time scale of regime II is $\frac{1}{2S} \ln(\frac{SL_{flow}^2}{\kappa})$ with L_{flow} the domain size. After

regime II, the filament starts to fold until it fills the whole domain (packed filaments similar to the Pierrehumbert strange eigenmode). It is unlikely that after regime II the velocity field could be considered as a linear function of space. In addition, when the domain of influence covers a significant portion of the domain, it is unlikely that the concentrations determining the concentration at $\mathbf{x}$ and time t are independent, which invalidates a basic assumption of LLST (*Tsang et al.*, 2005). However, LLST should be valid to predict the behavior of the passive scalar on a time scale $\frac{1}{2S}\ln(\frac{SL_{flow}^2}{\kappa})$.

Even though the mixing rate is not predicted by LLST, except in the particular case of a tracer initialized at scales much smaller than the domain and for intermediate times, it was argued that they might be useful in predicting the variance spectrum shape. For example, (1.38) has been shown to predict accurately the spectrum in the forced case (*Antonsen et al.*, 1996; *Haynes and Vanneste*, 2004). For the decaying case, *Fereday and Haynes* (2004) and *Tsang et al.* (2005) proposed a spectrum taking into account the fact that the decay rate is explained by a global mechanism, acting on the large scale, determining a mixing rate γ_2. They showed that

$$\gamma_2 \leqslant \gamma_2^L \tag{1.40}$$

and that the spectrum is given by:

$$E(k,t) \sim e^{-\gamma_2 t} k^{-1-G'(\lambda_*)} \int d\tau P_\tau(\tau) e^{-2\kappa k^2 \tau}, \tag{1.41a}$$

$$\text{with } G(\lambda_*) - \lambda_* G'(\lambda_*) - \gamma_2 = 0. \tag{1.41b}$$

Fereday proposed an euristic proof for this result, using a similar reasoning as for (1.38), assuming, at small wavenumber, a large-scale forcing decaying at a (unknown) rate γ_2. In particular, for sufficiently small diffusion, there is a range of the spectrum exhibiting a power law behavior $k^{-1-G'(\lambda_*)}$. It can be shown that this corresponds

to k^0 if LLST are valid ($\gamma_2 = \gamma_2^L$) and to k^{-1} in the forced situation $\gamma_2 = 0$, the slope of the spectrum in a log-log plot being intermediate between -1 and 0 for any $0 < \gamma_2 < \gamma_2^L$. It was argued that a flat spectrum was a necessary and sufficient condition for the validity of LLST by *Tsang et al.* (2005). Both *Fereday and Haynes* (2004) and *Tsang et al.* (2005) supported their findings with numerical simulations.

The success of LLST for predicting the shape of the spectrum in a wide range of situations is probably because the time for variance to cascade from a wavenumber corresponding to the large scale to the diffusive cutoff is the mixing time scale from the largest scale of the flow to the diffusive cutoff, which is also the time span $\frac{1}{2S}\ln(\frac{SL_{flow}^2}{\kappa})$ of regime II in *Fereday and Haynes* (2004). However, one can question the validity of (1.21) on this time scale.

Local and global control of fluctuation decay

Tsang et al. (2005) argued, like *Sukhatme and Pierrehumbert* (2002); *Voth et al.* (2003); *Fereday and Haynes* (2004), that a global mechanism explains the decay when LLST are not valid. However, it does not propose a precise mechanism and it is not clear how it should be different from eddy diffusivity. The issue of the validity of LLST was explored in more depth by *Haynes and Vanneste* (2005) with an eigenmode approach. This paper appears very important, as it might propose a pathway to a reconciliation between the eddy diffusivity and the LLST approaches.

Haynes and Vanneste (2005) studied a $\delta-$correlated Kraichnan-Kazantsev flow and renewing flows for which closed equations exists for the multipoint correlations. This allows to diagonalize the advection-diffusion operator $\mathcal{L}_\kappa$ acting on the covariance $\Gamma(\mathbf{r},t) \equiv \langle\phi(\mathbf{x}+\mathbf{r},t)\phi(\mathbf{r},t)\rangle$ (It is not isotropic but it is assumed homogeneous for simplicity, however *Haynes and Vanneste* (2005) argues that mathematical derivation of the spectrum of eigenvalues does not necessitate spacial homogeneity but

complicates the mathematical developments). The flow and the scalar are respectively 2π and $2\pi P$ periodic in both directions of space. The spectrum of eigenvalues of $\mathcal{L}_{\kappa=0}$ was shown to have a continuous part $[l, +\infty)$ that depends on its local behavior near $\mathbf{r} = 0$ and a discrete part. In particular it was shown that $l = \gamma_2^L$ as defined in (1.34) and that the discrete spectrum depends on the global structure of $\mathcal{L}_{\kappa=0}$ and on the ratio P between the scalar and velocity fields spatial periods, the eigenvalues being $\mathcal{O}(\frac{1}{P^2})$ as $P \to \infty$. It was also shown that, in the limit of small diffusion, the spectrum of eigenvalues of L_κ is discrete. The eigenvalues larger than l are separated by gaps scaling like $\frac{1}{\ln \kappa}$. The smallest eigenvalue larger than l converges to l very slowly, in $\frac{1}{\ln^2 \kappa}$. To each eigenvalue Λ_0 of the discrete spectrum of $\mathcal{L}_{\kappa=0}$ corresponds an eigenvalue of $\mathcal{L}_\kappa$ converging to Λ_0 in κ^σ, with σ some real strictly positive and strictly smaller than one.

In the limit of an infinitely small diffusion, whether the control of the fluctuation decay is local or global is determined by the existence of a discrete part in the spectrum of $\mathcal{L}_{\kappa=0}$. Without a discrete part, the control is local and the prediction of LLST are exact. With a discrete part, the decay is controlled globally. This theory also shows the slow convergence of the decay rate as $\kappa \to 0$.

1.4 Our approach

1.4.1 The numerical setup

We use a large-scale two-dimensional flow to capture some features of stratospheric mixing. Contrary to many numerical models used to study chaotic advection or to verify the theoretical results of LLST, we opted for a dynamically consistent flow solution of the barotropic two dimensional Navier-Stokes equations in a $2\pi \times 2\pi$ periodic domain. The equation for the vorticity ω is:

$$\frac{\partial \omega}{\partial t} + \mathbf{u} \cdot \nabla \omega = F - R_0 \omega + \nu \nabla^2 \omega \tag{1.42}$$

F is a forcing term that injects energy at wavenumber 3:

$$F_{\mathbf{k}} = \begin{cases} 0.002 \text{ if } \mathbf{k} = (\pm 3, 0) \text{ or } \mathbf{k} = (0, \pm 3) \\ 0 \text{ otherwise} \end{cases} \tag{1.43}$$

This large-scale forcing can be seen as a very crude parametrization for planetary scale Rossby wave breaking. Because energy tends to cascade to the largest scale, we use a Rayleigh friction term with $R_0 = 0.0002$. The injection of energy, together with the Rayleigh dissipation and the periodicity of the domain, causes the emergence of two large scale vortices moving very slowly compared to the characteristic advective time scale of the large-scale flow $\frac{L}{U}$ (U and L are respectively the typical length and velocity scales of the large-scale flow). We think that these large-scale vortices can produce chaotic advection. However, we did not check rigorously the applicability of chaotic advection. Nevertheless, trajectories are chaotic and the energy spectrum is strongly non-local (it scales like k^{-4}, with k the horizontal wavenumber, in the initial range which extends over about one and a half decade). A snapshot of the vorticity field is shown on figure 1–7.

The forcing term F injects enstrophy that is dissipated by a viscosity ν. The magnitude of the viscosity is chosen such that the Reynolds number $Re = \frac{UL}{\nu}$ is of the same order as a Peclet number $Pe = \frac{UL}{\kappa}$ calculated in stratospheric flows with an estimate for the horizontal diffusivity as discussed below (1.1). The order of magnitude of the Reynolds number is 10^3.

Our model also advects passive tracers, integrating the advection-diffusion equation (1.6). The model uses the pseudospectral method for both the vorticity and the passive tracers concentration on a 512×512 grid. The fast Fourier transforms are provided by FFTW (*Frigo and Johnson*, 2005). The Fourier series are truncated at $K_{max} = \lfloor 512/3 \rfloor$ to avoid aliasing. The time-stepping algorithms are leap-frog

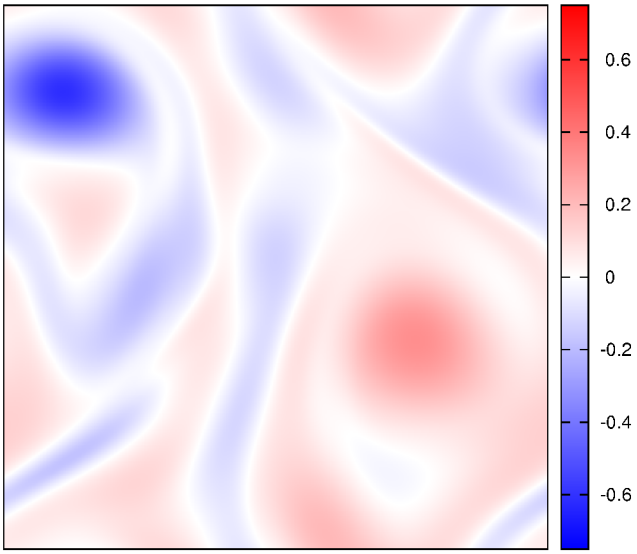

Figure 1–7: Snapshot of the output of the model for the vorticity.

for the advection and Crank-Nicholson for the viscosity. The computational mode is dissipated by a weak Robert filter with parameter 0.001. The leap-frog and the Crank- Nicolson schemes are accurate at second order in time.

The accuracy of the algorithm was tested on a solid-body rotation. The behavior of the RMS error between the simulation and the known analytical solution shows a superalgebraic convergence (also called spectral accuracy): the order of the spatial accuracy increases with the spatial resolution. This is consistent with the theoretical knowledge we have on convergence of truncated Fourier series of infinitely differentiable functions. The reader interested in such results can refer to *Peyret* (2002). Spectral accuracy is one of the strengths of the pseudospectral methods: there is a substantial accuracy gain over finite-difference or finite- element schemes when simulating a function that is sufficiently differentiable. It has been shown numerically (*Orszag*, 1971) that spectral schemes are as accurate as finite-difference schemes running at twice the resolution in the simulation of incompressible flows.

1.4.2 The chemistry

We focus on a bimolecular chemical reaction

$$A + B \longrightarrow C, \tag{1.44}$$

similar to (1.5) and for reactants in stoichiometric quantities. With C_A, C_B and C_C, the concentrations of A, B and C respectively, the equation for the Eulerian fields $C_i(\mathbf{x}, t)$, $i = A, B, C$ are:

$$\frac{\partial C_A}{\partial t} + \mathbf{u} \cdot \nabla C_A = \kappa \nabla^2 C_A - k_c C_A C_B \tag{1.45a}$$

$$\frac{\partial C_B}{\partial t} + \mathbf{u} \cdot \nabla C_B = \kappa \nabla^2 C_B - k_c C_A C_B \tag{1.45b}$$

$$\frac{\partial C_C}{\partial t} + \mathbf{u} \cdot \nabla C_C = \kappa \nabla^2 C_C + k_c C_A C_B \ , \tag{1.45c}$$

where k_c is the chemical reaction rate and κ the scalar diffusion. We have also implemented these advection-diffusion-reaction equation in the pseudospectral model using a forward Euler time stepping method, which is only accurate at first order. It was impossible to use the leap-frog scheme for the chemistry because of stability problems. There are some simple implicit second order stable schemes but the pseudospectral method needs an explicit scheme, in order to avoid operator splitting methods.

The superalgebraic convergence was observed for $k_c = 0$ and for very slow chemistry compared to the advection. However, we have observed that for larger reaction rates the spectral accuracy vanishes. More work is needed to valid, quantify and understand this behavior. In the limit of a very fast, instantaneous, chemical reaction, the passive tracer $\phi \equiv C_A - C_B$ determines both reactant concentrations, as we

shall see in the second chapter[1] . As a consequence, for an instantaneous chemical reaction, we use the model without chemistry to advect ϕ and the convergence is superalgebraic.

1.4.3 Preliminary results

We briefly summarize some preliminary results, which where presented at the 2009 European Geosciences Union general assembly and at the 2010 Institute for Mathematics and its Applications workshop on mixing in complex flows. Some of these results are also discussed in *Ait-Chaalal* (2008). They motivated the research presented in the following chapters.

Our work is based on the study of the chemical reaction (1.44) , and in particular on the effect of κ, which defines an effective resolution as in *Tan et al.* (1998); *Wonhas and Vassilicos* (2002, 2003). The diffusion κ is chosen such that the Prandtl number $Pr \equiv \frac{\nu}{\kappa}$ is larger than one. For various κ and various chemical reaction rate k_c, we run an ensemble of simulations. Each member is defined by the initial condition on the vorticity, taken from a long simulation of the statistically stationary flow solution of (1.42).

Studying the ensemble average of the domain mean of C_C, concentration of the product of the chemical reaction (1.44), we have obtained similar results as *Tan et al.* (1998), as discussed in section 1.2.2. More specifically, for various initial conditions, we obtained that $\langle\overline{C_C}\rangle \propto \kappa^{-p(t)}$ (the brackets are for the ensemble average and the overbar for the domain average). The function $p(t)$ depends on the initial condition on the tracer and on the reaction rate. This scaling has been shown to perform well for an instantaneous chemistry, but also for a chemistry as fast as the large-scale

[1] Subtracting (1.45a0 and (1.45b) shows that $\phi \equiv C_A - C_B$ is a passive scalar. If the reaction is infinitely fast, A and B cannot coexist and ϕ determines completely C_A and C_B, being equal to the former when it is positive and to the latter when it is negative

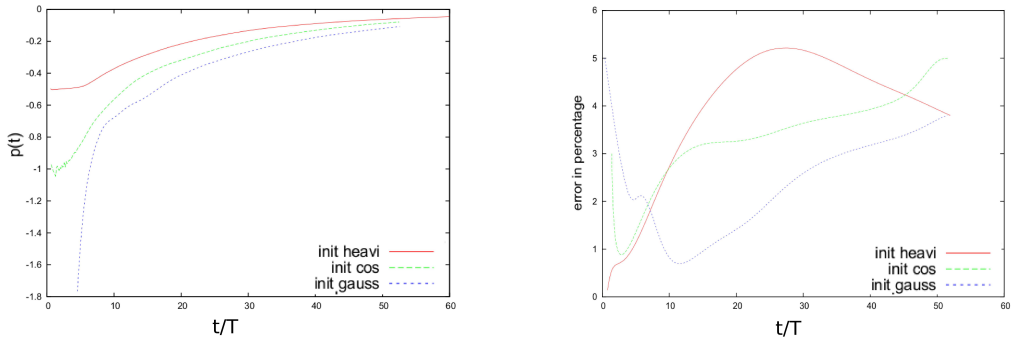

Figure 1–8: Left: Function $p(t)$ determined from a linear regression between $\ln\langle\overline{C_C}\rangle$ and $\ln\kappa$ using a least squares regression method. The chemistry is infinitely fast and three different initial conditions are used (figure 1–9). Each regression is performed on 6 points corresponding to $Pr \equiv \frac{\nu}{\kappa} = 1, 2, 4, 8, 16, 32$. Right: corresponding asymptotic standard error. The time axis is normalized by the large-scale turnover time T.

advection and a chemistry one hundred times slower. The function $p(t)$ is shown on figure 1–8 for an instantaneous chemical reaction, for three different initial conditions named INIT_HEAVI, INIT_COS and INIT_GAUSS (figure 1–9):

$$\begin{aligned}
&\phi(x,y,t=0) = A_0 \operatorname{sgn} x && \text{INIT_HEAVI} \\
&\phi(x,y,t=0) = A_0 \frac{\pi^2}{4} \cos x \cos y && \text{INIT_COS} \\
&\phi(x,y,t=0) = A_1 (e^{-\frac{(x+\frac{\pi}{2})^2+(y-\frac{\pi}{2})^2}{2(\frac{\pi}{3})^2}} - e^{-\frac{(x-\frac{\pi}{2})^2+(y+\frac{\pi}{2})^2}{2(\frac{\pi}{3})^2}}) && \text{INIT_GAUSS} ,
\end{aligned} \tag{1.46}$$

for $-\pi \leq x < \pi$ and $-\pi \leq y < \pi$. The passive tracer ϕ is defined as $C_A - C_B$ and A_1 is chosen such that the domain average of A and B is the same for all three initial conditions.

The function $p(t)$ for sharp initial gradients (INIT_HEAVI) is consistent with the results of *Tan et al.* (1998). In particular $p(t) \approx -\frac{1}{2}$ as long as the contact line

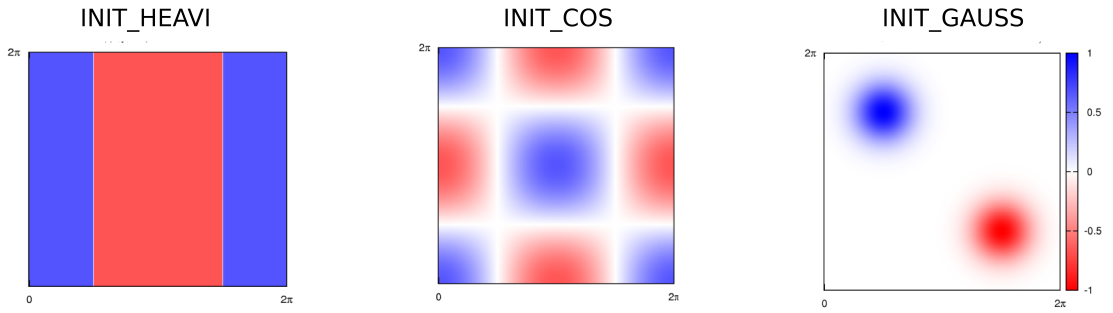

Figure 1–9: Initial conditions on the tracer field, as defined in (1.46). Each color indicates a different tracer. The field are normalized with the maximum concentration in the domain.

between the reactants is the same one-dimensional material line for all diffusions [1] and then seems to converge to 0. Also, the theoretical framework built by *Wonhas and Vassilicos* (2002, 2003) might be relevant for INIT_HEAVI but not for the others initial conditions, as the on/off assumption on the scalar field is violated.

1.5 Structure of the thesis

In order to understand the function $p(t)$ we have adopted a Lagrangian straining theory approach. However, we did not go much farther than examining the case of an infinitely fast reaction for a clearly defined one-dimensional contact line between the reactants. In chapter 2, we show how the Lagrangian straining properties of the flow determine the production of C. Chapter 3 examines in detail the probability density function of the reactants and of their gradients. Chapter 4 is more general and deals with the decay of passive tracer fluctuations in the two-dimensional Navier-Stokes model described above, as opposed to kinematics flows which are usually used to study LLST.

[1] For small enough times, the tracer filaments do not merge under the action of diffusion and are only determined by the flow. We will elaborate on this in chapter 2.

CHAPTER 2
Fast chemical reaction in a two-dimensional Navier-Stokes flow: Initial regime

In this chapter we study the instantaneous bimolecular reaction $A + B \longrightarrow C$ in a flow solution of the two dimensional barotropic Navier-Stokes equation. We use a local Lagrangian stretching theory approach to determine how the flow controls the dynamics of the contact line between the reactants, the reactants' gradients along this line and the domain average of the concentration of the product. We investigate the effect of the diffusion κ of the reactants on the reaction. The manuscript which constitutes this chapter was submitted to Physical Review E in June 2011, the revised version was resubmitted in December 2011.

Fast chemical reaction in a two-dimensional Navier-Stokes flow: Initial regime

F. Ait-Chaalal [1], M.S. Bourqui[1,2] and P. Bartello[1,3]

[1]Department of Atmospheric and Oceanic Sciences, McGill University, Montréal, QC, Canada

[2]Department of Chemistry, McGill University, Montréal, QC, Canada

[3]Department of Mathematics and Statistics, McGill University, Montréal, QC, Canada

Published in Physical Review E, Volume: 85 Issue: 4 Article Number: 046306 DOI: 10.1103/PhysRevE.85.046306, April 2012.

Abstract

This paper studies an infinitely fast bimolecular chemical reaction in a two-dimensional bi-periodic Navier-Stokes flow. The reactants in stoichiometric quantities are initially segregated by infinite gradients. The focus is placed on the initial stage of the reaction characterized by a well-defined one dimensional material contact line between the reactants. Particular attention is given to the effect of the diffusion κ of the reactants. This study is an idealized framework for isentropic mixing in the lower stratosphere and is motivated by the need to better understand the effect of resolution on stratospheric chemistry in Climate-Chemistry Models.

Adopting a Lagrangian stretching theory approach, we relate theoretically the ensemble mean of the length of the contact line, of the gradients along it and of the modulus of the time derivative of the space-average reactant concentrations (here called the chemical speed) to the joint probability density function of the finite time Lyapunov exponent λ with two times τ and $\widetilde{\tau}$. The time $\frac{1}{\lambda}$ measures the stretching time scale of a Lagrangian parcel on a chaotic orbit up to a finite time t, while τ measures it in the recent past before t, and $\widetilde{\tau}$ in the early part of the trajectory. We show that the chemical speed scales like $\kappa^{\frac{1}{2}}$ and that its time evolution is determined by rare large events in the finite time Lyapunov exponent distribution. The case of smooth initial gradients is also discussed. The theoretical results are tested with an ensemble of direct numerical simulations (DNS) using a pseudospectral model.

2.1 Introduction

The stratospheric ozone chemistry resulting from Climate-Chemistry Models is thought to be sensitive to the spatial resolution. It was shown by *Edouard et al.* (1996) that the simulated spring ozone depletion inside the polar vortex is very sensitive to the horizontal grid size. However *Searle et al.* (1998a,b) pointing out some flaws in the former work, suggested that resolution is not crucial for ozone depletion inside the polar vortex during cold enough winters because chlorine, the relevant catalyst for ozone destruction, is totally activated regardless the resolution. Nevertheless, they suggested that at the outer edge of the vortex (the surf zone), where mixing is important, the filamentary structures exhibited by chemical fields (e.g. *Waugh and Plumb* (1994)) are not represented by low resolution models. The deactivation of polar vortex chlorine by low-latitude nitrogen oxide, a process controlling ozone concentrations at the outer edge of the mid-winter Arctic polar vortex, was studied numerically by *Tan et al.* (1998). Assuming two dimensional mixing on isentropes on time scales smaller than two weeks and using reanalysis data to advect chemicals, they found that the production of chlorine was strongly dependent on the tracer diffusion coefficient. They proposed that the product's concentration scales like $\kappa^{p(t)}$ where $p(t)$ is a positive decreasing function of time which depends on initial conditions. This problem was addressed from a theoretical point of view by *Wonhas and Vassilicos* (2002) which showed, for an infinitely fast bimolecular chemistry, that the function $p(t)$ is given by $1 - D(t)/2$ where $D(t)$ is the box counting fractal dimension of the contact line between the reactants, defined as the zero isoline of a tracer ϕ equal to the difference between the two reactants' fields. Their main assumption on the geometric configuration of ϕ is that of an on/off field, which allows to link the slope of the tracers' variance spectrum to the box counting fractal dimension of the contact line, and the variance to the first moment of the modulus of

ϕ. This interesting approach is however limited by the unrealisticness of the on/off fields assumption.

Here, in the absence of this assumption, we propose to focus on the case where the contact line is a material line unaffected by diffusion (fractal dimension equals to one). This is true during the early stage of the reaction, before tracer filaments start to merge under the action of diffusion. To our knowledge, a detailed analysis of this regime has not appeared in the literature despite its relevance to the atmosphere on time scales of several days to weeks. We develop a mathematical framework which relates the effect of diffusion on the reactant concentration and its time evolution to the statistics of Lagrangian stretching properties (LSP) of advected parcels in the flow. This approach has been widely used to describe the asymptotic decay of passive tracers in the Batchelor regime of turbulence or in chaotic advection (for Lagrangian stretching theories and further developments, see *Antonsen et al.* (1996); *Balkovsky and Fouxon* (1999); *Sukhatme and Pierrehumbert* (2002); *Fereday et al.*; *Fereday and Haynes* (2004); *Tsang et al.* (2005); *Haynes and Vanneste* (2005)). In addition, this approach was recently applied to the long term decay of fast reacting chemicals by *Tsang* (2009).

Our assumptions are those of a two dimensional statistically isotropic, homogeneous and stationary non linear Navier-Stokes flow. We use corresponding ensembles of direct numerical simulations to verify the analytical relations between the LSP and chemistry. Although this flow gives a very simplified representation of stratospheric mixing, it can be argued that it is relevant for scales larger than approximately 40km (*Haynes and Anglade*, 1997)). We vary the diffusion coefficient κ of tracers to study the effect of resolution, employing a similar approach to *Tan et al.* (1998); *Wonhas and Vassilicos* (2002). This is justified by noting that the smallest scales of the flow are determined by the balance of advective and diffusive processes and thus scale like

$\kappa^{\frac{1}{2}}$. Considering that small-scale tracer structures are generated by the large-scale field, the viscosity of the field is chosen larger than the diffusion. Hence, tracers evolve in a smooth velocity field, which allows to differentiate it at the tracers' finite scale and interpret their behavior in the framework of Lagrangian chaos. It has been shown in *Ngan and Shepherd* (1999a,b) that the concept of chaotic advection, where a spatially coarse flow produces chaotic tracer trajectories, was applicable to two-dimensional mixing in the stratospheric surf zone. In addition it has been argued (*Bartello*, 2000)) that in barotropic, β-plan two-dimensional turbulence, relatively coarse velocity fields reproduce quite accurately the fine structures of the tracer field when the spectrum of energy is steeper than k^{-3}, which is relevant both in the stratosphere (*Koshyk and Hamilton*, 2001)) and in the enstrophy cascade in two-dimensional turbulence (*Kraichnan*, 1967)).

We focus on the initial regime of an infinitely fast chemical reaction between two segregated reactants in stoichiometric quantities. The main emphasis is placed on the case where the reactants are initially separated by a sharp gradient, while the case of a smooth gradient is briefly discussed. Figure 2–1 illustrates this regime. With T the integral time scale of the flow, the contact line does not depend on diffusion at $\frac{t}{T} = 1$ and $\frac{t}{T} = 3$, but gradients become clearly smoother when diffusion increases. The time span of this regime depends on the diffusion: at $\frac{t}{T} = 8$ the contact line seems to be the same for Prandtl numbers $Pr = 16$ and $Pr = 128$ but is clearly different for $Pr = 1$. When the diffusion is larger, filaments merge earlier, making the contact line dependent on diffusion at a smaller time.

This approach is relevant to the chlorine deactivation at the outer edge of the winter time polar vortex, which is very fast compared to advective and diffusive time scales (*Tan et al.*, 1998)). It is also of general interest in isolating and investigating the effect of two-dimensional turbulent mixing on chemical reactions. A separate

paper, in preparation, will focus on the case of a more complicated contact line (box counting fractal dimension between 1 and 2), which corresponds to the intermediate and time asymptotic regime.

This paper is organized as follows. Section II. describes our approach and methodology. We show that with infinitely fast chemistry, average concentrations of reactants and product are simple linear functions of the first moment of the modulus of the passive tracer concentration ϕ defined as the difference between the reactant fields. This approach is rather general in the study of infinitely fast bimolecular reactions (*Corrsin*, 1958; *Sokolov and Blumen*, 1991; *Wonhas and Vassilicos*, 2002; *Tsang*, 2009). In particular, this implies that the reaction is controlled by the diffusive flux across the isoline $\phi = 0$, noted $\mathcal{L}$. The importance of the behavior of $\mathcal{L}$ for chemistry in complex flows or complex geometric configurations of chemical fields has been highlighted in *Adrover et al.* (2002); *Martinand and Vassilicos* (2007) respectively. This section also describes the numerical model and the simulated flow, including the spatial configuration and the probability density function (pdf) of the FTLE. Section III. describes the theoretical and numerical results. We derive analytical expressions for the lengthening of $\mathcal{L}$, for the gradients advected along $\mathcal{L}$ and finally for the diffusive flux across $\mathcal{L}$, the latter being equal to the time derivative of the space-average reactants concentrations. We compare the theory to ensembles of numerical simulations. Finally, conclusions are drawn in section IV.

2.2 Methodology

2.2.1 The limit of infinite chemistry

We consider the bimolecular chemical reaction $A + B \longrightarrow C$ with C_A, C_B and C_C, the concentrations of A, B and C respectively. Eulerian equations describing the

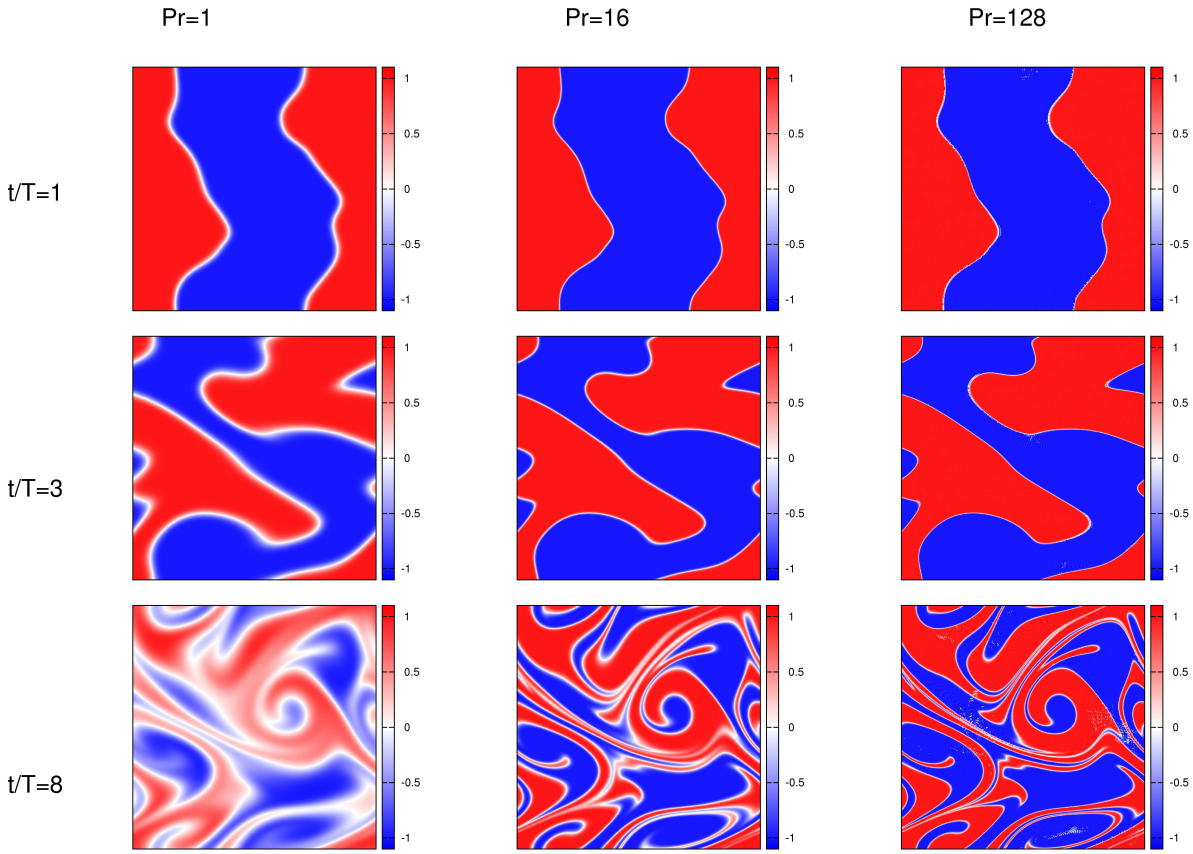

Figure 2–1: Reactant fields in a bi-periodic domain $[-\pi, \pi]^2$. Colors (red, positive values, and blue, negative values) show the two reactants A and B. From left to right Pr $= 1, 16, 128$ and from top to bottom $\frac{t}{T} = 1, 3, 8$. The Prandtl number Pr is defined as the ratio of the viscosity of the fluid to the tracer diffusion. Since the viscosity is fixed, an increasing Pr means a decreasing diffusion. T is the integral time scale of the flow.

evolution of $C_i(\mathbf{x},t)$, $i = A, B, C$, in the flow $\mathbf{u} = (u, v)$ are:

$$\frac{\partial C_A}{\partial t} + \mathbf{u}\cdot\nabla C_A = \kappa\nabla^2 C_A - k_c C_A C_B \tag{2.1a}$$

$$\frac{\partial C_B}{\partial t} + \mathbf{u}\cdot\nabla C_B = \kappa\nabla^2 C_B - k_c C_A C_B \tag{2.1b}$$

$$\frac{\partial C_C}{\partial t} + \mathbf{u}\cdot\nabla C_C = \kappa\nabla^2 C_C + k_c C_A C_B \ , \tag{2.1c}$$

where k_c is the chemical reaction rate and κ the diffusion, which is assumed equal for all tracers. The quantity $\phi = C_A - C_B$ is a passive tracer which obeys the simple advection-diffusion equation

$$\frac{\partial \phi}{\partial t} + \mathbf{u}\cdot\nabla\phi = \kappa\nabla^2\phi \tag{2.2}$$

We assume that ϕ has zero spatial average, which is equivalent to having the reactants in stoichiometric balanced ratio. Under the fast chemistry hypothesis ($k_c \longrightarrow \infty$), we can assume without loss of generality that the reactants A and B are segregated (i.e. A and B do not overlap spatially). In fact, even if they are collocated at time $t = 0$, they can not coexist at a later time $t > 0$ since they react instantaneously where both fields are together non-zero. It follows that:

$$\begin{cases} C_A(\mathbf{x},t) = \phi(\mathbf{x},t) & \text{and } C_B(\mathbf{x},t) = 0 \quad \text{if } \phi(\mathbf{x},t) > 0 \\ C_B(\mathbf{x},t) = -\phi(\mathbf{x},t) & \text{and } C_A(\mathbf{x},t) = 0 \quad \text{if } \phi(\mathbf{x},t) < 0 \end{cases} \tag{2.3}$$

Defining with an over-bar the average over the whole domain, we have:

$$\overline{C_A} = \overline{C_B} = \frac{\overline{|\phi|}}{2} \tag{2.4a}$$

$$\overline{C_C} = \frac{\overline{|\phi(t=0)|} - \overline{|\phi|}}{2}. \tag{2.4b}$$

Consequently, studying the decay of the reactants of an infinitely fast chemical reaction in stoichiometric balanced ratio is equivalent to studying the decay of the first moment of the modulus of a passive tracer ϕ of zero spatial average. For an

incompressible flow, it can be shown with the divergence theorem that the decay rate of the total reactant quantity for an infinite reaction equals the diffusive flux across the contact line between A and B, namely $\mathcal{L} = \{\mathbf{x}|\phi(\mathbf{x}) = 0\}$, oriented in a counterclockwise direction around the area where A is located:

$$\begin{aligned} \mathcal{A}\overline{\frac{dC_A}{dt}} = \mathcal{A}\overline{\frac{dC_B}{dt}} = \frac{1}{2}\mathcal{A}\overline{\frac{d|\phi|}{dt}} &= -\kappa \int_{\mathcal{L}(t)} \nabla\phi \cdot \mathbf{n}\, dl \\ &= -\kappa \int_{\mathcal{L}(t)} |\nabla\phi|\, dl, \end{aligned} \tag{2.5}$$

where $\mathcal{A}$ is the total area of the domain and $\mathbf{n}$ the vector normal to $\mathcal{L}$ and pointing outside the area where A is located. The contact line is by definition an isoline of ϕ, which gives the last equality in (2.5). Hereafter, $-\overline{\frac{d|\phi|}{dt}}$ is called the chemical speed.

2.2.2 The numerical model

The flow

The numerical model integrates the vorticity equation:

$$\frac{\partial\omega}{\partial t} + \mathbf{u}\cdot\boldsymbol{\nabla}\omega = F - R_0\omega + \nu\nabla^2\omega \tag{2.6}$$

where $\omega = \boldsymbol{\nabla}\times\boldsymbol{u}$ is the vorticity, F the forcing term, R_0 the Rayleigh friction and ν the viscosity. The equation is integrated in a bi-periodic domain $(x, y) \in [-\pi, \pi]^2$ on a 512×512 grid using the pseudo-spectral method. The fast Fourier transforms are provided by FFTW (*Frigo and Johnson*, 2005). The Fourier series are truncated at $K_{max} = 512/3$ to avoid aliasing. The time stepping algorithms are leap-frog for the advection and Crank-Nicholson for the viscosity. The computational mode is dissipated by a weak Robert filter with parameter 0.001. The forcing term F has the following form in Fourier space:

$$F_{\mathbf{k}} = \begin{cases} 0.002 \text{ if } \mathbf{k} = (\pm 3, 0) \text{ and } \mathbf{k} = (0, \pm 3) \\ 0 \text{ otherwise} \end{cases} \tag{2.7}$$

The energy tends to concentrate in the largest scales of the flow because of the inverse energy cascade inherent to two-dimensional turbulence. As a consequence, we use a Rayleigh friction term with $R_0 = 0.0002$ in the vorticity equation (2.6) to balance the injection of energy through F. The viscosity is $\nu \simeq 5.57 \times 10^{-4}$ and results in a Reynolds number Re of the order of 10^3. It has deliberately been chosen to be relatively low for reasons explained in the Introduction.

A snapshot of the vorticity field is depicted in figure 2–4 (top left). With brackets for an ensemble average, the flow has an RMS velocity $\langle \mathbf{u} \cdot \mathbf{u} \rangle^{\frac{1}{2}} \simeq 0.08$ and a mean enstrophy $Z = \frac{1}{2}\langle \omega^2 \rangle \simeq 0.009$, which corresponds to an advective time scale $T = Z^{-\frac{1}{2}} \sim 10$ (*Bartello*, 2000). Hereafter, T is used to normalize time and can also be estimated from the mean strain rate $\langle S \rangle$, where $S = \left(\left(\frac{\partial u}{\partial x} \right)^2 + \frac{1}{4} \left(\frac{\partial u}{\partial y} + \frac{\partial v}{\partial x} \right)^2 \right)^{\frac{1}{2}}$ (here expressed in Cartesian coordinates for an incompressible flow). In two dimensional turbulence, we have $\langle (2S)^2 \rangle = \langle \omega^2 \rangle$ (e.g. *Lapeyre* (2002)). The distribution of the strain is close to a Rayleigh distribution [1] , as a consequence we have $\langle S^2 \rangle \approx \frac{4}{\pi} \langle S \rangle^2$. Finally, we have $T \approx \sqrt{\frac{\pi}{2}} \frac{1}{2\langle S \rangle}$. The term $\sqrt{\frac{\pi}{2}}$ being of the order of unity, the turnover time can be evaluated from $\frac{1}{2\langle S \rangle}$. The mean strain rate is about 0.05 in our flow (see figure 2–2 for the whole distribution), which gives approximately the same estimate as $Z^{-\frac{1}{2}}$ for T.

Finite Time Lyapunov Exponents (FTLE)

Definition and properties. The finite time Lyapunov exponent is defined as the rate of exponential increase of the distance between the trajectories of two fluid parcels that are initially infinitely close. If $\boldsymbol{\delta l}(t)$ is the distance at time t between two parcels that start at $\boldsymbol{x}$ and $\boldsymbol{x} + \boldsymbol{\delta l_0}$ at time $t = 0$, then the FTLE $\lambda(\boldsymbol{x}, t)$ at $\boldsymbol{x}$

[1] It would be exactly a Rayleigh distribution if the velocity derivatives had Gaussian statistics and where statistically independent.

over the time interval t is

$$\lambda(\boldsymbol{x},t)=\frac{1}{t}\max_{\alpha}\lim_{|\boldsymbol{\delta l_0}|\to 0}\Big\{\ln\frac{|\boldsymbol{\delta l(t)}|}{|\boldsymbol{\delta l_0}|}\Big\}\ , \tag{2.8}$$

where the maximum is calculated over all the possible orientations α of $\boldsymbol{\delta l}_0$. The unit vector with the orientation $\psi_+(\mathbf{x},t)$ of $\boldsymbol{\delta l}_0$ at the maximum is called a singular vector and we note it $\boldsymbol{\psi_+}(\mathbf{x},t)\equiv(\cos\psi_+,\sin\psi_+)$. It defines a Lagrangian stretching direction. It follows from (2.8) that the FTLE converges to the strain rate as $t\to 0$. For large times, the large deviation theory suggests that the FTLE pdf P_λ in chaotic flows without KAM (Kolmogorov, Arnold, and Moser) surfaces (*Ott*, 2002) can be well approximated by:

$$\widetilde{P}_\lambda(t,\lambda)=\sqrt{\frac{tG''(\lambda_0)}{2\pi}}\exp(-tG(\lambda)), \tag{2.9}$$

where $G(\lambda)$, the Cramer or rate function, is concave with its minimum at λ_0 satisfying $G(\lambda_0)=G'(\lambda_0)=0$. Moreover, λ_0 is the infinite-time Lyapunov exponent: $\lim_{t\to\infty}P_\lambda(t,\lambda)=\delta(\lambda_0-\lambda)$ where δ is the Dirac delta function. The convergence of the Lyapunov exponents is very slow and typically algebraic in time (*Tang and Boozer*, 1996). The form (2.9) has been numerically verified and is widely used to approximate the asymptotic form of FTLE pdfs in simple ergodic flows with chaotic advection (e.g *Antonsen et al.* (1996); *Haynes* (2005); *Tsang* (2009)).

Computation and description. The distance $\boldsymbol{\delta l}$ between two trajectories initially infinitely close is solution of

$$\frac{d\boldsymbol{\delta l}}{dt}-\mathbf{S}.\boldsymbol{\delta l}=0, \tag{2.10}$$

where the tensor $\mathbf{S}=\nabla\mathbf{u}(\mathbf{X},t)$ is the velocity gradient tensor along a trajectory $\mathbf{X}(\mathbf{x},t)$. The distance $\boldsymbol{\delta l}$ can be calculated by $\boldsymbol{\delta l}=\mathbf{M}\boldsymbol{\delta l}_0$, where the resolvent matrix $\mathbf{M}$ is solution of $\frac{d\mathbf{M}}{dt}-\mathbf{SM}=0$ and is equal to the identity at $t=0$. The

finite time Lyapunov exponent λ is the log of the largest eigenvalue of $[\mathbf{M}^T\mathbf{M}]^{\frac{1}{2t}}$, with the singular vector $\boldsymbol{\psi}_+$ the associated eigenvector. The FTLE are obtained using the method described in *Abraham and Bowen* (2002) from the trajectories computed offline using a fourth order Runge-Kutta scheme with a trilinear interpolation on the velocity field. The time step is 0.1, which corresponds to a hundredth of the turnover time. The tensor $\mathbf{S}$ is calculated along the trajectories to obtain $\mathbf{M}$ and consequently λ and $\boldsymbol{\psi}_+$.

We estimate the FTLE pdfs as normalized histograms over 100 realizations of the flow, differing by their initial vorticity field. We initialize a trajectory at every grid point of our 512^2 domain, which results of a total of about 26×10^6 trajectories calculated. Each realization is run for a time span of $25T$. The FTLE pdfs are shown at different times in figure 2–2. The variance of the FTLE decreases with time while the peak of the distribution converges toward $\lambda_{max} \sim 0.02$. The FTLE are significantly smaller than the strain rates probably because of vorticity that inhibits the stretching of material elements (*McWilliams*, 1984) and because of the reorientation of the local strain axis along a trajectory (e.g. *Chertkov et al.* (1995)). In order to estimate whether these pdfs are asymptotically well approximated by (2.9), we define

$$G_e(\lambda, t) = -\frac{\ln(P_\lambda(t, \lambda))}{t} + \frac{\ln t}{2t} + \frac{A_e(t)}{t}, \tag{2.11}$$

where $A_e(t)$ is chosen such that $\min_\lambda G_e(\lambda, t) = 0$. Figure 2–3 shows the time evolution of G_e. The convergence for large values of λ, typically larger than the ensemble mean $\langle\lambda\rangle$ is satisfactory. However, the convergence for small values is much slower. It is particularly difficult to get the Cramer function for small values of λ (*Vanneste*, 2010). This is not a concern for the present study because only values of λ larger than their average are relevant. Nevertheless, we can get an estimate of the Cramer function assuming it is symmetric, as represented on 2–3. We have fitted the average

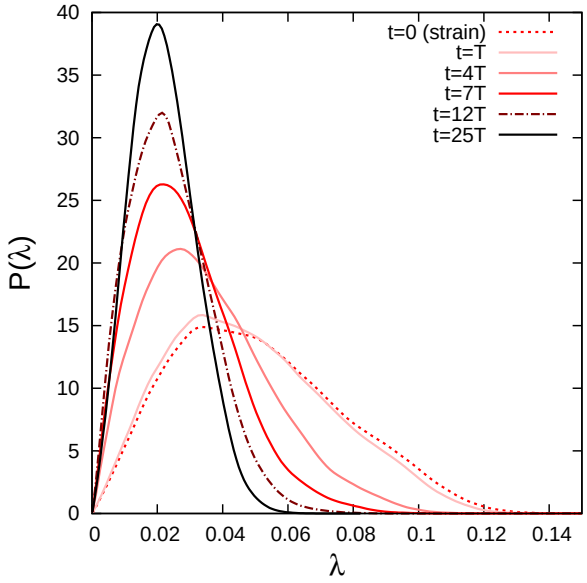

Figure 2–2: Density P_λ of the finite-time Lyapunov exponents shown at different times between $t = 0$ and $t = 25T$.

of the Cramer function for times larger that $15T$ for values of λ larger than 0.02 with a second order polynomial (Gaussian approximation) and obtained the estimate for values smaller than $\langle\lambda\rangle$ using symmetry.

The FTLE maps are shown in figure 2–4. For small times the strain field is dominated by large scales because of the high viscosity. However filamentary structures appear shortly, becoming finer and finer until they reach the resolution of the Eulerian model (the trajectories are initiated at every grid point of the Eulerian model). It is interesting to note that we get very similar structures as *Lapeyre* (2002), despite our much coarser velocity field. This is a manifestation of chaotic advection: the finite scales of a tracer are determined by the large-scale properties of the flow. It has been argued, in ergodic systems, that the singular vectors converge exponentially in time (*Goldhirsch et al.*, 1987), faster than the Lyapunov exponents, whose convergence is algebraic (*Goldhirsch et al.*, 1987; *Tang and Boozer*, 1996; *Lapeyre*, 2002). The "freezing" of the large-scale patterns in the FTLE maps (figure 2–4) may

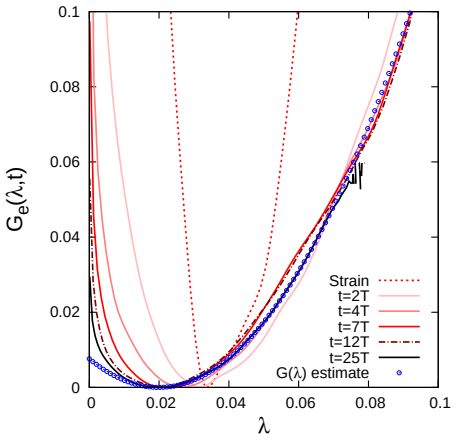

Figure 2–3: Function $G_e(\lambda, t)$ plotted at different times ($0 < t/T < 25$). G_e is defined such that P_λ - plotted in figure 2–2 - can be written $\propto -tG_e(\lambda, t)$ with $\min_\lambda G_e = 0$. We note the asymmetry of G_e and the faster convergence for FTLE larger than their ensemble mean. The time asymptotic form of G_e is the Cramer function G corresponding to the longtime FTLE pdf P_λ. An estimate of G is given by the blue circles, using a method detailed in the text.

be interpreted as a manifestation of the convergence of the singular vectors. In fact, *Tang and Boozer* (1996) argued that in ergodic and conservative chaotic dynamical systems, the Lyapunov exponents varies slowly along lines (the $\hat{\mathbf{s}}$ lines) which defines the stable direction in which neighboring points asymptotically converge. The filamentary structures in figure 2–4 may be interpreted as being these $\hat{\mathbf{s}}$ lines. This has been verified experimentally through the computation of the singular vectors (not shown), their convergence being particularly fast for trajectories originating in areas of the flow dominated by strain.

In the theoretical developments of part III.B and III.C, we will neglect the time evolution of the Lyapunov vectors and will only take into account the time evolution of the Lyapunov exponents.

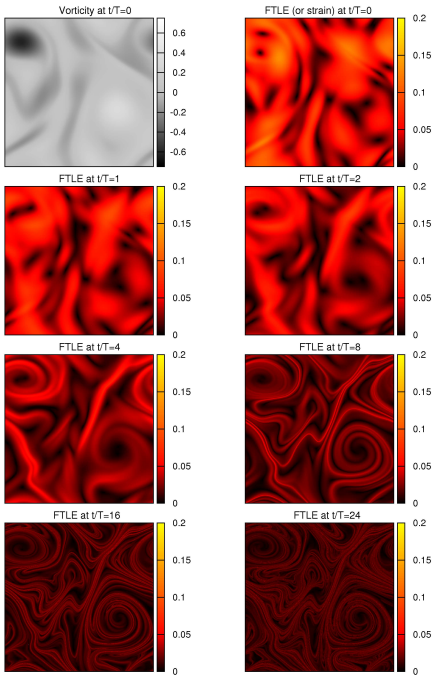

Figure 2–4: FTLE maps calculated at different times and displayed at starting locations of trajectories in the bi-periodic domain $[-\pi, \pi]^2$. In the top row are shown the vorticity (left) and the strain (right) at $t = 0$. In the following panels, ordered from left to right and top to bottom are shown the FTLE maps for $\frac{t}{T} = 1, 2, 4, 8, 16, 24$.

The tracers

The passive scalar ϕ is integrated with equation (2.2), using the same numerical scheme as for the vorticity. The numerical simulations are performed for eight different Prandtl numbers $Pr = \frac{\kappa}{\nu} = 2^i$ for $0 \leq i \leq 7$. Consequently the Peclet number $Pe = PrRe$, which measures the ratio of the advective to the diffusive time scale, ranges from 10^3 to 10^5.

We use two different initial conditions on the tracer for $(x, y) \in [-\pi, \pi]^2$:

$$\phi(x, y, t = 0) = A_0 \operatorname{sgn} x \qquad \text{for infinite initial gradients} \tag{2.12}$$

$$\phi(x, y, t = 0) = A_0 \frac{\pi^2}{4} \cos x \cos y \qquad \text{for smooth initial gradients} \quad , \tag{2.13}$$

where $\operatorname{sgn} x$ is the sign of x and A_0 is twice the initial domain average concentration of both A and B in the box. The first initial condition allows represents the case of sharp (actually infinite) gradients separating areas of well mixed reactants and the second one the case of smooth gradients.

2.2.3 The ensemble analysis

For each value of Prandtl number and for each initial condition, we run an ensemble of 34 simulations (or members). Each member is defined by different initial condition on the vorticity, taken from a long simulation of the statistically stationary flow solution of (2.6).

2.3 Theoretical and numerical results

Our goal here is to describe and understand the initial evolution of the first moment of $|\phi|$. In other words, we would like to integrate (2.5). We first consider how a material line stretches in a Lagrangian framework (III.A), and then how gradients on the contact line evolve under the action of both the diffusion and the flow along a Lagrangian trajectory (III.B). Paragraph III.C deals with the chemical speed. We focus on the initial condition where the reactants are separated by a sharp gradient before discussing the case of smoother gradients (III.D).

2.3.1 Lengthening of the contact line $\mathcal{L}$

Theory

We consider a line element $\boldsymbol{\delta l_0}$ along the contact line $\mathcal{L}(t=0) \equiv \mathcal{L}_0$. Its coordinates are $\delta l_0(\cos\alpha, \sin\alpha)$. The angle α is the initial orientation of the line element. It is transformed at time t into an element $\boldsymbol{\delta l} = \mathbf{M}\boldsymbol{\delta l_0}$ whose norm is:

$$\begin{aligned} |\boldsymbol{\delta l}| &= \left[\boldsymbol{\delta l_0}^T \mathbf{M}^T \mathbf{M} \boldsymbol{\delta l_0}\right]^{\frac{1}{2}} \\ &= |\boldsymbol{\delta l_0}| \left[e^{2\lambda t}\cos^2(\psi_+ - \alpha) + e^{-2\lambda t}\sin^2(\psi_+ - \alpha)\right]^{\frac{1}{2}}. \end{aligned} \tag{2.14}$$

The resolvent matrix $\mathbf{M}$ was introduced in II.B.2.b. The angle α and consequently the angle $\gamma \equiv \psi_+ - \alpha$ between the initial orientation and the singular vector can be assumed uniformly distributed between 0 and 2π and statistically independent of the chaotic orbit because the contact line is chosen arbitrarily with respect to the flow. Integrating over the Lyapunov exponent λ, the angle γ and the initial contact line, gives the ensemble average $\langle L \rangle$ of the length L of $\mathcal{L}$ (brackets are for ensemble averages). With P_λ the probability density distribution of λ, we have:

$$\langle L \rangle = L_0 \int_{\lambda=0}^{\infty} \int_{\gamma=0}^{2\pi} \left[e^{2\lambda t} \cos^2 \gamma + e^{-2\lambda t} \sin^2 \gamma \right]^{\frac{1}{2}} P_\lambda(t, \lambda)\, d\lambda \frac{d\gamma}{2\pi}. \tag{2.15}$$

The length L_0 is the initial length of the contact line. Equation (2.15) gives the actual length with no diffusion. Given the chaotic and closed (periodic) nature of the flow, we can only neglect diffusion as long as the contact line has not folded on itself. Indeed, when two filaments of $\mathcal{L}$ are brought together at a distance smaller than the diffusive cutoff, they merge under the action of diffusion. The time span of the regime where (2.15) is expected to be valid can be approximated with the mix-down time T_{mix} from the the largest scale L of the flow to the diffusive cutoff L_κ which is, according to *Thuburn and Tan* (1997), $\frac{1}{\lambda} \ln(L/L_\kappa)$, where λ is the thinning rate of a fluid element, i.e the Lyapunov exponent. It follows that T_{mix} depends on the trajectory we are considering. To obtain an estimate of T_{mix}, we use $\lambda \approx \langle S \rangle$ and $L_\kappa \approx \sqrt{\frac{\kappa}{\langle S \rangle}}$:

$$T_{mix} \approx T \ln Pe = T \ln RePr, \tag{2.16}$$

The length $\langle L \rangle$ can be approximated by L_E when we neglect the sine term in (2.15), i.e. when the contact line elements have equilibrated with the flow: their length converge to a function that grows exponentially at a rate given by the FTLE, the initial orientation α of the contact line being "forgotten". This is valid for

$t \gg \frac{1}{4\langle S\rangle} \approx \frac{T}{2}$.

$$\langle L\rangle \underset{t\gg\frac{T}{2}}{\sim} L_E = L_0 \int_{\lambda=0}^{\infty}\int_{\gamma=0}^{2\pi} P_\lambda(t,\lambda)\,|\cos\gamma|\, e^{\lambda t} d\lambda\, \frac{d\gamma}{\pi}$$
$$= \frac{2L_0}{\pi}\int_0^{\infty} P_\lambda(t,\lambda) e^{\lambda t} d\lambda. \tag{2.17}$$

If we assume $P_\lambda(t,\lambda) \propto e^{-G_e(\lambda,t)t}$, with G_e a concave positive function, integrating (2.17) with the steepest descent method, we obtain:

$$L_E \propto \int_0^{\infty} e^{[\lambda - G_e(\lambda,t)]t} d\lambda = e^{\max_\lambda[\lambda - G_e(\lambda,t)]t}. \tag{2.18}$$

Asymptotically, we have:

$$L_E \asymp e^{\lambda_1 t}, \tag{2.19}$$

where

$$\lambda_1 = \max_\lambda[\lambda - G(\lambda)] \tag{2.20}$$

is the Legendre transform of G evaluated in one. The value of λ_1 from our numerical estimate of G (figure 2–3) is 0.027.

Numerical results

The theoretical predictions $\langle L\rangle$ and L_E are compared to the numerical calculations in figure 2–5. The integration of (2.15) using our numerical estimate of P_λ reproduces very accurately the initial lengthening of the contact line for $t \lesssim T_{mix}(Pr)$. The derivative of the mean length of the contact line mean length at $t = 0$ is 0 because contracting line elements statistically compensate with stretching line elements due to randomness of α. The inflection of $\ln\langle L\rangle$ around $\frac{t}{T} = 2.5$ is due to two opposite effects: the equilibration of the contact line with the flow accelerates the growth of the line, while the shift of the FTLE pdf toward smaller values decelerates it, as shown by the L_E curve.

As seen on figure 2–5, $\langle L \rangle$ and L_E have a behavior very close to an exponential increase at the rate $\lambda_1 \approx 0.027$ after a couple of turnover times. This is consistent with the fast convergence of G_e for large FTLE (figure 2–3). A behavior close to this exponential increase can actually be seen in the simulations with large Prandtl numbers for a window of turnover times from around $4T$ to $6T$. Note that numerical simulations with even larger Prandtl numbers would have increased this time window only marginally since dividing the diffusion by two extends its time span by only half a turnover time (2.16). The reason is that the convergence of G_e, at least for larger than average FTLE, has a time scale close to the advective time scale. Further investigations are needed to explain this fact.

It is worth noting that the lengthening of a material contour is determined by rare events in the tail of the FTLE distribution. The maximum $\max_{\lambda}[\lambda - G_e(\lambda, t = NT)]$ is achieved by values of λ in the 42% quantile of the distribution for $N = 2$, 27% for $N = 4$, 13% for $N = 7$, and 3% for $N = 15$. Even though those events become exponentially rare because of the convergence of the FTLE pdfs toward a Dirac distribution, their contributions to the ensemble average of the contact line become exponentially important in the average of exponentials (2.15).

2.3.2 Lagrangian advection of the gradients along the contact line $\mathcal{L}$

In this section, we calculate the time evolution of the gradient of ϕ along a Lagrangian trajectory on the contact line for infinite initial gradients. We take into account the time evolution of the Lyapunov exponents. The singular vectors are taken equal to the forward Lyapunov vectors: $\psi_+(\mathbf{x}, t) = \Psi_+(\mathbf{x})$. As noted in part II.B.2, since the singular vectors converge rapidly, we expect this approximation to yield an accurate estimate of the gradients because the singular vectors converge rapidly, as noted in part II.B.2.

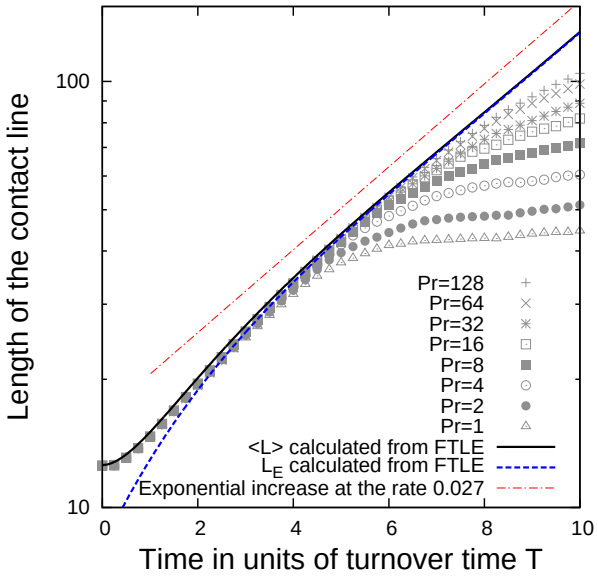

Figure 2–5: Ensemble average of the length of the contact line (infinite initial gradient case). The symbols correspond to ensemble averages of DNS for different Prandtl numbers $Pr = 1, 2, 4, 8, 16, 32, 64$ and 128. The black solid line corresponds to $\langle L \rangle$, as estimated from the FTLE pdf using (2.15), and the blue dotted line to L_E as estimated using the FTLE pdf with simplified expression (2.17). The red dotted line corresponds to an exponential increase at a rate $\lambda_1 = \max_{\lambda}[\lambda - G(\lambda)] \approx 0.027$, which corresponds to the asymptotic behavior in the inviscid limit (2.19). The latter has been shifted vertically for clarity. We note the log scale in the y-axis

Advection-diffusion equation in a co-moving frame

We consider a fluid element on the contact line and we note $\mathbf{X}_{\mathcal{L}}$ its trajectory:

$$\frac{d\mathbf{X}_{\mathcal{L}}}{dt} = \mathbf{u}(\mathbf{X}_{\mathcal{L}}, t) \text{ with} \qquad \mathbf{X}_{\mathcal{L}}(t=0) = \mathbf{X}_{0\mathcal{L}}, \tag{2.21}$$

where $\mathbf{X}_{0\mathcal{L}}$ is the initial location of the contact line element we are following. We define a new coordinate $\mathbf{r}$ corresponding to a frame co-moving with $\mathbf{X}_{\mathcal{L}}$:

$$\mathbf{r} = \mathbf{x} - \mathbf{X}_{\mathcal{L}}. \tag{2.22}$$

Writing the concentration field $\chi(\mathbf{r},t) \equiv \phi(\mathbf{x},t)$, we can show (*Monin and Yaglom*, 1975)) using (2.2) and (2.21) that:

$$\frac{\partial \chi}{\partial t} + [\mathbf{u}(\mathbf{X}_{\mathcal{L}} + \mathbf{r}, t) - \mathbf{u}(\mathbf{X}_{\mathcal{L}}, t)] \cdot \nabla \chi = \kappa \nabla^2 \chi. \tag{2.23}$$

Assuming a separation of scale between velocity and tracer scales, we can write $[\mathbf{u}(\mathbf{X}_{\mathcal{L}} + \mathbf{r}, t) - \mathbf{u}(\mathbf{X}_{\mathcal{L}}, t)]$ at the first order in $\mathbf{r}$. We basically assume that the characteristic width of the contact zone is much smaller than the velocity scale.

$$\frac{\partial \chi}{\partial t} + \mathbf{r}^T \cdot \nabla \mathbf{u}(\mathbf{X}_{\mathcal{L}}, t) \cdot \nabla \chi = \kappa \nabla^2 \chi. \tag{2.24}$$

Locally, along the contact line, the concentration of ϕ only varies in the direction perpendicular to the contact line, assuming that, for $t \lesssim T_{mix}$, the curvature of the contact line is much larger than the width of the contact zone where the gradients are concentrated. This is relevant because the stirring in chaotic advection produces elongated structures by nature. As a consequence, as noted previously in a similar case (*Balluch and Haynes*, 1997)), the field χ has to be of the form:

$$\chi(\mathbf{r},t) = \widetilde{\chi}(\mathbf{k} \cdot \mathbf{r}, t) = \widetilde{\chi}(\eta, t), \tag{2.25}$$

where $\mathbf{k}$ is a vector perpendicular to the contact line and η a coordinate along $\mathbf{k}$. Substituting (2.25) into (2.24) (with $\mathbf{S}(t) = \nabla \mathbf{u}(\mathbf{X}_{\mathcal{L}}, t)$) and equaling the zero and first order terms in $\boldsymbol{r}$, we can show that (*Balluch and Haynes*, 1997)):

$$\frac{d\mathbf{k}}{dt} + \mathbf{S}^T.\mathbf{k} = 0 \tag{2.26a}$$

$$\frac{\partial \widetilde{\chi}}{\partial t} = \kappa \left|\mathbf{k}\right|^2 \frac{\partial^2 \widetilde{\chi}}{\partial \eta^2}. \tag{2.26b}$$

Equation (2.26a) is actually the equation of a wavenumber $\mathbf{k}$ advected with the trajectory $\mathbf{X}_{\mathcal{L}}$. Noting its similarity with (2.10), it is clear that the FTLE is also the maximum exponential growth rate of a wavenumber $\mathbf{k}$ (or equivalently of a passive tracer

gradient in the absence of diffusion). This is an alternate and classical definition of FTLE (*Lapeyre*, 2002)). Considering the resolvent matrix $\mathbf{N}$ such that $\mathbf{k} = \mathbf{N}\mathbf{k}_0$, where $\mathbf{k}_0 = k_0(-\sin\alpha, \cos\alpha)$ is the initial value of $\mathbf{k}$, the finite time Lyapunov exponent λ is the log of the largest eigenvalue of $[\mathbf{N}^T\mathbf{N}]^{\frac{1}{2t}}$ with $(-\sin\psi_+, \cos\psi_+)$ the associated eigenvector. As a consequence, we have

$$\begin{aligned} |\boldsymbol{k}|^2 &= \boldsymbol{k_0}^T\mathbf{N}^T\mathbf{N}\boldsymbol{k_0} \\ &= |\boldsymbol{k_0}|^2 \left[e^{2\lambda t}\cos^2(\psi_+ - \alpha) + e^{-2\lambda t}\sin^2(\psi_+ - \alpha)\right]. \end{aligned} \tag{2.27}$$

With the assumption $\psi_+(\mathbf{x}, t) = \Psi_+(\mathbf{x})$, equation (2.26$b$) can be written

$$\frac{\partial\widetilde{\chi}}{\partial\Theta} = \kappa k_0^2 \frac{\partial^2\widetilde{\chi}}{\partial\eta^2} \tag{2.28}$$

using the rescaled time

$$\Theta = \left[\tau e^{2\lambda t}\cos^2\gamma + \widetilde{\tau}\sin^2\gamma\right]. \tag{2.29}$$

We have reintroduced $\gamma = \Psi_+ - \alpha$, a random and uniformly distributed angle between 0 and 2π (see III.A.1). The quantities τ and $\widetilde{\tau}$ are two equivalent times defined as follows:

$$\tau = \frac{\int_0^t e^{2u\lambda(u)}du}{e^{2t\lambda(t)}} \text{ and } \widetilde{\tau} = \int_0^t e^{-2u\lambda(u)}du. \tag{2.30}$$

The time τ, introduced by *Antonsen et al.* (1996) and called "equivalent time" by *Haynes and Vanneste* (2004) evaluates the stretching time scale of a Lagrangian parcel in the recent past because chaotic trajectories are characterized by positive Lyapunov exponents. Similarly, the equivalent time $\widetilde{\tau}$ measures the stretching rate in the early part of the trajectory. As a consequence, we expect τ and $\widetilde{\tau}$ to have the same statistics, to be asymptotically equivalent as $t \to 0$ and to become independent at larger times. It has been argued (*Haynes and Vanneste*, 2004)) that the pdf of τ converges to a time asymptotic form, which is suggested for our flow in figure 2–6

where we have plotted the pdf of $\frac{1}{\tau}$ calculated together with the Lyapunov exponent on each Lagrangian trajectory (II.2.B). The statistics of $\widetilde{\tau}$ (not shown), calculated the same way, are not distinguishable from these of τ.

Solution (infinite initial gradient case)

The initial gradient along the contact line is infinite, while the reactants are well mixed in their respective domain with a concentration equal to A_0. As a consequence, we take:

$$\widetilde{\chi}(\eta, t=0) = A_0 \operatorname{sgn} \eta. \tag{2.31}$$

The solution of (2.28) with the initial condition (2.31) is:

$$\widetilde{\chi}(\eta, t) = A_0 \frac{2}{\sqrt{\pi}} \int_0^{\frac{\eta}{2\sqrt{\kappa\Theta}}} e^{-l^2} dl = A_0 \operatorname{Erf}\big(\frac{\eta}{2k_0\sqrt{\kappa\Theta}}\big). \tag{2.32}$$

The function Erf is the Gauss error function. It follows from (2.25) and (2.32):

$$\begin{aligned} \chi(\mathbf{r}, t) &= A_0 \operatorname{Erf}\big(\frac{\mathbf{n}\cdot\mathbf{r}}{2\sqrt{\kappa}} \sqrt{\frac{|\mathbf{k}|/k_0}{\Theta}}\big) \\ &= A_0 \operatorname{Erf}\big(\frac{G_{\mathcal{L}}}{2\sqrt{\kappa}} \mathbf{n}\cdot\mathbf{r}\big) \end{aligned} \tag{2.33}$$

with

$$\mathbf{n} = \frac{\mathbf{k}}{|\mathbf{k}|} \tag{2.34}$$

the unit vector normal to the contact line and

$$\begin{aligned} G_{\mathcal{L}} &= \sqrt{\frac{|\mathbf{k}|/k_0}{\Theta}} \\ &= \sqrt{\frac{e^{2\lambda t}\cos^2\gamma + e^{-2\lambda t}\sin^2\gamma}{\tau e^{2\lambda t}\cos^2\gamma + \widetilde{\tau}\sin^2\gamma}}. \end{aligned} \tag{2.35}$$

The norm $|\nabla\phi_{\mathcal{L}}|$ of the gradient of the field ϕ on the contact line (where $\chi = 0$), i.e. at the location of the trajectory $\mathbf{X}_{\mathcal{L}}$ characterized by the Lagrangian stretching

properties $(\lambda, \tau, \widetilde{\tau}, \gamma)$ is

$$|\nabla \phi_{\mathcal{L}}| = |\nabla_{\mathbf{r}} \chi \cdot \mathbf{n}|_{\mathbf{r}=0} = \frac{A_0}{\sqrt{\pi \kappa}} G_{\mathcal{L}}(t, \lambda, \tau, \widetilde{\tau}, \gamma). \tag{2.36}$$

Ensemble average of the gradient along the contact line

To perform the ensemble average $\langle |\nabla \phi_{\mathcal{L}}| \rangle$ of the modulus of the gradient of ϕ along the contact line, we introduce the joint pdf $\widetilde{P}$ of $(\lambda, \tau, \widetilde{\tau})$. As noted previously, the orientation γ is assumed uniformly distributed between 0 and 2π and independent from the random vector $(\lambda, \tau, \widetilde{\tau})$. If we consider a trajectory $\mathbf{X}_{\mathcal{L}}$ of a contact line element $\boldsymbol{\delta l}$, the gradient on it is equal to $|\nabla \phi_{\mathcal{L}}|$ on a length $|\boldsymbol{\delta l}|$, defined in (2.10). As a consequence, with (2.36) and (2.10), we obtain:

$$\begin{aligned} \langle |\nabla \phi_{\mathcal{L}}| \rangle &= \frac{\langle |\nabla \phi_{\mathcal{L}}| \, |\boldsymbol{\delta l}| \rangle}{\langle |\boldsymbol{\delta l}| \rangle} \\ &= \frac{A_0}{\sqrt{\pi \kappa}} \frac{L_0}{\langle L \rangle} \iiint \frac{e^{2\lambda t} \cos^2 \gamma + e^{-2\lambda t} \sin^2 \gamma}{\sqrt{\tau e^{2\lambda t} \cos^2 \gamma + \widetilde{\tau} \sin^2 \gamma}} \\ &\quad \widetilde{P}(t, \lambda, \tau, \widetilde{\tau}) \, d\lambda \, d\tau \, d\widetilde{\tau} \, \frac{d\gamma}{2\pi}. \end{aligned} \tag{2.37}$$

The integration is performed between 0 and ∞ for λ, τ and $\widetilde{\tau}$ and between 0 and 2π for γ. Hereafter, these bounds will be omitted. For times sufficiently large ($t \gg \frac{1}{2\langle S \rangle} \approx T$), we neglect the $\sin^2$ terms under the integral in (2.37) and in the expression for $\langle L \rangle$ and we obtain, in the limit of a contact line equilibrated with the flow:

$$\langle |\nabla \phi_{\mathcal{L}}| \rangle \underset{t \gg T}{\sim} \frac{2A_0}{\sqrt{\pi^3 \kappa}} \frac{L_0}{L_E} \iint \frac{e^{\lambda t}}{\sqrt{\tau}} P_{\lambda,\tau}(t, \lambda, \tau) \, d\lambda \, d\tau, \tag{2.38}$$

where $P_{\lambda,\tau}$ is the time dependent joint pdf of λ and τ. The joint density of $(\lambda, \frac{1}{\tau})$ is pictured on figure 2–7. The frequencies λ and $\frac{1}{\tau}$ are clearly dependent, especially when they are small, even at times much larger than the advective time scale (e.g. $t = 20T$ and $t = 25T$). The computation of the Spearman Rho correlation coefficient clearly confirms this dependence Previous studies (e.g *Antonsen et al.* (1996);

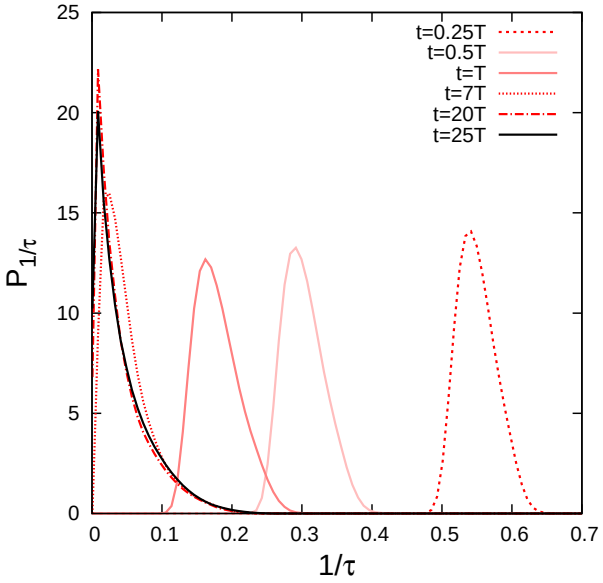

Figure 2–6: Probability density function of $\frac{1}{\tau}$ plotted at different times. The equivalent time τ is defined in (2.30).

Haynes and Vanneste (2004)) have assumed the independence between λ and τ at times much larger than the Lagrangian correlation time, here shorter than or of the order of the advective time scale. This may be appropriate in simple ergodic chaotic flows. However, two dimensional Navier-Stokes flows, including two-dimensional turbulence, exhibit coherent structures (vortices, filaments of vorticity, etc...) that seem to prevent this independence to be achieved. Nevertheless, the dependence is weaker for large values of λ, which precisely dominate the integral (2.38). Approximating $P_{\lambda,\tau}$ by the product of its marginal densities P_λ and P_τ, we obtain that $|\nabla\phi_{\mathcal{L}}|$ can be approximated by the simple expression $\frac{A_0}{\sqrt{\pi\kappa\tau}}$

Comparison with the numerical results

The ensemble average of the modulus of the gradient along the contact line have been calculated on the 34 ensemble members and for the whole range of Prandtl numbers $Pr = \frac{\kappa}{\nu} = 2^i$ for $0 \leq i \leq 7$. We calculate λ, τ and $\widetilde{\tau}$ on each trajectory, which permits the numerical integration of (2.37) and (2.38). Numerical results are

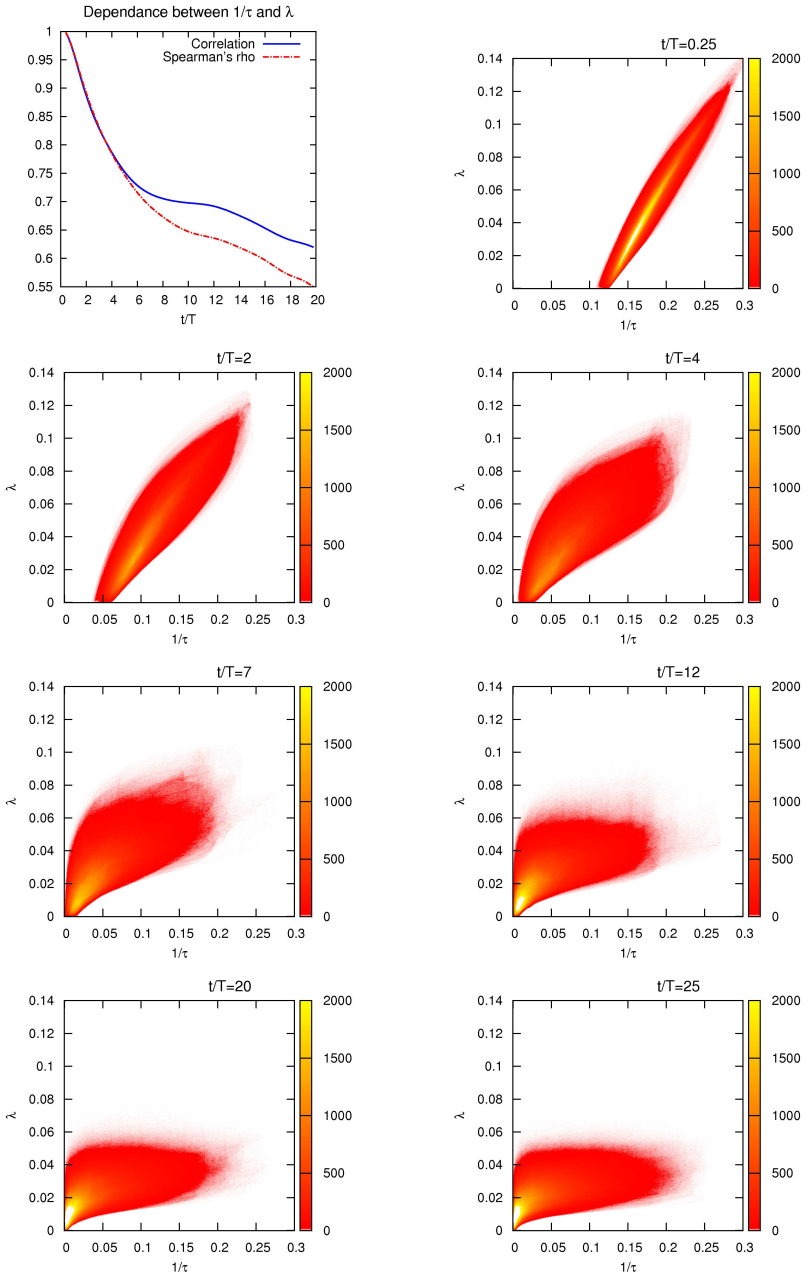

Figure 2–7: Correlation between λ and $\frac{1}{\tau}$ as a function of time (top left) and joint pdf of $(\lambda, \frac{1}{\tau})$, as estimated from the numerical simulations and plotted at different times $\frac{t}{T} = 0.25, 2, 4, 7, 12, 20$ and 25

displayed on figure 2–8 and are compared with the theoretical results of the previous paragraph. The joint statistics of $(\lambda, \tau, \widetilde{\tau})$ are referred to as the Lagrangian stretching properties (LSP).

The ensemble averages of the gradient calculated from the DNS and multiplied by $\frac{\sqrt{\kappa\pi}}{A_0}$ are shown for Prandtl numbers ranging from 2 to 128 in figure 2–8. For large enough diffusion (small enough Pr), the curves become virtually identical, showing the dependence in $\kappa^{-\frac{1}{2}}$ of the gradient suggested by equation (2.37). This regime seems to be valid for times up to $3.5T$ at $Pr = 2$ and up to $6T$ at $Pr = 16$. This timescale corresponds to that estimated by equation (2.16) modulo a factor 2 and coincides with the regime where the advection alone accounts for the lengthening of the contact line (figure 2–5). The departure at small diffusion comes from the fact that the infinite gradient hypothesis becomes inaccurate in the numerical simulations given the finite size of the grid. We can reproduce the curves at large Prandtl number by solving the derivative with respect to η in (2.28) using the initial condition on the gradient $\frac{\partial \chi_t}{\partial \eta}|_{t=0} = \frac{A_0}{2\delta_0\sqrt{\pi}} e^{-\frac{\eta^2}{4\delta_0^2}}$, with δ_0 a length corresponding to a grid point. We find that the previous developments stand with $G_{\mathcal{L}}$ (2.35) replaced by $G_{\mathcal{L},\kappa} = \sqrt{\frac{e^{2\lambda t}\cos^2\gamma + e^{-2\lambda t}\sin^2\gamma}{\frac{\delta_0^2}{\kappa} + [\tau e^{2\lambda t}\cos^2\gamma + \widetilde{\tau}\sin^2\gamma]}}$ which is a function of κ. The expression $G_{\mathcal{L}}$ is a good approximation of $G_{\mathcal{L},\kappa}$ when the initial gradients imposed by the grid $\frac{A_0}{\delta_0}$ are large compared to $\frac{A_0}{\sqrt{\kappa\tau}}$ ($\sqrt{\kappa\tau}$ can be interpreted as the diffusive cutoff). This is not the case for $Pr = 64$ and $Pr = 128$ in our simulations.

The evolution of $\frac{\sqrt{\kappa\pi}}{A_0}\langle|\nabla\phi_{\mathcal{L}}|\rangle$ estimated using (2.37) with the LSP is provided on figure 2–8. It captures very well the behavior of ensemble mean gradients for small Prandtl numbers. A very slight underestimation is seen that could be due to numerical artifacts or to our approximation taking the singular vectors constant in the theoretical developments. We also show $\frac{\sqrt{\kappa\pi}}{A_0}\langle|\nabla\phi_{\mathcal{L}}|\rangle$ approximated by (2.38). It overestimates the gradients at small times, a discrepancy which decreases with time

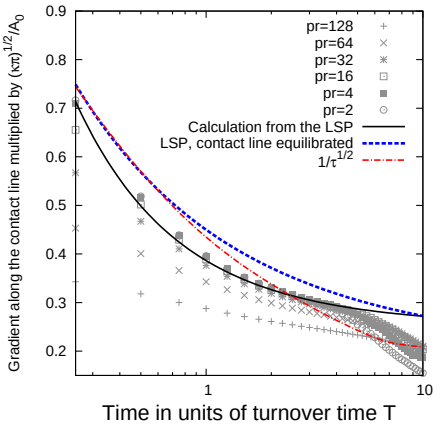

Figure 2–8: Ensemble average of the gradients advected with the contact line, multiplied by $\frac{\sqrt{\kappa\pi}}{A_0}$, in the sharp gradient case. The symbols correspond to ensemble averages over the 34 DNS members for different Prandtl numbers $Pr = 2, 4, 16, 32, 64, 128$. The lines correspond to the calculation from the Lagrangian stretching properties (LSP): in green from (2.37) and in blue from (2.38), considering a perfectly equilibrated contact line with the flow. The red line is $\frac{1}{\sqrt{\tau}}$ and corresponds to (2.38) with λ and τ statistically independent. We note the log scale in the time axis.

as the contact line equilibrates with the flow. The quantity $\frac{1}{\sqrt{\tau}}$, also shown in figure 2–8 neither performs well at small times for the same reason as (2.38), nor at larger times because of the missing dependence of τ with λ.

2.3.3 Time evolution of $\langle \frac{d\overline{|\phi|}}{dt} \rangle$

Theory

Having formulated the evolution of the contact line and the gradient, we can now express the chemical speed $-\langle \frac{d\overline{|\phi|}}{dt} \rangle$ by ensemble averaging (2.5). We use the expression of $|\boldsymbol{\delta l}|$ in (2.14), with $\psi_+ = \Psi_+$, for dl and the expression $|\nabla \phi_{\mathcal{L}}|$ in (2.36)

for $|\nabla\phi|$.

$$-\langle\frac{d\overline{|\phi|}}{dt}\rangle = \frac{L_0 A_0}{\sqrt{\pi}\mathcal{A}}\sqrt{\kappa}\left\langle\frac{e^{2\lambda t}\cos^2\gamma + e^{-2\lambda t}\sin^2\gamma}{\sqrt{\tau e^{2\lambda t}\cos^2\gamma + \widetilde{\tau}\sin^2\gamma}}\right\rangle$$

$$= \frac{L_0 A_0}{\sqrt{\pi}\mathcal{A}}\sqrt{\kappa}\iiiint\frac{e^{2\lambda t}\cos^2\gamma + e^{-2\lambda t}\sin^2\gamma}{\sqrt{\tau e^{2\lambda t}\cos^2\gamma + \widetilde{\tau}\sin^2\gamma}}$$

$$\widetilde{P}(t,\lambda,\tau,\widetilde{\tau})\,d\lambda\,d\tau\,d\widetilde{\tau}\,\frac{d\gamma}{2\pi} \tag{2.39}$$

$$\underset{t\gg T}{\sim}\frac{2L_0 A_0}{\sqrt{\pi^3}\mathcal{A}}\sqrt{\kappa}\iint\frac{e^{2\lambda t}}{\sqrt{\tau}}P_{\lambda,\tau}(t,\lambda,\tau)\,d\lambda\,d\tau\,. \tag{2.40}$$

The chemical speed scales like $\kappa^{\frac{1}{2}}$, which is a direct consequence of the scaling of the gradients like $\kappa^{-\frac{1}{2}}$, the contact line length being independent of the diffusion in the regime considered. Indeed, comparing equation (2.39) with (2.37) leads to the simple relationship between the ensemble means:

$$-\langle\frac{d\overline{|\phi|}}{dt}\rangle = \frac{\kappa}{\mathcal{A}}\langle L\rangle\langle|\nabla\phi_{\mathcal{L}}|\rangle. \tag{2.41}$$

This relationship was actually previously justified and used to calculate the gradients (2.37).

Numerical results

Figure 2–9 shows $-\frac{1}{\sqrt{\kappa}}\langle\frac{d\overline{|\phi|}}{dt}\rangle$ for various Prandtl numbers estimated from the ensemble DNS and the result of equation (2.39) using LSP. Like for the gradients, the curves converge together when the diffusion gets larger, for times shorter than T_{mix}. The limit curve best fulfills the infinite gradient hypothesis and consequently matches very well the estimate from equation (2.39) calculated from the Lagrangian stretching properties.

The general behavior of the chemical speed can be interpreted in light of equation (2.41). The initial decrease is mainly due to the decrease of the gradients, as observed previously. Then, it is dominated by the increase of the contact line, the gradients decreasing very slowly. Figure 2–9 shows the exponential increase at a rate $\lambda_1 \approx$

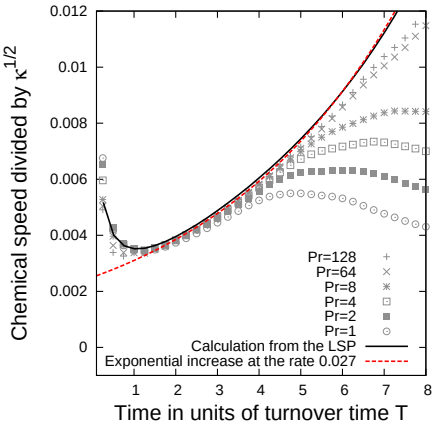

Figure 2–9: Ensemble average of the chemical speed in the sharp gradient case divided by the diffusion $\sqrt{\kappa}$. The symbols correspond to numerical results from the 34 members ensemble, for different Prandtl numbers $Pr = 1, 2, 4, 8, 64, 128$. The blue solid line (calculation from the LSP) corresponds to (2.39). The exponential increase at a rate $\lambda_1 = 0.027$, in red, corresponds to the expected asymptotic regime of (2.39).

0.027. The timescale corresponding to the minimum of the chemical speed can be estimated from the timescale of the decrease of the gradient, which is of the order of T [1]

2.3.4 Alternative initial condition on the tracers: smooth gradients

The following calculations are extending the analytical results for an initial condition on the tracers with smooth gradients and are validated numerically with the initial condition (2.13). We neglect the diffusion to determine the evolution of the gradients. In the inviscid limit, a gradient along a Lagrangian trajectory obeys the wavenumber equation (2.26*a*) (e.g. *Lapeyre* (2002)), whose solution is given by

[1] Assuming that it is the time scale for the decrease of $\frac{1}{\sqrt{\tau}}$, this estimate is obtained by direct calculation of $\frac{1}{\sqrt{\tau}}$ from (2.30) taking $\lambda \approx S$. The latter approximation is justified because the Lyapunov exponent is very close to the strain rate where the trajectory originates for times smaller than T, as shown on figures 2–4 and 2–2. The fact that we find a time scale of the order of T validates the approximation $\lambda \approx S$ a posteriori.

(2.27). Together with (2.14), we obtain the ensemble average of (2.5):

$$-\langle\frac{d\overline{|\phi|}}{dt}\rangle = \beta\kappa \iint P_\lambda(t,\lambda)\left[e^{2\lambda t}\cos^2\gamma + e^{-2\lambda t}\sin^2\gamma\right]\frac{d\gamma}{2\pi}\,d\lambda \tag{2.42}$$

$$\underset{t\gg\frac{T}{2}}{\sim} \frac{\beta}{2}\kappa \int P_\lambda(t,\lambda)\, e^{2\lambda t} d\lambda \propto e^{\max_\lambda[2\lambda - G_e(\lambda,t)]t} \tag{2.43}$$

$$\asymp e^{\lambda_2 t}.$$

with

$$\lambda_2 = \max_\lambda[2\lambda - G(\lambda)] \tag{2.44}$$

the Legendre transform of G evaluated in two and $\beta = \frac{L_0\langle|\nabla\phi_{\mathcal{L}}|\rangle(t=0)}{\mathcal{A}}$.

The dependence of the chemistry on the diffusion is, like in the sharp gradient case, algebraic but the exponent is now 1. Our numerical simulations are consistent with this prediction: figure 2–10 shows the chemical speed divided by the diffusion. For small times, all the curves are virtually identical, which confirms the κ dependence of the chemical speed.

The calculation of $-\langle\frac{d\overline{|\phi|}}{dt}\rangle$ using (2.42) with the pdf P_λ reproduces very well the initial increase of the chemical speed, as shown on figure 2–10. Interestingly, the chemical speed has now a similar evolution as the contact line (figure 2–5). Indeed, equations (2.15) and (2.42) are very similar. The quantity integrated over the density of λ is just squared in (2.42) compared to (2.15). Using our numerical estimate of the Cramer function through (2.44), λ_2 can be estimated at 0.09, which is about three times λ_1. The chemical speed increases much faster than twice the contact line, which would be the case for a uniform Lyapunov exponent. In the sharp gradient case, the chemical speed rather scales like $e^{\lambda_1 t}$, because of the action of diffusion on the gradient. This suggests a slower chemistry, which may be surprising since the chemistry, controlled by a diffusive flux, is expected to be faster when the gradients are sharper. Actually, the chemistry is not faster than in the sharp gradient case,

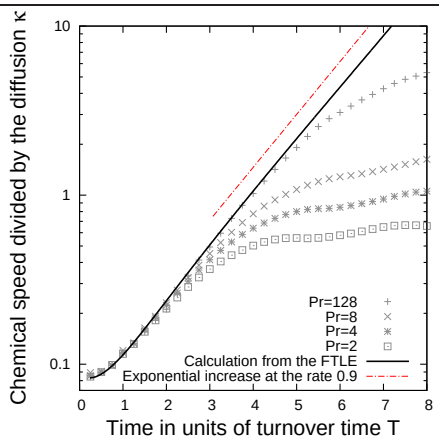

Figure 2–10: Ensemble average of the chemical speed, in the smooth gradient case, divided by κ. The dotted lines correspond to numerical results from the 34 members ensemble, for different Prandtl numbers $Pr = 2, 4, 8, 128$. The solid line (calculation from the LSP) correspond to (2.42) The exponential increase at a rate 0.09 corresponds to the expected asymptotic regime of (2.42), as expressed in (2.43) and has been shifted vertically for clarity. We note the log scale in the y-axis

precisely because of the difference in the initial gradients magnitude, but it increases much faster.

2.4 Concluding remarks

We have studied an infinitely fast bimolecular chemical reaction in a two-dimensional Navier-Stokes flow at moderate Reynolds number with chaotic advection. The computation of the probability distribution function of the Lyapunov exponents suggests that large deviation theories may be relevant to describe its behavior after a few turnover times. We defined $G_e(\lambda, t)$ such that the FTLE pdf scales like $e^{-tG_e(\lambda,t)}$ and $\min_{\lambda} G_e(\lambda, t) = 0$. The function G_e satisfactorily converges to a Cramer function G in a couple of turnover times, at least for exponents larger than their mean value.

*. We have investigated the early regime (≈ 5 turnover times of the flow) of the reaction, corresponding to the time window where the contact line is a clearly defined material line that does not depend on diffusion. We postulate that this time window is limited by the mix-down time scale from the large scales to the diffusive cutoff

and scales like the log of the Peclet number. We have related, both theoretically and numerically, the Lagrangian stretching properties of the flow, as captured by the joint pdf of the Lyapunov exponents λ and two equivalent times τ and $\widetilde{\tau}$ (2.30), to the following quantities:

- **The ensemble average contact line length between the reactants $\langle L \rangle$.** After a brief transient corresponding to the equilibration of the contact line with the flow, i.e. to the alignment of the contact line elements with the direction corresponding to the maximum growth, independent of its initial orientation, the contact line lengthens like $e^{\max_{\lambda}[\lambda - G_e(\lambda,t)]t}$ which converges in time to $e^{\lambda_1 t}$, where λ_1 is the Legendre transform of G evaluated in one and is determined by rare large events in the FTLE distribution.
- **The ensemble mean of the gradients along the contact line $\langle |\nabla \phi_{\mathcal{L}}| \rangle$.** It scales like $\kappa^{-\frac{1}{2}}$ and is determined by the pdf of $(\lambda, \tau, \widetilde{\tau})$ through (2.37). The influence of $\widetilde{\tau}$ diminishes with time as the contact line is equilibrating with the flow. The dependence between λ and τ is crucial to accurately predict $\langle |\nabla \phi_{\mathcal{L}}| \rangle$. Our main assumption was the stationarity of the Lyapunov vectors, justified by their fast exponential convergence in time. It would be interesting to extend this work without this assumption to precise the conditions of its applicability.
- **The ensemble mean chemical speed.** The chemical speed is defined as the modulus of the time derivative of the sum of the two reactants' mean domain concentrations. It scales like $\kappa^{\frac{1}{2}}$ in the limit of infinite initial gradients. This scaling is consistent with *Wonhas and Vassilicos* (2002) in the special case of a contact line of dimension one separating two on/off fields. The ensemble average chemical speed is proportional to the product of $\langle L \rangle$ and $\langle |\nabla \phi_{\mathcal{L}}| \rangle$. Hence, an initial decrease of the chemical speed is related to the decrease of the gradients, while a later regime is dominated by the lengthening of the

contact line and is consequently equivalent to $e^{\max_{\lambda}[\lambda - G_e(\lambda,t)]t}$. Both the contact line length and the chemical speed are determined by very rare events in the tail of the FTLE distribution. This points out the importance of considering the distribution of the FTLE, which is not always taken into account in the literature (*Sokolov and Blumen*, 1991; *Karolyi and Tél*, 2005, 2007)).

The case of smooth gradients exhibits some significant differences. The gradients increase instead of decreasing and are initially not affected by diffusion. The two main consequences are that the chemistry scales like κ and increases exponentially in time at a rate determined by even rarer events in the tail of the FTLE distribution (2.43).

The theory developed in this paper should allow to predict the evolution of the pdfs of the gradients along the contact line and of the passive tracer ϕ, which would be a very robust way to test it. This will be the subject of a future paper. Another paper in preparation which takes into account the fractal structure of the contact line in order to investigate the intermediate regime, where the chemical production reaches a maximum, and the long term decay of the reactants.

Some interesting open questions about the Lagrangian properties of a two-dimensional Navier-Stokes flow have arisen from this study. What determines the initial time evolution of the FTLE pdf? What determines the shape of the Cramer function G? Is it possible to predict the asymptotic form of the pdf of $\frac{1}{\tau}$? More importantly, the dependence between τ and λ seems to be a major difference with simple prescribed flows used in the literature to study chaotic advection, which may not be, as a consequence, representative of dynamically consistent flows. Studying the joint pdf of (λ, τ) may happen to be useful to better understand the mixing of both passive and active tracers in two-dimensional Navier-Stokes flows with chaotic advection, particularly when using Lagrangian stretching theory approaches.

Acknowledgments. This research was supported by the Natural Sciences and Engineering Research Council of Canada (NSERC). We thank an anonymous reviewer that contributed very significantly to improve the theoretical development of part III.B.

CHAPTER 3
Fast chemical reaction in a two-dimensional Navier-Stokes flow: Probability distribution in the initial regime

In this chapter, we use the theory developed in chapter 2 to determine the probability distribution function of the gradient of the reactants along the contact line and of the reactants. This allows to test the relevance of this theory in more detail. Also, knowing how these pdfs depend on resolution might be helpful when building sub-grid parametrization for the chemistry. The manuscript which constitutes this chapter was submitted to Physical Review E in October 2011: F. Ait-Chaalal, M.S. Bourqui and Peter Bartello (2011). Fast chemical reaction in a two-dimensional Navier-Stokes flow: Probability distribution in the initial regime

Fast chemical reaction in a two-dimensional Navier-Stokes flow: Probability distribution in the initial regime

F. Ait-Chaalal [1], M.S. Bourqui[1,2] and P. Bartello[1,3]

[1]Department of Atmospheric and Oceanic Sciences, McGill University, Montréal, QC, Canada

[2]Department of Chemistry, McGill University, Montréal, QC, Canada

[3]Department of Mathematics and Statistics, McGill University, Montréal, QC, Canada

Manuscript submitted to Physical Review E in October 2011.

Abstract

We study an instantaneous bimolecular chemical reaction in a two-dimensional chaotic, incompressible and closed Navier-Stokes flow. Areas of well mixed reactants are initially separated by infinite gradients. We focus on the initial regime, characterized by a well-defined one-dimensional contact line between the reactants. The amount of reactant consumed is given by the diffusive flux along this line, and hence relates directly to its length and to the gradients along it. We show both theoretically and numerically that the probability distribution of the modulus of the gradient of the reactants along this contact line multiplied by $\kappa^{\frac{1}{2}}$ does not depend on the diffusion κ and can be inferred, after a few turnover times, from the joint distribution of the finite time Lyapunov exponent λ and the frequency $\frac{1}{\tau}$. The equivalent time τ measures the stretching time scale of a Lagrangian parcel in the recent past, while $\frac{1}{\lambda}$ measures it on the whole chaotic orbit. At smaller times, we predict the shape of this gradient distribution taking into account the initial random orientation between the contact line and the stretching direction. We also show that the probability distribution of the reactants is proportional to $\kappa^{\frac{1}{2}}$ and to the product of the ensemble mean contact line length with the ensemble mean of the inverse of the gradient along it. Besides contributing to the understanding of fast chemistry in chaotic flows, the present study based on a Lagrangian stretching theory approach provides results that pave the way to the development of accurate subgrid parametrizations in models with insufficient resolution for capturing the length scales relevant to chemical processes, for example in Climate-Chemistry Models.

3.1 Introduction

Chemical reactions in the stratosphere have been shown to be sensitive to the numerical spatial resolution when the chemistry is fast compared to advective processes (*Tan et al.*, 1998; *Edouard et al.*, 1996). It was proposed by *Tan et al.* (1998) that the product concentration of the deactivation of polar vortex chlorine by low latitudes nitrogen oxide at the edge of the stratospheric Northern hemisphere winter time polar vortex scales like $\kappa^{p(t)}$, with κ being the reactant diffusion. Later on, *Wonhas and Vassilicos* (2002) argued that $p(t)$ can be expressed as $1-D(t)/2$, where $D(t)$ is the box counting fractal dimension of the contact line between the reactants. Here we focus on the initial regime of an instantaneous bimolecular chemical reaction in a two dimensional Navier-Stokes flow characterized by chaotic trajectories (this provides an idealized framework for isentropic dynamics in the stratosphere). By definition, the initial regime is characterized by a well-defined one-dimensional contact line (i.e. $D = 1$). The reactants are initially separated by infinite gradients. This regime has a time span of several turnover times of the large-scale flow. It is consequently consistent with the study of chemical tracers in the stratosphere over several days or weeks. These time scales are typical of the wintertime ozone depletion in the midlatitude stratosphere, or of the seasonal "ozone hole" formation.

In a previous work (*Ait-Chaalal et al.*, under review) dealing with this regime, we have shown that the ensemble mean reactant concentration time derivative scales like $\kappa^{\frac{1}{2}}$ and can be predicted accurately from the Lagrangian stretching properties of the flow. Here we investigate the statistical properties of the chemical production and of the reactants concentrations.

In section II, we explain how the study of an infinitely fast chemical reaction $A + B \longrightarrow C$ simplifies into the study of a passive tracer whose concentration field ϕ is defined as the difference between the concentrations fields of the two reactants

A and B . The rate at which the reactants disappear is the diffusive flux of ϕ along the contact line, and hence depends on both its length and the gradients along it. In section III, we give some theoretical relations between, on one hand, the contact line length and the gradients of the reactants along it, and, on the other hand, the Lagrangian stretching properties of the flow. In section IV, we focus on the probability distribution of the reactants concentration. Section V describes the Lagrangian stretching properties of a two-dimensional Navier-Stokes flow and section VI presents some numerical simulations to test the theoretical results of sections III and IV in the flow introduced in section V.

3.2 Finite time Lyapunov exponents and chemical production in a chaotic flow

We consider the bimolecular chemical reaction $A + B \longrightarrow C$ in stoichiometric quantities. One molecule of A reacts locally with one molecule of B to give one molecule of C. As a result, the field $\phi = C_A - C_B$, defined as the difference between the reactants' concentration fields C_A and C_B, is independent of the chemistry. If, in addition, the reaction is instantaneous, A and B cannot coexist at the same location. Consequently, the fields C_A and C_B, and their spatial average over a closed domain denoted by an overbar, can be retrieved from ϕ as follows (*Corrsin*, 1958; *Sokolov and Blumen*, 1991):

$$\begin{cases} C_A(\mathbf{x},t) = \phi(\mathbf{x},t) \text{ and } C_B(\mathbf{x},t) = 0 & \text{if } \phi(\mathbf{x},t) > 0 \\ C_B(\mathbf{x},t) = -\phi(\mathbf{x},t) \text{ and } C_A(\mathbf{x},t) = 0 & \text{if } \phi(\mathbf{x},t) < 0 \end{cases} \tag{3.1a}$$

$$\overline{C_A} = \overline{C_B} = \frac{\overline{|\phi|}}{2} \tag{3.1b}$$

Because a molecule of A always react with a molecule of B locally, the tracer ϕ is passive and follows the classical advection-reaction equation:

$$\frac{\partial \phi}{\partial t} + \mathbf{u} \cdot \nabla \phi = \kappa \nabla^2 \phi. \tag{3.2}$$

If A and B are separated by a contact line $\mathcal{L} = \{\mathbf{x}|\phi(\mathbf{x}) = 0\}$ of dimension one oriented in a counterclockwise direction such that it encloses reactant A (domain D_A), the time derivative of the reactants in an incompressible closed flow is:

$$\mathcal{A}\overline{\frac{dC_A}{dt}} = \mathcal{A}\overline{\frac{dC_B}{dt}} = \frac{1}{2}\mathcal{A}\overline{\frac{d|\phi|}{dt}} = -\kappa \int_{\mathcal{L}(t)} \nabla\phi \cdot \mathbf{n} dl, \tag{3.3}$$

where $\mathcal{A}$ is the total area of the domain and $\mathbf{n}$ a unit vector normal to $\mathcal{L}(t)$ pointing outward from D_A. We call $-\overline{\frac{d|\phi|}{dt}}$ the chemical speed. Furthermore, on every line element dl of $\mathcal{L}(t)$, the quantities $\frac{\kappa}{2}\nabla\phi \cdot \mathbf{n} dl$ of A and B are consumed. As a consequence, knowing the length of $\mathcal{L}(t)$ and the probability distribution of $|\nabla\phi|$ along it, gives a comprehensive statistical description of the chemistry in the domain.

If the trajectories are chaotic, equation (3.3) allows to link the chemical speed to the Lagrangian stretching properties of the trajectories as captured by the finite time Lyapunov exponents (FTLE), defined as the rate of exponential increase of the distance between the trajectories of two fluid parcels that are initially infinitely close. If $\boldsymbol{\delta l}(t)$ is the distance between two parcels that start at $\mathbf{x}$ and $\mathbf{x} + \boldsymbol{\delta l_0}$, then the FTLE $\lambda(\mathbf{x}, t)$ at $\mathbf{x}$ over the time interval t is

$$\lambda(\mathbf{x}, t) = \frac{1}{t} \max_{\alpha} \left\{ \ln \frac{|\boldsymbol{\delta l}|}{|\boldsymbol{\delta l_0}|} \right\}, \tag{3.4}$$

where the maximum is calculated over all the possible orientations α of $\boldsymbol{\delta l}_0$. The unit vector with the orientation $\psi_+(\mathbf{x}, t)$ of $\boldsymbol{\delta l}_0$ at the maximum defines a "singular vector" $\boldsymbol{\psi}_+(\mathbf{x}, t) \equiv (\cos\psi_+, \sin\psi_+)$. In the inviscid limit, it can be shown, with the conservation of tracer concentration for Lagrangian parcels, that $\lambda(\mathbf{x}, t)$ is also the rate of exponential increase of a gradient initially aligned with the unit vector $\boldsymbol{\psi}_-(\mathbf{x}, t) \equiv (-\sin\psi_+, \cos\psi_+)$ perpendicular to $\boldsymbol{\psi}_+$.

We can calculate FTLE and singular vectors in an incompressible flow using the velocity gradient tensor $\mathbf{S} \equiv \nabla\mathbf{u}(\mathbf{X}, t)$ along a trajectory $\mathbf{X}(\mathbf{x}, t)$. The distance

$\boldsymbol{\delta l}$ between two trajectories initially infinitely close is solution of $\frac{d\boldsymbol{\delta l}}{dt} - \mathbf{S}(t).\boldsymbol{\delta l} = 0$ and is given by $\boldsymbol{\delta l} = \mathbf{M}\boldsymbol{\delta l}(\boldsymbol{t = 0})$ where the resolvent matrix $\mathbf{M}$ is solution of $\frac{d\mathbf{M}}{dt} - \mathbf{S}(t).\mathbf{M} = 0$. The finite time Lyapunov exponent $\lambda(t)$ is given by the log of the largest eigenvalue of $[\mathbf{M}^T\mathbf{M}]^{\frac{1}{2t}}$, with $\boldsymbol{\psi}_+$ the associated eigenvector.

In ergodic chaotic dynamical systems, it has been shown that the FTLE converge to an infinite time Lyapunov exponent independent of the initial position $\mathbf{x}$, while the singular vectors converge to the forward Lyapunov vector $\boldsymbol{\Psi}_+ \equiv (\cos\Psi_+, \sin\Psi_+)$ that depend on $\mathbf{x}$ (Osedelec theorem, *Oseledec* (1968)). The convergence of the Lyapunov exponent is very slow and algebraic in time (*Tang and Boozer*, 1996) while the convergence of the Lyapunov vector is much faster, and typically exponential (*Goldhirsch et al.*, 1987). A discussion specific to high Reynolds number two-dimensional Navier-Stokes flows is available in *Lapeyre* (2002). Here we will only take into account the time dependence of the FTLE, assuming the singular vector field is only a function of space, not of time, equal to the forward Lyapunov vector field. This assumption will allow us to link the evolution of a gradient along a trajectory to the Lagrangian straining properties of the flow, while taking into account the diffusion (see (3.11) below)

An element $\boldsymbol{\delta l_0} = |\boldsymbol{\delta l_0}|\,(\cos\alpha, \sin\alpha)$ of the contact line at the initial time is advected at time t into an element $\boldsymbol{\delta l}$ whose squared norm is

$$\begin{aligned} |\boldsymbol{\delta l}|^2 &= \boldsymbol{\delta l_0}^T \mathbf{M}^T\mathbf{M}\boldsymbol{\delta l_0} \\ &= |\boldsymbol{\delta l_0}|^2 \left[e^{2\lambda t}\cos^2(\psi_+ - \alpha) + e^{-2\lambda t}\sin^2(\psi_+ - \alpha)\right] \end{aligned} \tag{3.5}$$

Noting that the angle $\psi_+ - \alpha$ is random (the contact line is chosen independently of the flow), we can show, averaging over λ, ψ_+ and α, that the total ensemble average

length of the contact line is (brackets are for an ensemble average):

$$\begin{aligned}&\langle L\rangle(t) = \\ &L_0 \int_0^{\pi} \int_0^{\infty} \tfrac{d\gamma}{\pi} dl P_\lambda(t,l) \sqrt{e^{2lt}\cos^2\gamma + e^{-2lt}\sin^2\gamma},\end{aligned} \tag{3.6}$$

with L_0 the initial length of $\mathcal{L}$ and $P_\lambda(t,l)$ the time dependent probability density of λ. Henceforth, the integration bounds over l and γ will be implicit and the same as in (3.6). This expression is valid when the diffusion is not taken into account. For large times, when two filaments are brought together at a distance smaller that the diffusive cutoff, they merge under the action of diffusion. We think the time span of this regime to be well approximated by the mix-down time scale $T_{mix} \approx \frac{1}{2\lambda} \ln L_e \sqrt{\frac{\lambda}{\kappa}}$ from the largest scale L_e of the flow to the diffusive cutoff (*Thuburn and Tan*, 1997). If the strain S is an estimation of λ, which is the case for the flow we study section V and VI (figure 3–1), and if $\frac{2}{S}$ is an estimate for the integral time scale T of the flow, which is also true in our flow, we get that

$$T_{mix} \approx T \ln Pe = T \ln RePr, \tag{3.7}$$

where Pe is the Peclet number, Re the Reynolds number and $Pr = \frac{Pe}{Re}$ the Prandtl number. Our previous work *Ait-Chaalal et al.* (under review) has shown that (3.6) is very accurate on time scales of the order of T_{mix} in the flow we describe in section V.

We follow an element $\boldsymbol{\delta l_0}$ of the initial contact line along a Lagrangian trajectory $\mathbf{X}_\mathcal{L}$ and we define the coordinate $\mathbf{r}$ corresponding to a frame co-moving with $\mathbf{X}_\mathcal{L}$:

$$\mathbf{r} = \mathbf{x} - \mathbf{X}_\mathcal{L}, \tag{3.8}$$

where $\boldsymbol{x}$ is the Eulerian coordinate. We can write the advection-diffusion reaction in this frame and assume the existence of a local 1-D solution $\chi_t(z)$, with z the coordinate normal to the contact line, because the tracers have a filamentary structure.

Linearizing the velocity in $\boldsymbol{r}$ in the comoving frame because the velocity is large scale and using the stationarity of the Lyapunov vectors, we can show that, for an initial profile of tracer $A_0\delta(z)$, with δ the Dirac delta function, the solution is (*Ait-Chaalal et al.*, under review):

$$\begin{aligned}\chi_t(z) &= A_0 \,\mathrm{Erf}\left(\tfrac{zG}{2\sqrt{\kappa}}\right)\\ \text{with } G &= \sqrt{\tfrac{e^{2\lambda t}\cos^2(\Psi_+-\alpha)+e^{-2\lambda t}\sin^2(\Psi_+-\alpha)}{\tau e^{2\lambda t}\cos^2(\Psi_+-\alpha)+\widetilde{\tau}\sin^2(\Psi_+-\alpha)}}.\end{aligned} \tag{3.9}$$

The concentration A_0 is the initial concentration of reactants A and B in their respective domain. The function Erf is the Gauss error function defined on $\mathbb{R}$ as follows: $x \longmapsto \frac{2}{\sqrt{\pi}}\int_0^x e^{-t^2}dt$. The two quantities τ and $\tilde{\tau}$ are:

$$\tau = \frac{\int_0^t e^{2u\lambda(u)}du}{e^{2t\lambda(t)}} \text{ and } \widetilde{\tau} = \int_0^t e^{-2u\lambda(u)}du. \tag{3.10}$$

The time τ has been introduced through the wavenumber growth along Lagrangian trajectories by *Antonsen et al.* (1996) and was called an equivalent time by *Haynes and Vanneste* (2004). Because the trajectories are chaotic, $\frac{1}{\tau}$ is the stretching rate in the recent past (i.e approximately over the last correlation time). *Haynes and Vanneste* (2004) have argued that when the correlation time of the stretching is much smaller than the time scale of the decay of the mean Lyapunov exponent, τ becomes independent of λ at large times and that its probability distribution converges to a time independent form. The time $\widetilde{\tau}$ is also an equivalent time that measures the stretching rate in the early part of the trajectory. As a consequence, we expect τ and $\widetilde{\tau}$ to have the same statistics, to be asymptotically equivalent as $t \to 0$ (typically for times smaller than the correlation time of the stretching) and to become independent at larger times. From (3.9), we can see that the gradient along the contact line $|\nabla\phi_{\mathcal{L}}| \equiv \frac{\partial\chi_t(z)}{\partial z}\big|_{z=0}$ is:

$$|\nabla\phi_{\mathcal{L}}| = \tfrac{A_0}{\sqrt{\pi\kappa}}G \tag{3.11}$$

3.3 Probability distribution of the reactant gradients on the contact line

The distribution of $|\nabla\phi_{\mathcal{L}}|\,\frac{\sqrt{\pi\kappa}}{A_0}$ on the contact line can be inferred from the joint distribution of G (eq. 3.11) and λ when we considered an ensemble of trajectories on the the contact line. In particular, it does not depend on κ. the probability density function (pdf) of $|\nabla\phi_{\mathcal{L}}|\,\frac{\sqrt{\pi\kappa}}{A_0}$ along the contact line $P_{G,\mathcal{L}}$ is given by:

$$P_{G,\mathcal{L}}(t,g) = \frac{\iint \frac{d\gamma}{\pi} dl P_{G,\lambda}(t,g,l)\sqrt{e^{2lt}\cos^2\gamma + e^{-2lt}\sin^2\gamma}}{\iint \frac{d\gamma}{\pi} dl P_{\lambda}(t,l)\sqrt{e^{2lt}\cos^2\gamma + e^{-2lt}\sin^2\gamma}}, \tag{3.12}$$

where we have introduced the joint pdf $P_{G,\lambda}$ of G and λ. Considering an orbit characterized by $(\lambda,\tau,\widetilde{\tau},\Psi_+,\alpha)$, expression (3.12) can be derived noting that $\frac{\sqrt{\pi\kappa}}{A_0}\,|\nabla\phi_{\mathcal{L}}|$ is equal to $G(t,\lambda,\tau,\widetilde{\tau},\Psi_+,\alpha)$ on a fraction of the contact line

$$\frac{|\boldsymbol{\delta l}|\,/\,|\boldsymbol{\delta l_0}|}{\langle L\rangle/L_0} = \frac{\sqrt{e^{2\lambda t}\cos^2(\Psi_+-\alpha) + e^{-2\lambda t}\sin^2(\Psi_+-\alpha)}}{\iint \frac{d\gamma}{\pi} dl P_{\lambda}(t,l)\sqrt{e^{2lt}\cos^2\gamma + e^{-2lt}\sin^2\gamma}}. \tag{3.13}$$

For times such that $t \gg \frac{1}{4\lambda}$, the sine terms in (3.12) can be neglected: the gradients are equilibrating with the flow and the time asymptotic form of G is $\frac{1}{\sqrt{\tau}}$ (see (3.9)). As a consequence, for $t \gg \frac{1}{4\lambda} \approx \frac{T}{4}$, $P_{G,\mathcal{L}}(t,g)$ is asymptotically equivalent to $P_{G,\mathcal{L},\infty}$:

$$P_{G,\mathcal{L}}(t,g) \sim P_{G,\mathcal{L},\infty}(t,g) = \frac{\int dl P_{\frac{1}{\sqrt{\tau}},\lambda}(t,g,l)e^{lt}}{\int dl P_{\lambda}(t,l)e^{lt}}, \tag{3.14}$$

where $P_{\frac{1}{\sqrt{\tau}},\lambda}$ is the joint pdf of $\frac{1}{\sqrt{\tau}}$ and λ. It is worth noting that if τ and λ were independent, which is expected at the very long times, the pdf of g along the contact line would be equal to the pdf of $\frac{1}{\sqrt{\tau}}$. This can be seen writing the bivariate density $P_{\frac{1}{\sqrt{\tau}},\lambda}$ as the product of its marginal densities in (3.14).

3.4 Probability distribution of the reactants concentrations

The reactants are in stoichiometric quantity and their initial concentration in their respective domain is A_0. As a consequence, it follows from (3.1) that the pdfs of C_A, C_B can be inferred directly from the pdf of $|\phi|$. The corresponding random

variable will be noted Φ. Our objective is to understand its dependence with κ and with time, as well as its shape.

The profile of the tracer gradient close to the contact line is given by (3.9), an expression that should be valid as long as the contact line is well-defined with a curvature larger than $\frac{\sqrt{\kappa}}{g}$, which is expected as long as $t < T_{mix}$. We assume that an $\epsilon \ll 1$ can be chosen such that, for all members, the length

$$\delta_t = 2\chi_t^{-1}\big(A_0(1-\epsilon)\big) = \frac{4\sqrt{\kappa}}{G}\,\mathrm{Erf}^{-1}(1-\epsilon) \tag{3.15}$$

satisfies $L_a \equiv \sqrt{\mathcal{A}} \gg \delta_t \gg \sqrt{\kappa\tau}$. The range $[-\frac{\delta_t}{2}, \frac{\delta_t}{2}]$ is where $|\chi_t|$ takes values smaller than $A_0(1-\epsilon)$. This can be seen noting that χ_t is a monotonic odd increasing function with $\chi_t(\pm\frac{\delta_t}{2}) = \pm A_0(1-\epsilon)$. In fact, we have $\frac{L_a}{\sqrt{\kappa\tau}} \ll 1$ because $\frac{L_a}{\sqrt{\frac{\kappa}{S}}} \sim \sqrt{Pe}$ is very large by assumption (the Peclet number in the simulations presented in section VI will be of the order of 10^3 to 10^5). However, $\frac{1}{\tau}$ is in general different from S: the former measures a Lagrangian stretching rate in the recent past while the latter measures an Eulerian stretching rate (for a comparison in the flow considered in section VI, one can refer to figure 1, noting that the strain is the Lyapunov exponent at small times). It is possible to choose δ_t far from both L_a and $\sqrt{\kappa\tau}$ because we are considering a well-defined contact line between areas of well mixed reactants. As mentioned earlier, this is expected to be true for $t < T_{mix}$.

If we consider a profile χ_t of tracer around the contact line in the range $[-\frac{\delta_t}{2}, \frac{\delta_t}{2}]$, the cumulative distribution function (cdf) of Φ, i.e. the probability of having Φ smaller than a given value ϕ, is

$$f_\Phi(\phi) = \frac{\chi_t^{-1}(\phi)}{\frac{\delta_t}{2}} = \frac{\chi_t^{-1}(\phi)}{\chi_t^{-1}(A_0(1-\epsilon)} = \frac{\mathrm{Erf}^{-1}(\frac{\phi}{A_0})}{\mathrm{Erf}^{-1}(1-\epsilon)} \tag{3.16}$$

and stands for values of ϕ in the range $[0, A_0(1-\epsilon)]$. We multiply by $\frac{\langle\delta_t\rangle\langle L\rangle}{\mathcal{A}}$ to obtain the cdf F_ϕ in the whole domain of area $\mathcal{A}$ because values in the range $[0, A_0(1-\epsilon)]$

are achieved on a sub-domain of area $\langle\delta_t\rangle\langle L\rangle$:

$$F_\Phi(\phi) = \frac{\langle\delta_t\rangle\langle L\rangle}{\mathcal{A}} \frac{\mathrm{Erf}^{-1}(\frac{\phi}{A_0})}{\mathrm{Erf}^{-1}(1-\epsilon)}. \tag{3.17}$$

Using equation (3.15) to calculate $\langle\delta_t\rangle$, we have:

$$F_\Phi(\phi) = \frac{4}{\mathcal{A}}\sqrt{\kappa}\langle L\rangle\langle\frac{1}{G}\rangle\,\mathrm{Erf}^{-1}(\frac{\phi}{A_0}) \text{ for } \phi \in [0, A_0(1-\epsilon)]. \tag{3.18}$$

Finally, the probability density is the derivative of the cdf with respect to ϕ:

$$P_\Phi(\phi) = \frac{4}{\mathcal{A}A_0}\sqrt{\kappa}\langle L\rangle\langle\frac{1}{G}\rangle\,\mathrm{Erf}^{-1'}\left(\frac{\phi}{A_0}\right) \text{ for } \phi \in [0, A_0(1-\epsilon)]. \tag{3.19}$$

A direct consequence of well mixed reactants away from the well-defined contact line is the term $\mathrm{Erf}^{-1'}$ (derivative of the inverse of the Gauss error function). It expresses that the shape of the pdf is an increasing function and can be directly related to the shape of the profile of the tracer field close to the contact line. The density P_Φ is proportional to $\sqrt{\kappa}\langle L\rangle$ because the area where the field ϕ takes non-trivial values (i.e significantly different from the initial value A_0) is proportional to $\sqrt{\kappa}\langle L\rangle$: its length is $\langle L\rangle$ while its width is controlled by diffusive processes. Finally the term $\langle\frac{1}{G}\rangle$ depicts the effect of the mean gradient, with a decrease of the gradient along the contact line explaining an increase in the probability of small values of $|\phi|$.

3.5 Statistics of the Lagrangian stretching properties in a two-dimensional Navier-Stokes flow

The numerical model integrates the following vorticity equation using the pseudo-spectral method:

$$\frac{\partial\omega}{\partial t} + \mathbf{u}\cdot\nabla\omega = F - R_0\omega + \nu\nabla^2\omega, \tag{3.20}$$

where ω is the vorticity, F a forcing term at wavenumber 3:

$$F_{\mathbf{k}} = \begin{cases} 0.002 \text{ if } \mathbf{k} = (\pm 3, 0) \text{ and } \mathbf{k} = (0, \pm 3) \\ 0 \text{ otherwise} \end{cases} \tag{3.21}$$

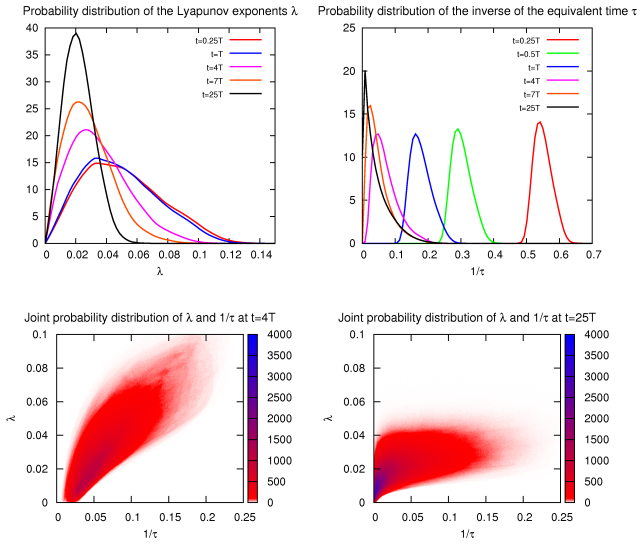

Figure 3–1: Probability density of the Lyapunov exponents (top left), of the inverse of the equivalent time τ defined in (3.10) (top right) for $0 < t \leq 25T$. We note that the density of λ at $t = 0.25T$ is roughly the density of the strain. At the bottom, their joint density at $t = 4T$ (left) and $t = 25T$ (right).

$R_0 = 0.0002$ the Rayleigh friction and $\nu = 5.57\,10^4$ the viscosity. The equation is integrated in a doubly periodic box $[-\pi, \pi] \times [-\pi, \pi]$ on a 512×512 grid. The integral time scale of the flow $T \equiv \sqrt{\frac{2}{\langle \omega^2 \rangle}} \approx \frac{2}{S}$, where the brackets stand for an ensemble average, will be used to normalize the time axis. The Reynolds number is of the order of 10^3.

Trajectories are computed using a fourth order Runge-Kutta scheme with a trilinear interpolation on the velocity field. On each trajectory, we integrate the resolvent matrix $\mathbf{M}$ such that $\frac{d\mathbf{M}}{dt} = \mathbf{SM}$ with $\mathbf{S} = \frac{\partial u_j}{\partial x_i}$ the velocity gradient tensor along the trajectory and $\mathbf{M}(t = 0)$ the identity matrix. The largest eigenvector of the symmetric positive matrix $\mathbf{M}^T\mathbf{M}$ is $e^{2\lambda t}$, where λ is the Lyapunov exponent on the trajectory at the finite time t. This method is described in more detail in *Abraham and Bowen* (2002). We also calculate the equivalent times τ and $\widetilde{\tau}$ through a numerical integration of (3.10). The trajectories are computed for hundred

realizations of the flow, each realization spanning 25 turnover times. This gives access to the statistics of λ, τ, $\widetilde{\tau}$ and G involved in equations (3.12) and (3.14).

Figure 3–1 shows the time evolution of the pdf of λ and $\frac{1}{\tau}$. The pdf of λ converges to the pdf of the strain P_s as $t \to 0$ because the strain is the FTLE on each chaotic orbit for an infinitely small time (see (3.4)). The pdf does not evolve much during the first turnover time, as the correlation time is expected to be of the order of T, or larger. Then, the variance of the FTLE decreases while the density shifts toward smaller values as time increases. The peak of the density saturates at $\lambda_{max} = 0.02$, which we think is a rough estimate of the infinite time Lyapunov exponent. For a more detailed description of the FTLE, the reader can refer to *Ott* (2002) in chaotic flows, to *Lapeyre* (2002) in two-dimensional turbulence and to *Abraham and Bowen* (2002); *Ngan and Shepherd* (1999b); *Waugh and Abraham* (2008) in geophysical flows. For times smaller than one turnover time, the pdf of $\frac{1}{\tau}$ shifts toward smaller value, its shape being only slightly affected. This can be interpreted assuming that λ does not evolve much on trajectories and can be estimated by the strain S where the trajectory originates. Hence, $\tau \approx 2S/(1 - e^{-2St})$, which gives $\frac{1}{\tau} \approx \lambda + \frac{1}{t}$ for $t \ll \frac{1}{2S}$. The pdf $P(t, x)$ of $\frac{1}{\tau}$ is then approximated by $P_s(x - \frac{1}{t})$ where P_s is the pdf of the strain. In addition, as we expected in section II, we observe that the density of $\frac{1}{\tau}$ converges to a time independent form.

Figure 3–1 also shows the joint pdf of λ and $\frac{1}{\tau}$ at $t = 4T$, well within the time range where we think (3.12) should be a satisfying description of the gradient pdf. The joint pdf at $t = 25T$ shows this dependence is still important at large times. Previous studies (e.g *Antonsen et al.* (1996)) have assumed the independence between λ and τ at long times. This is relevant in simple chaotic flows. However, two dimensional Navier-Stokes flow exhibit coherent structures (vortices, filaments of vorticity, etc...) probably making the Lagrangian correlation time dependent on

the trajectories. In particular, very long correlation times could be associated with trajectories trapped in vortices, where the stretching rate is particularly weak. This could explain the strong dependence between large values of τ and small values of λ.

3.6 Numerical results

3.6.1 Gradients along the contact line

The numerical simulations are performed for eight different Prandtl numbers $Pr \equiv \frac{\nu}{\kappa} = 2^i$ for $0 \leq i \leq 7$. For each one we run an ensemble of 34 simulations integrating equations (3.2) and (3.20) in the periodic box. Each member is defined by its initial condition on the flow, taken as the vorticity field every turnover time of a long time simulation of the statistically stationary flow solution of (3.20). For each member, we use the following initial condition on the tracer:

$$\phi(x, y, t = 0) = 2A_0(H(x) - \frac{1}{2}) \text{ for } (x, y) \in [-\pi, \pi]^2, \tag{3.22}$$

where H is the Heaviside step function. In other words, in one half of the box, $C_A = A_0$ and $C_B = 0$, and in the other half $C_A = 0$, and $C_B = A_0$. A and B are separated by initially infinite gradients. This is not exactly true in the numerical integrations because of the finite resolution of the model and has to be kept in mind for an accurate interpretation of the numerical results.

For each member we determine the coordinates of the contact line $\mathcal{L}$ with a time increment $\frac{T}{4}$ using the library DISLIN (*Michels*, 2010)). We calculate the modulus of the gradient of ϕ at each of these coordinates using bilinear interpolation. We then multiply it by $\frac{\sqrt{\pi\kappa}}{A_0}$ in order to obtain a physical quantity that scales like G in equation (3.9) and which we name $G_{e,Pr}$. A weighted histogram of $G_{e,Pr}$ is calculated every time increment $\frac{T}{4}$ using as weight the length enclosed by three consecutive points of $\mathcal{L}$ centered in the point where $G_{e,Pr}$ is estimated. This is necessary since the points

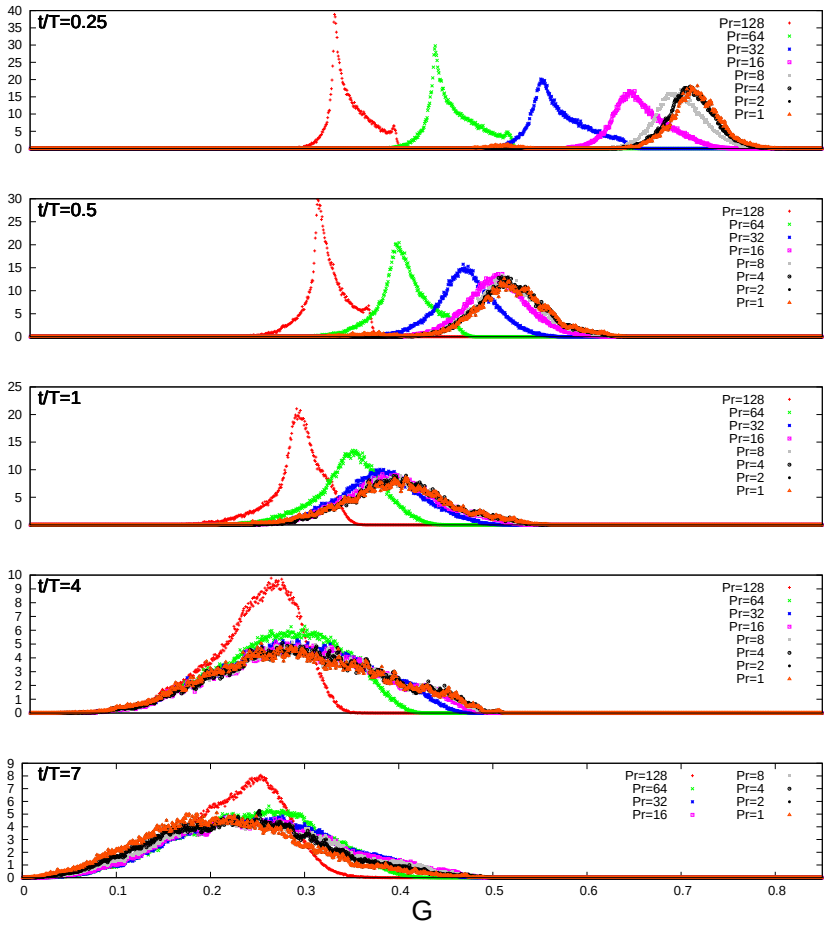

Figure 3–2: Probability density $P_{G,1\leq Pr\leq 128}$ of $G_{e,Pr} = \frac{\sqrt{\pi\kappa}}{A_0}|\nabla\phi_{\mathcal{L}}|$ where $|\nabla\phi_{\mathcal{L}}|$ is the modulus of the gradient of ϕ along the line $\mathcal{L} = \{\mathbf{x}|\phi(\mathbf{x}) = 0\}$. These pdf are obtained from an ensemble of 34 direct numerical simulations and plotted here for $t = \frac{1}{4}T, \frac{1}{2}T, T, 4T$ and $7T$

are not equidistant. The probability densities obtained after normalization of these histograms are noted $P_{G,Pr}$.

On figure 3–2 we plot $P_{G,Pr}$ for different Prandtl numbers and different times. We observe:

- When time becomes shorter, as observed from $t = 4T$ to $t = 0.25T$, the independence of $G_{e,Pr}$ to Pr, as predicted in sections III and IV, is not verified. As a matter of fact, the gradient cannot be considered as infinite at the initial time because of the finite grid size of the numerical model. This effect can be quantified: we can solve the advection diffusion equation in a Lagrangian co-moving frame with a contact line element for the tracer profile around this line with the initial condition on the gradients $\frac{\partial \chi_t}{\partial z}|_{t=0} = \frac{A_0}{2\delta_0\sqrt{\pi}} e^{-\frac{x^2}{4\delta_0^2}}$ (δ_0 is a length corresponding to a grid point). We get:

$$\begin{array}{l} |\nabla \phi_{\mathcal{L}}| = \frac{A_0}{\sqrt{\pi\kappa}} G_\kappa \\ \text{with } G_\kappa = \sqrt{\frac{e^{2\lambda t}\cos^2(\Psi_+ - \alpha + e^{-2\lambda t}\sin^2(\Psi_+ - \alpha)}{\frac{\delta_0^2}{\kappa} + [\tau e^{2\lambda t}\cos^2(\Psi_+ - \alpha) + \widetilde{\tau}\sin^2(\Psi_+ - \alpha)]}}, \end{array} \tag{3.23}$$

  where G_κ now depends on diffusion through the term $\frac{\delta_0^2}{\kappa}$ (this expression has to be compared to G in (3.9)). The initial gradient cannot be assumed infinite when the diffusive cutoff $\sqrt{\kappa\tau}$ is of the order of the grid size δ_0. The time scale T_{Pr} where this effect is important can be evaluated by comparing the two terms $\frac{\delta_0^2}{\kappa}$ and $[\tau e^{2\lambda t}\cos^2(\Psi_+ - \alpha) + \widetilde{\tau}\sin^2(\Psi_+ - \alpha)]$ in the denominator of G_κ^2. Approximating λ with S, we find $T_{Pr} \approx \frac{1}{2S}\ln(1 + \frac{2\delta_0^2}{\frac{\nu}{S}}Pr)$, which gives respectively $T_{Pr}/T = 0.12; 0.25; 0.45; 0.75; 1.2; 1.6$ for $Pr = 4; 8; 16; 32; 64; 128$. This calculation is consistent with the numerical results presented on figure 3–2, the pdf $P_{G,Pr}$ being independent of Pr for $t \gtrsim T_{Pr}$

- At $t = 4T$, the densities $P_{G,Pr=128}$ and $P_{G,Pr=64}$ are different from $P_{G,Pr\leq 32}$. Because of the finite resolution of the model, gradients at the high end of these

distributions cannot be resolved. This explains the strong asymmetry of these densities. This effect is also observed at other times: in particular, it explains the kick at the very high end of the densities $P_{G,Pr\geq 32}$ at $t = 0.25T$.

- At $t = 7T$, the densities $P_{G,Pr}$ are not anymore independent of Pr because we are at $t \gtrsim T_{mix}(\kappa)$ for all the Prandtl numbers

In order to remain consistent with the infinite initial gradient hypothesis, we will only consider small enough Prandtl numbers. We compare on figure 3–3 the numerical results to the theoretical predictions $P_{G,\mathcal{L}}$ (3.12), $P_{G,\mathcal{L},\infty}$ (3.14), and to the pdf of $\frac{1}{\sqrt{\tau}}$.

- For $t \lesssim T$, only $P_{G,\mathcal{L}}$ shows some success in predicting $P_{G,Pr}$. This is consistent with (3.12) which states that the effect of γ cannot be neglected at times smaller than T.
- For $t = 4T$, $P_{G,\mathcal{L}}$ and $P_{G,\mathcal{L},\infty}$ are much more similar because the contact line elements have equilibrated with the flow (their orientation does not depend anymore on their initial orientation α). The agreement between $P_{G,\mathcal{L}}$ and $P_{G,Pr}$ is very good.
- For $t = 7T$, $P_{G,\mathcal{L}}$ and $P_{G,\mathcal{L},\infty}$ are even closer. $P_{G,\mathcal{L},\infty}$ fails to predict $P_{G,Pr=1}$ but performs reasonably for $P_{G,Pr=32}$. Actually, an estimate of T_{mix} from (3.7) gives $4.5T$ for $Pr = 1$ and $6.5T$ for $Pr = 32$, which is consistent with the discrepancy between $P_{G,Pr=1}$ and $P_{G,Pr=32}$ at $t = 7T$.

It is worth observing that the pdf of $\frac{1}{\sqrt{\tau}}$ fails to predict $P_{G,Pr}$ because of the dependence of λ with τ, which is significant even at very long times (section V)[1] . We observe that the time scale for the much simpler $P_{G,\mathcal{L},\infty}$ to become a good prediction

[1] The similarity between the pdf of $\frac{1}{\sqrt{\tau}}$ and $P_{G,Pr=1}(t = 7T)$ (figure 3–3) is not explained by our theory, as showed by the significant difference between the pdf of $\frac{1}{\sqrt{\tau}}$ and $P_{G,\mathcal{L}}$.

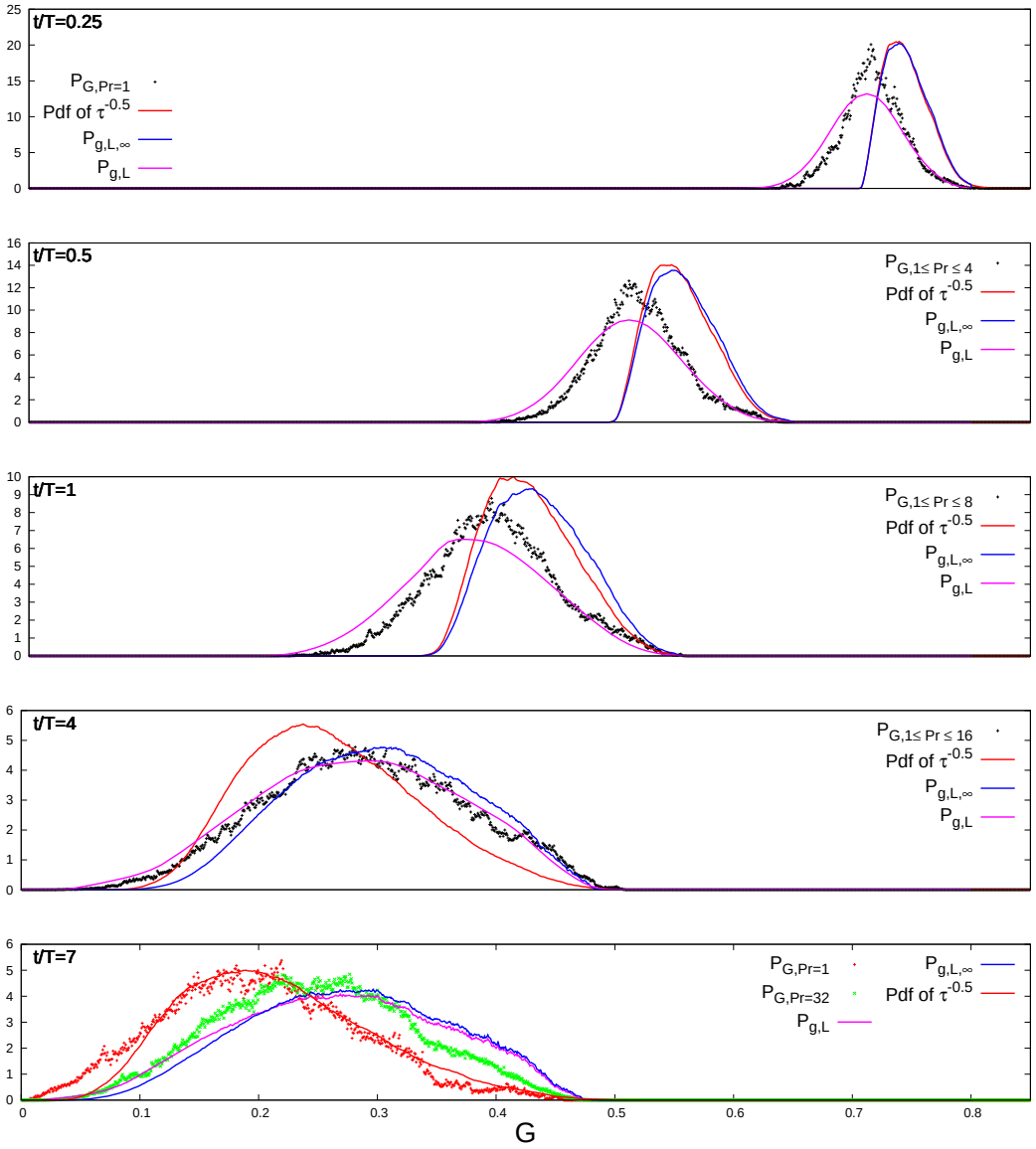

Figure 3–3: Comparison between $P_{G,Pr}$ obtained from the direct numerical simulations and the theoretical predictions $P_{G,\mathcal{L}}$ (eq. 3.12), $P_{G,\mathcal{L},\infty}$ (eq. 3.14) and the pdf of $\frac{1}{\sqrt{\tau}}$ (τ is defined in (3.10)), obtained from the calculation of the Lagrangian stretching properties of the flow calculated with the trajectories. We have only plotted the curves $P_{G,Pr}$ corresponding to direct numerical simulations consistent with the infinite initial gradient hypothesis.

for the gradient, i.e the timescale for $P_{G,\mathcal{L}}$ to converge to $P_{G,\mathcal{L},\infty}$, seems to be of the order of T_{mix}. This non-trivial behavior may be determined by the dependence of τ with $\widetilde{\tau}$ (3.10). If we had $\tau \sim \widetilde{\tau}$, which is expected as $t \to 0$, this convergence would have been of the order of $\frac{1}{2\lambda} \approx \frac{1}{2S} \approx \frac{T}{2}$ (equations (3.11) and (3.12)). It is one order of magnitude longer. The reason could lie in the fact that $\widetilde{\tau}$ and τ quickly become independent.

Equation (3.12), where the joint pdf of λ and G is replaced by the joint pdf of λ and G_κ, is a fair approximation to $P_{G,Pr\leq 32}$ at any time (not shown). This extends our results to finite initial gradients, but concentrated on length scales not large compared to the diffusive cutoff of the flow, such that a Lagrangian straining theory approach remains possible.

3.6.2 Reactants' fields

We calculate the pdf Q_{Pr} of $\widetilde{\phi} \equiv A_0 - |\phi|$ using our 34 simulations ensemble for the entire range of Prandtl numbers. On figure 3–4, we show Q_{Pr} for $Pr = 1, 4, 8$ and 32 and for $0.25T \leq t \leq 7T$. Our objective is to compare the theoretical prediction (3.19) to these numerical results.

Figure 3–5 shows $\sqrt{Pr}Q_{Pr}$ for a wide range of Prandtl numbers over the first few turnover times. The dependence in $\sqrt{\kappa}$ predicted in (3.19) is well achieved, except at small times ($t = 0.25T$) especially for small diffusion ($Pr = 32$), i.e. when the infinite gradient assumption is again violated in the numerical simulations. It also fails at $t = 7T$ because $T > T_{mix}$.

Next, we compare the time dependence predicted in (3.19) to the numerical results. For $Pr = 8$, we show the product of Q_{Pr} with $\sqrt{Pr}\frac{1}{\langle 1/G\rangle\langle L\rangle}$ on figure 3–6. The contact line length $\langle L\rangle$ is calculated from P_λ using (3.6), and $\langle 1/G\rangle$ from the integral $\int_0^\infty \frac{1}{g} P_{G,\mathcal{L}}(t,g)dg$ where $P_{G,\mathcal{L}}$ is defined in (3.12). The densities P_λ and $P_{G,\mathcal{L}}$ are determined as explained in section V from the computation of Lagrangian

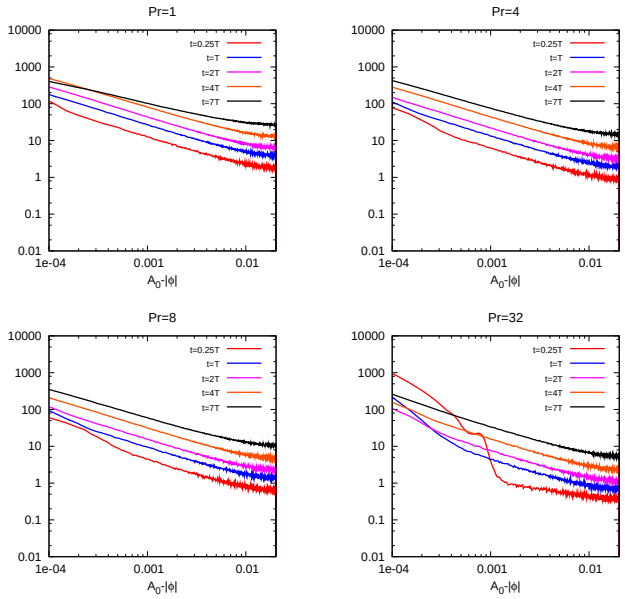

Figure 3–4: Numerically determined pdf Q_{Pr} of $\widetilde{\phi} \equiv A_0 - |\phi|$ at different times $t = \frac{1}{4}T, T, 2T, 4T$ and $7T$ and for Prandtl numbers $Pr = 1, 4, 8$ and 32. Log-log scale.

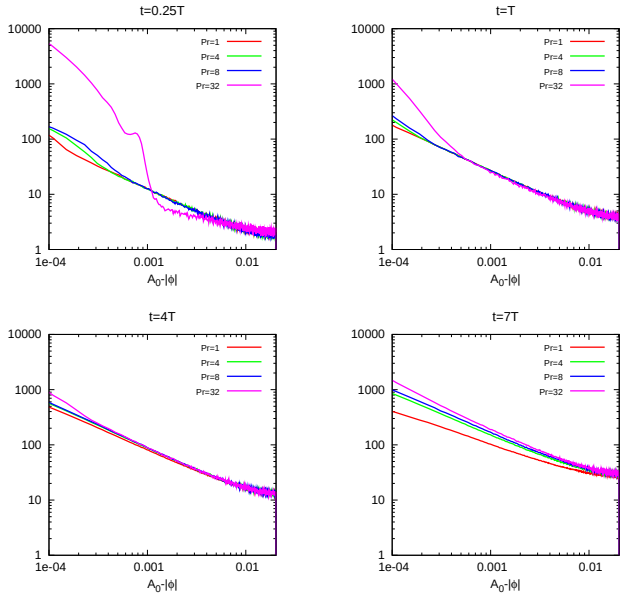

Figure 3–5: Numerically determined pdf Q_{Pr} of $\widetilde{\phi} \equiv A_0 - |\phi|$ multiplied by $\sqrt{Pr}$ for $Pr = 1, 4, 8$ and 32 and $t = \frac{1}{4}T, T, t = 4T$ and $7T$. Log-log scale.

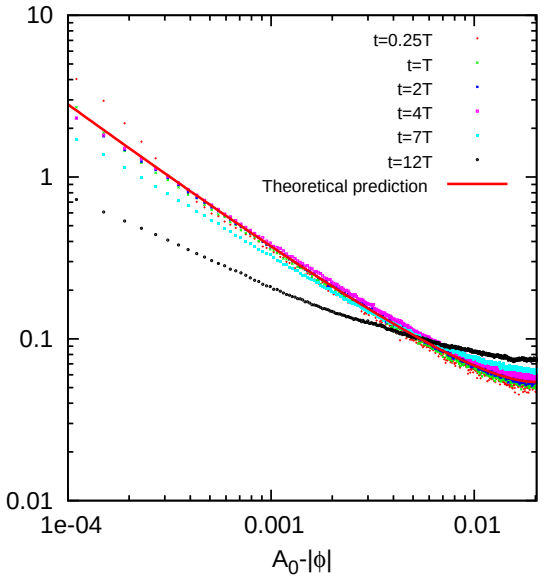

Figure 3–6: Time evolution of $Q_{Pr=8}\sqrt{Pr}\frac{1}{\langle 1/G\rangle\langle L\rangle}$. $\langle L\rangle$ and G are defined respectively in equations (3.6) and (3.9) and are calculated from trajectories, as described in section V. The red curve (theoretical prediction) corresponds $\frac{4\sqrt{\nu}}{\mathcal{A}A_0}\,\mathrm{Erf}^{-1'}\left(\frac{A_0-\tilde{\phi}}{A_0}\right)$, where Erf is the Gauss error function. Log-log scale.

trajectories. The curves converge together, except at very small times for values of $|\phi|$ close to A_0 ($\widetilde{\phi}$ close to 0). As expected, (3.19) does not work either for $t > T_{mix}$, as shown by the curves $t = 7T$ and $t = 12T$.

The shape of the reactants' pdf shown as $Q_{Pr=8}\sqrt{Pr}\frac{1}{\langle 1/G\rangle\langle L\rangle}$ on figure 3–6 is very well reproduced by $\frac{4\nu}{\mathcal{A}A_0}\,\mathrm{Erf}^{-1'}\left(\frac{A_0-\tilde{\phi}}{A_0}\right)$, which confirms the theoretical prediction (3.19).

3.7 Conclusion and discussion

We have considered the early regime of an instantaneous bimolecular chemical reaction in a two-dimensional Navier-Stokes flow, for segregated reactants initially separated by infinite gradients. The time scales considered here are shorter than the mix-down time scale from the integral length scale to the diffusive cutoff (T_{mix} given in (3.7)). Assuming that the singular vector associated with a FTLE does not depend on time and is equal to the forward Lyapunov vector, we have adopted a Lagrangian

straining theory approach and showed numerically its success in predicting (a) the statistics of the diffusive flux of fast reacting chemicals along their interface (3.12), and thus the chemical speed, (b) the probability distribution of the reactants (3.19). We have put the emphasis on the effect of the reactants diffusion, showing (a) that the distribution of the gradients along the contact line, rescaled by $\kappa^{\frac{1}{2}}$, does not depend on κ (b) that the distribution of the reactant concentration, when it is not too close to A_0, is proportional to $\kappa^{\frac{1}{2}}$.

At the very early stage, for about one turnover time, predicting these statistics requires knowing the joint statistics of λ, τ and $\widetilde{\tau}$ (equation 3.9). At moderate time scales (a few turnover times), the knowledge of the joint pdf of λ and τ is sufficient. More work is needed to understand these distributions, i.e the marginal distributions of λ, τ and $\widetilde{\tau}$ and how these three variables depend on each other.

Previous studies (*Waugh et al.*, 2006; *Waugh and Abraham*, 2008) investigating the two-dimensional mixing in the upper layer of the ocean suggest that it might be possible to recover the distribution of λ from the distribution of the strain (which is λ as $t \to 0$), a more accessible Eulerian quantity, and from the time evolution of the mean Lyapunov exponent $\langle\lambda\rangle$. Specifically, they observed that the distribution of $\frac{\lambda}{\langle\lambda\rangle}$ does not change significantly in time over several turnover times and is given by a Weibull distribution. We have observed the same behavior in our flow (not shown), with the distribution of the strain being very well approximated by a Weibull distribution of shape parameter 1.8[1] . The time evolution of $\langle\lambda\rangle$ in a chaotic ergodic flow was theoretically predicted by *Tang and Boozer* (1996), a prediction which was shown to perform well in the mixing layer of the ocean (*Abraham and Bowen*,

[1] This is very close to a Rayleigh distribution (Weibull distribution of shape parameter 2), which is the distribution of the norm of a vector whose components are independent from each other and follow Gaussian statistics

2002). The decrease of the Lyapunov exponent along a trajectory is related to the reorientation of the strain axis and to the effect of vorticity (e.g. *Chertkov et al.* (1995)). However, other mechanisms, specific to two-dimensional dynamically consistent Navier-Stokes flows (or in similar geophysical flows), could play a rôle. Although this deserves more investigation, we can speculate that parcels tend to stay longer in area of low strain than in areas of high strain. For example, a parcel can be captured in a vortex for a long time but travels very quickly in areas of high strain. Hence we would have two explanations for this shift: (a) the fact that regions with low strain (e.g vortices) have smaller velocities than regions of high strain; (b) the existence of barriers of transport at the edge of the vortices that act like parcel traps.

We have shown that the distribution of λ can be obtained from the strain distribution below one turnover time. Its time evolution at longer time scale has to be studied in more detail, especially its asymptotic form. The dependence between τ and λ is a complex issue which needs to be addressed. We expect it to be strongly dependent on the nature of the flow, especially on its Lagrangian correlation time. In our two-dimensional Navier-Stokes flow, areas of low stretching associated with long correlation times (e.g. vortices) could explain the strong dependence between λ and $\frac{1}{\tau}$ where they are both small compared to their ensemble mean (figure 3–1).

Some studies (e.g. *Fereday and Haynes* (2004); *Haynes* (2005)) have shown, both numerically and theoretically, the relevance of Lagrangian stretching theories when the length scale of the tracer are much smaller than the scale of the flow, like in the present study. However, this was done for simple prescribed smooth chaotic flows and in the long time decay. This theory was recently applied by *Tsang* (2009) to infinite chemistry in the long time decay. Here we apply it for the initial regime.

A comprehensive picture would be given by studying intermediate time scales, which will be the subject of a future paper.

CHAPTER 4
Decay of a passive tracer in a two-dimensional Navier-Stokes flow

In chapter 2, we explained that the concentration fields of two reactants A and B involved in an instantaneous bimolecular reaction can be inferred from a passive tracer ϕ defined as the difference between the two reactants' fields (equation (2.3)). Chapter 2 and chapter 3 dealt with the initial regime of the reaction between A and B. In chapter 4, we focus on the long-term decay of the passive tracer ϕ. This chapter consists of a preliminary version of a letter to be submitted to Physical Review Letters.

Chapter 4: Decay of a passive tracer in a two-dimensional Navier-Stokes flow

F. Ait-Chaalal [1], M.S. Bourqui[1,2] and P. Bartello[1,3]

[1]Department of Atmospheric and Oceanic Sciences, McGill University, Montréal, QC, Canada

[2]Department of Chemistry, McGill University, Montréal, QC, Canada

[3]Department of Mathematics and Statistics, McGill University, Montréal, QC, Canada

Preliminary version of a manuscript to be submitted to Physical Review Letters.

Abstract

We study numerically the decay of a passive tracer in a dynamically consistent flow solution of the two-dimensional Navier-Stokes equation and in the limit of small diffusion. We observe that the decay of the variance becomes quickly exponential. However, after a few tens of large-eddy turnover times, the decay rate changes. We interpret our results in light of theories developed for mixing in simple ergodic flows, in particular local Lagrangian stretching theories. It is found that they only can explain very partially the phenomenology we observe. In particular, they cannot capture the rôle of coherent vortices which is crucial, particularly in the very long-term decay.

4.1 Introduction: local Lagrangian stretching theories

The decay of a passive tracer ϕ in large-scale two-dimensional flows, like in chaotic advection or in the Batchelor regime turbulence, has been examined recently using local Lagrangian stretching theories (LLST). These are based on the decomposition of the tracer field in elementary sine (*Antonsen et al.*, 1996) or Gaussian functions (*Balkovsky and Fouxon*, 1999). Each element is followed on Lagrangian trajectories and the statistical and spectral properties of the field are recovered through an ensemble average on the stretching histories. In the limit of an infinitely small diffusion, theses theories predict the exponential decay of the variance $\langle\phi^2\rangle$, or mixing rate, the decay of higher order moments $\langle|\phi|^n\rangle$ (the brackets are for an ensemble average), the spectrum of variance (*Antonsen et al.*, 1996; *Yuan et al.*, 2000; *Fereday and Haynes*, 2004; *Haynes and Vanneste*, 2004; *Tsang et al.*, 2005) and the tracer probability distribution function (*Pierrehumbert*, 2000; *Sukhatme and Pierrehumbert*, 2002; *Fereday and Haynes*, 2004).

The decay of the statistical moments can be inferred from the probability density function (pdf) of the Lagrangian stretching rates, or finite-time Lyapunov exponents (FTLE). The FTLE λ measures the rate of exponential separation in time t of initially infinitely close trajectories. Large deviation theory (e.g. *Frisch* (1996); *Balkovsky and Fouxon* (1999); *Ott* (2002)) suggests that their pdf converges to a density proportional to $e^{-G(\lambda)t}$, where G, the rate or Cramèr function, is concave and satisfies $G(\lambda_0) = G'(\lambda_0) = 0$, where λ_0 is the mean Lyapunov exponent. Extending the results of *Balkovsky and Fouxon* (1999), which where obtained for a G parabolic or equivalently a Gaussian distribution, we conjecture that the decay rate γ_n^L of $\langle|\phi|^n\rangle$ is given by (the superscript L indicates that the result is obtained with

LLST):

$$\begin{cases} \gamma_n^L = \frac{n}{2}\lambda_* + G(\lambda_*) \quad \text{with} \quad G'(\lambda_*) = -n & \text{if} \quad \frac{n}{2} < -G'(0) \\ \gamma_n^L = G(0) & \text{if} \quad \frac{n}{2} \geq -G'(0) \end{cases} . \tag{4.1}$$

This corresponds to the expression for $n = 2$ in *Haynes and Vanneste* (2005). *Thiffeault* (2008) proposed a similar formulation but with $\frac{n}{2}$ replaced by n, which seems to be wrong.

Recently, the applicability of Lagrangian stretching theories has been questioned. It has been shown that they overestimated the mixing rate, sometimes by one order of magnitude, in real magnetically driven flows (*Voth et al.*, 2003). In addition, as showed in *Sukhatme and Pierrehumbert* (2002), they do not capture the phenomenology of the strange eigenmode observed in the long-term decay of a tracer in two-dimensional large-scale dynamical flows (*Pierrehumbert*, 1994; *Rothstein et al.*, 1999; *Sukhatme and Pierrehumbert*, 2002). The strange eigenmode is the factorization of the scalar field in a statistically stationary field and an exponentially decaying term. In particular it implies the selfsimilarity of the scalar field in time, when rescaled by the square root of the total variance. This is not consistent with the intermittency predicted by LLST (see equation (4.1)). The strange eigenmode is associated with tightly packed tracer filaments, the striation thickness corresponding to the diffusive cutoff (*Sukhatme and Pierrehumbert*, 2002).

However, it has been argued that LLST perform accurate predictions on the mixing rate and on higher order moments when the characteristic scale of the tracer is smaller than the velocity field scale (*Fereday and Haynes*, 2004; *Tsang et al.*, 2005; *Haynes and Vanneste*, 2005). Basically, LLST are thought to be valid when the tracer is initialized at small scales compared to the flow and on time scales that correspond to the mixing time from the flow scale L to the diffusive cutoff $\sqrt{\frac{\kappa}{S}}$ (κ

is the scalar diffusion, and S the average Eulerian strain, defined as the positive eigenvalue of the symmetric part of the velocity gradient tensor):

$$T_{mix} \approx \frac{1}{2S} \ln \frac{SL^2}{\kappa}. \tag{4.2}$$

After that, the decay of the tracer field is thought to be controlled by the decay of the gravest Fourier modes (*Fereday et al.*; *Sukhatme and Pierrehumbert*, 2002; *Fereday and Haynes*, 2004; *Haynes and Vanneste*, 2005). However, a LLST approach can predict the shape of the spectrum, even when the mixing rate is globally controlled and not predicted by LLST. This is because the characteristic time scale for variance to cascade from the largest scale to the diffusive cutoff is T_{mix}. The global control of the decay can be seen as an exponentially decaying injection of variance at the largest scale. Assuming a mixing rate γ_2, in general different from γ_2^L, *Fereday and Haynes* (2004) showed that $\gamma_2 \leq \gamma_2^L$ and suggested that the spectrum of variance, with k the horizontal wavenumber, is proportional to:

$$E(k,t,\kappa) \equiv e^{-\gamma_2 t} k^{-1-G'(\lambda_*)} \int d\tau P_\tau(\tau) e^{-2\kappa k^2 \tau}, \tag{4.3a}$$

$$\text{with } G(\lambda_*) - \lambda_* G'(\lambda_*) - \gamma_2 = 0 \tag{4.3b}$$

The function P_τ is the probability density function of $\tau \equiv \frac{\int_0^t e^{2u\lambda(u)} du}{e^{2t\lambda(t)}}$, a time measuring the stretching on a Lagrangian trajectory in the recent past. At sufficiently large time it becomes independent of λ and its pdf converges to a time independent form (*Antonsen et al.*, 1996; *Haynes and Vanneste*, 2004). When the decay rate is predicted by LLST, we have a spectrum proportional to

$$E^L(k,t,\kappa) = e^{-\gamma_2^L t} \int d\tau P_\tau(\tau) e^{-2\kappa k^2 \tau} \equiv e^{-\gamma_2^L t} E_0^L(k,\kappa) \tag{4.4}$$

which is flat in the inertial range. When γ_2 goes to 0, the spectrum converges to a Batchelor-like k^{-1} spectrum. It was argued that the validity of LLST to describe

the full phenomenology of the decay can be inferred from the observation of a flat spectrum k^0 (*Tsang et al.*, 2005).

4.2 Objectives and methodology

The theory we have briefly reviewed was built upon numerical simulations of simple kinematic flows, i.e. prescribed flows that are not solution of the equation of motion. Here we examine how this phenomenology applies to the decay of a tracer in a large-scale dynamically consistent flow solution of the barotropic two-dimensional Navier-Stokes equation:

$$\frac{\partial \omega}{\partial t} + \mathbf{u} \cdot \nabla \omega = F - R_0 \omega + \nu \nabla^2 \omega, \tag{4.5}$$

The vorticity $\nabla \times \mathbf{u}$ is denoted ω, F is a forcing term at wavenumber 3 to have a large scale flow, $R_0 = 0.0002$ is the Rayleigh friction and $\nu = 5.57\,10^4$ is the viscosity. The Reynolds number is of the order of 10^3. The equation is integrated using the pseudospectral method. We define $T \equiv \sqrt{\frac{2}{\langle \omega^2 \rangle}}$ the large-eddy turnover time. A passive tracer ϕ in this flow obeys:

$$\frac{\partial \phi}{\partial t} + \mathbf{u} \cdot \nabla \phi = \kappa \nabla^2 \phi. \tag{4.6}$$

We use different diffusions corresponding to Prandtl numbers $Pr \equiv \frac{\nu}{\kappa} =$ $1; 8; 16; 32; 64; 128$. We run two ensembles of 40 simulations with two different initial conditions:

$$\phi(x, y, t = 0) = A_0 \operatorname{sgn} x \qquad \text{INIT\_HEAVI} \tag{4.7}$$

$$\phi(x, y, t = 0) = A_0 \frac{\pi^2}{4} \cos x \cos y \qquad \text{INIT\_COS.} \tag{4.8}$$

A_0 is a constant that fixes the initial total concentration. Each member of the ensemble is distinguished by the initial condition on the vorticity, taken within a long-term run of the statistically stationary solution of (4.5).

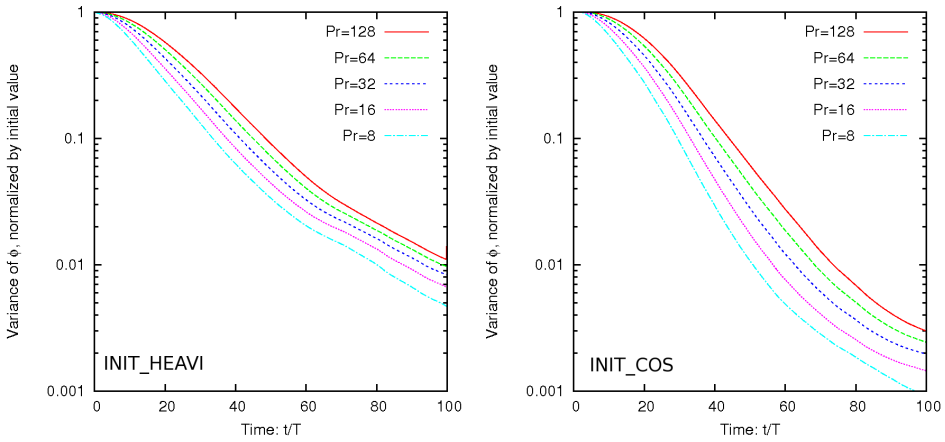

Figure 4–1: Decay of the tracer variance for $Pr \equiv \frac{\nu}{\kappa} = 8; 16; 32; 64; 128$ and for the two initial conditions INIT_HEAVI (4.7) and INIT_COS (4.8). The variance is normalized by its initial value. The scale is logarithmic on the abscissa.

4.3 Results

For INIT_HEAVI, we observe two exponential decays. The first one occurs from $t \approx 25T$ to $t \approx 60T$, and the second one from $t \approx 70T$. The decays for both initial conditions are pictured on figure 4–1. These two consecutive exponential decays have not been observed in the literature to our knowledge. We will refer to them as regime I and regime II. For INIT_COS, the second exponential decay is not very clear. However, we will refer to regime II for INIT_COS when considering diagnostics for $t \gtrsim 70T$.

4.3.1 Decay in regime I

In regime I, the decay rate of the n-order moment γ_n has an anomalous scaling with n, as shown on figure 4–2 and the tracer pdf evolves in time (figure 4–3, left panels). This could suggest that LLST are valid. In order to check it, we have estimated γ_2^L from the distribution of the FTLE in our flow, however it is not accurate enough to make quantitative conclusions. In addition, the convergence of $\gamma_2(\kappa)$ to γ_2^L is expected to be very slow (*Haynes and Vanneste* (2005)), which makes difficult the determination of the the infinitely-small diffusion mixing rate from finite diffusion

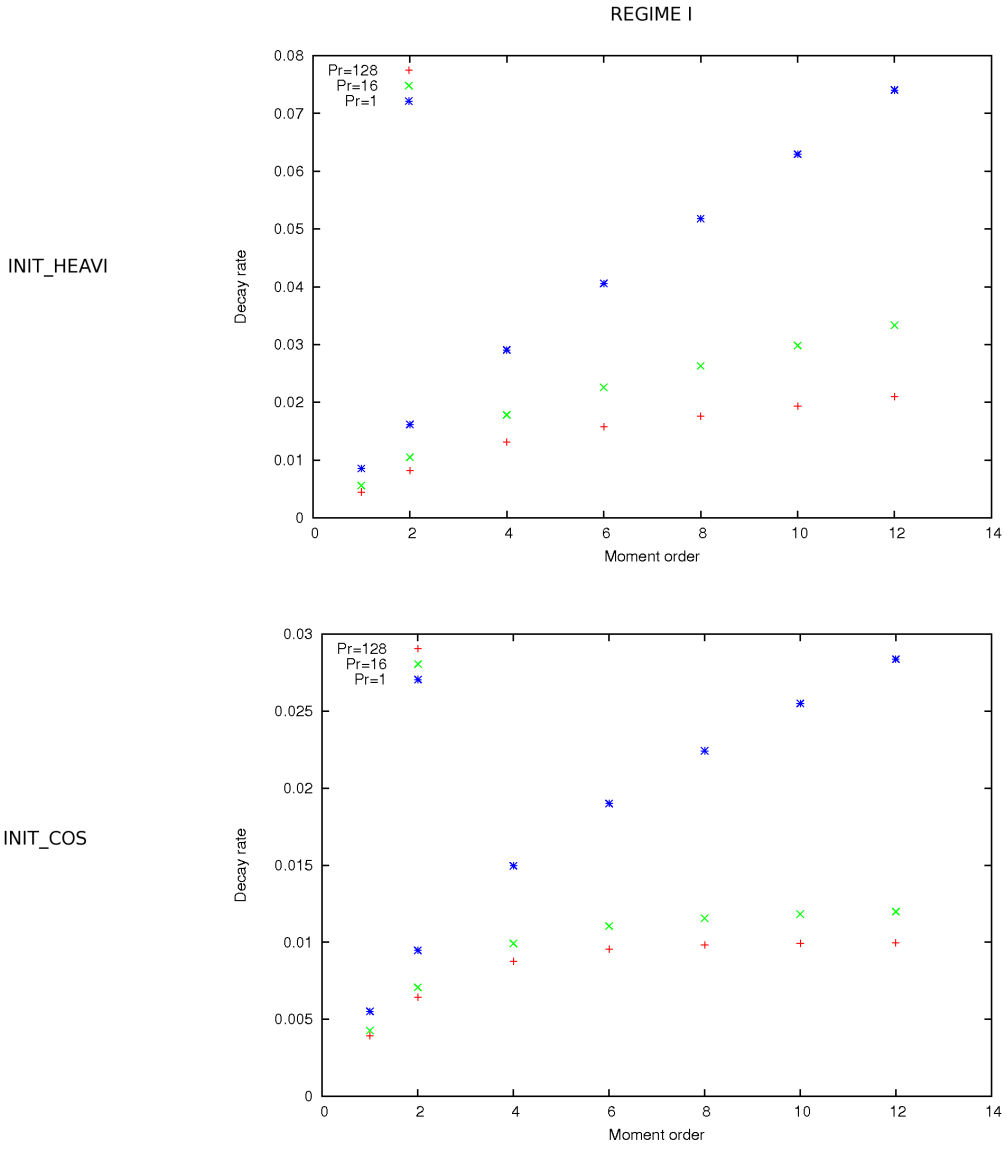

Figure 4–2: Top: exponential decay of the various moments $\langle|\phi|^n\rangle$ for $1 \leq n \leq 12$ in the first exponential decay (regime I, $25T \lesssim t \lesssim 60T$) for INIT_HEAVI (top) and INIT_HEAVI (bottom). We show $Pr = 1; 16; 128$. $Pr = 1$ is given to show a different situation where the decay is essentially controlled by diffusion. The vertical scale is not the same for the two plots.

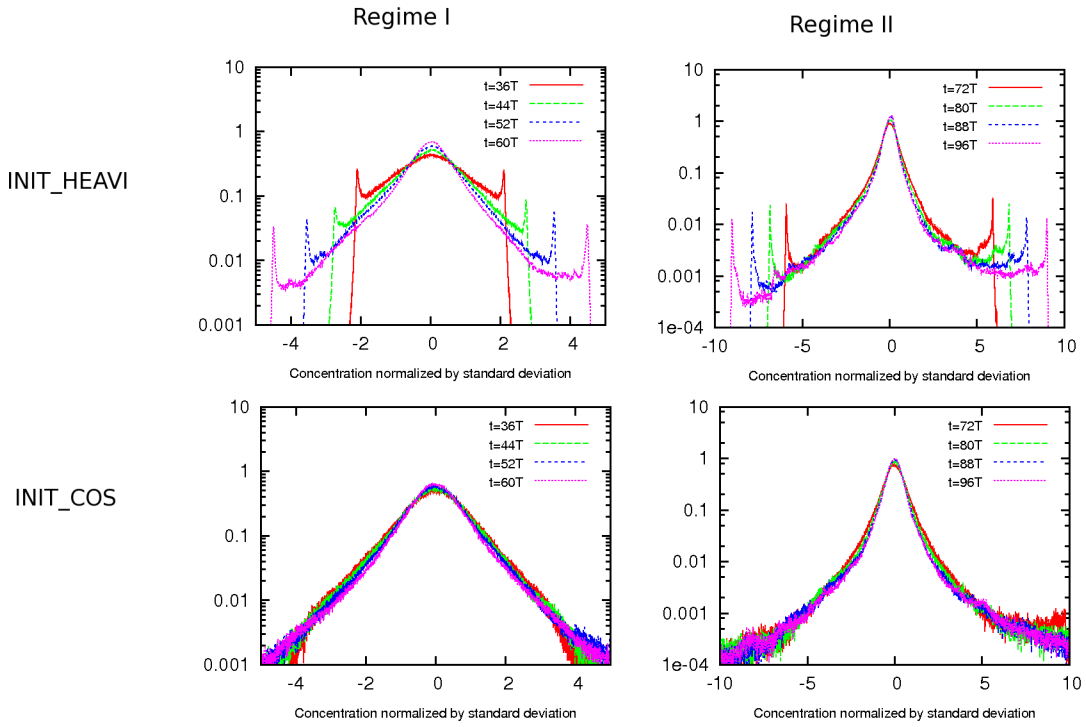

Figure 4–3: Probability distribution of the passive tracer ϕ, normalized by its standard deviation, at various times corresponding to regime I ($t = 36T; t = 44T; t = 52T; t = 60T$) on the left and to regime II ($t = 72T; t = 80T; t = 88T; t = 96T$) on the right. The two top panels correspond to INIT_HEAVI and the two bottom panels to INIT_COS. The Prandtl number is equal to 128. The scale is logarithmic in the abscissa.

simulations. The presence of spikes in the pdf for large values of $|\phi|$ (figure 4–3) correspond to tracer trapped in vortices and are crucial to determine the decay of high order moments. These phenomena cannot be captured by LLST because they involve transport barriers.

A global control of the decay is suggested by the k^{-1} spectrum (figure 4–4) and by the fact that the decay rate depends on the initial condition on the tracer field (figure 4–2). The spectrum, normalized by the total variance, is self-similar in time at each diffusion, as expected from (4.3a). This is shown on figure 4–4. Using

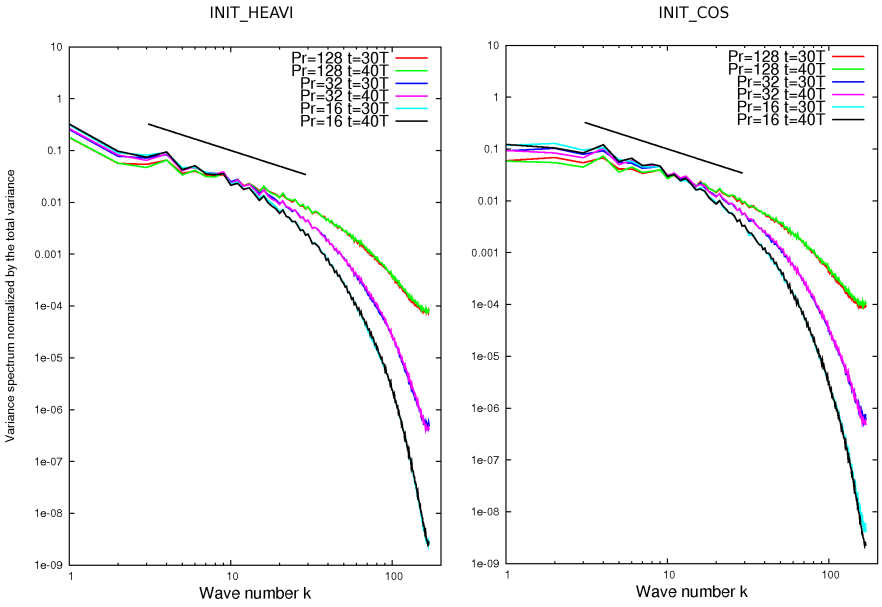

Figure 4–4: Ensemble average tracer variance spectrum for the initial condition INIT_HEAVI (left) and INIT_COS (right). We have represented three different Prandtl numbers $Pr = 128; 32; 16$ at two different times $t = 30T$ and $t = 40T$ corresponding to the regime I of the variance decay. The scale is log-log and the black line indicates a -1 slope.

a trajectory code and computing the FTLE using the same method as *Abraham and Bowen* (2002), we have estimated numerically the pdf P_τ of τ and have shown that it converges to a time independent form on a time scale of about $10T$. Using $P_\tau(t = 20T)$, we have computed $E_0^L(k, \kappa)$, defined in equation 4.4. On figure 4–5, we compare the spectrum from the numerical simulation, normalized by the total variance and multiplied by k, to what LLST predict, i.e. to $E_0^L(k, \kappa)$ normalized to fit the spectrum form the direct numerical simulation in the inertial range and multiplied by k. The match is very good, especially for INIT_HEAVI, and might confirm the relevance of using LLST to determine the shape of the spectrum.

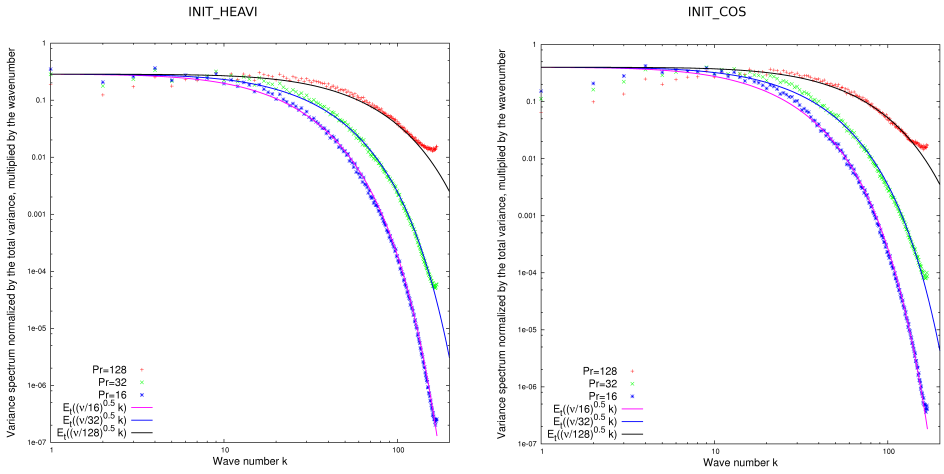

Figure 4–5: Comparison between the shape of the spectrum from the direct numerical simulations (DNS) and what local Lagrangian stretching theories (LLST) predict. The symbols correspond to the DNS and the solid lines to the LLST. The function $E_t(x)$ is proportional to $\int_0^\infty e^{-x^2\tau}\,d\tau$, the constant, common to all Pr, is chosen such that the spectra match the DNS in the inertial range. The scale is log-log and an horizontal line indicates a k^{-1} spectrum.

4.3.2 Decay in regime II

In regime II, the decay is much slower than in regime I. We will mainly discuss INIT_HEAVI, as regime II is not clear in INIT_COS and might necessitate longer simulations to be observed. The decay rate of the n-order moment γ_n also has an anomalous scaling with n (figure 4–7). However the reason for it seems different than in regime I. The presence of spikes in the pdf of ϕ at very large absolute values, which correspond to values very close to its initial value (figure 4–3), seems even more important than in regime II.

This can be conjectured noting that the variance decay in regime I varies much less from a member to another than in regime II. Figure 4–8 shows the decays for individual members. A major difference among members in regime II is the presence or the absence of tracer trapped in vortices, and the quantity trapped. Slower decays correspond to more tracer trapped in vortices (member 8 of figure 4–8). Tracer

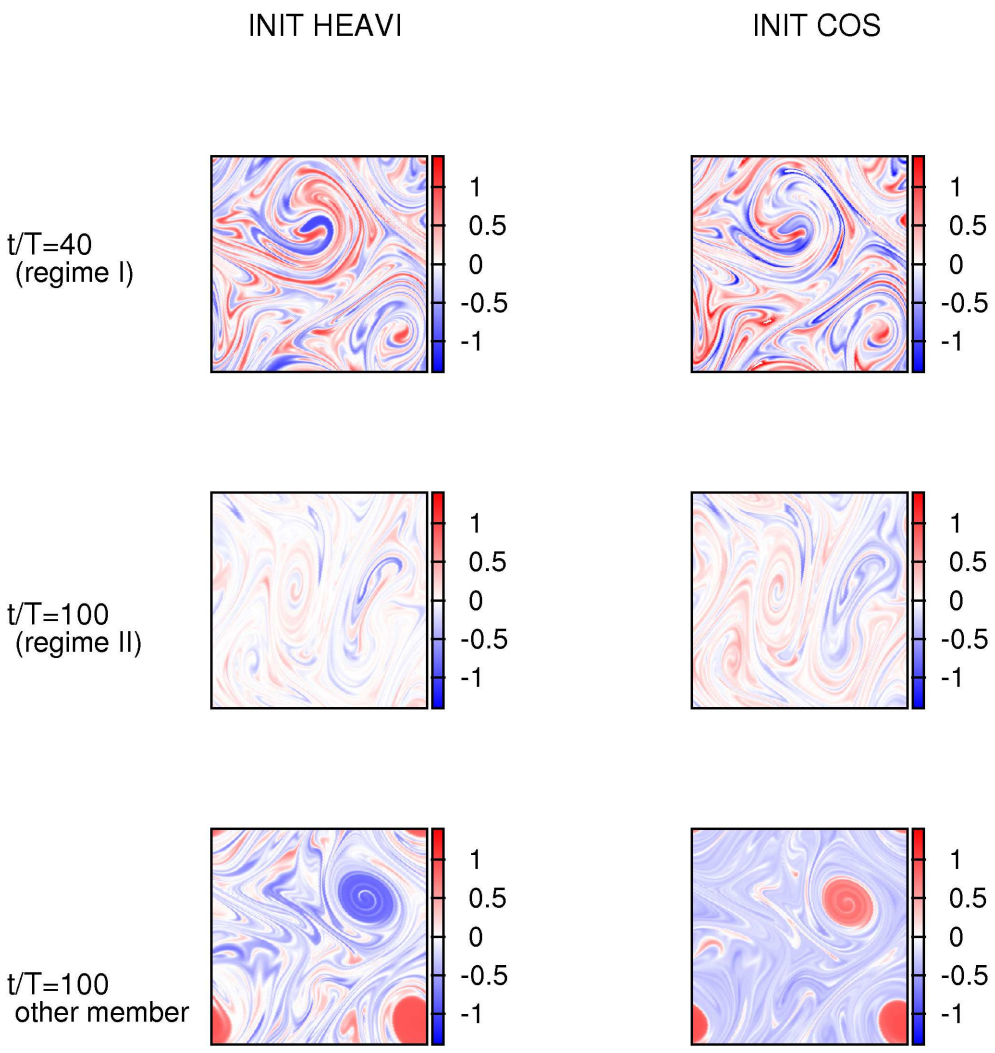

Figure 4–6: Examples of the tracer field in regime I at $t = 40T$ (the two top panels, member 3 of figure 4–8) and in regime II at $t = 100T$ (the four bottom panels corresponding to member 8 of 4–8). The left panels correspond to INIT_HEAVI and the right panels to INIT_COS. The fields are normalized by $|\overline{\phi}|(t = 0) = A_0$. We have plotted $\frac{\phi}{A_0}$ for $t = 40T$ and $\frac{2}{\pi}\tan^{-1}(10\frac{\phi}{A_0})$ for $t = 100T$, in order to be able to see clearly both the filamentary structures and the tracer trapped in vortices. The Prandtl number is equal to 128.

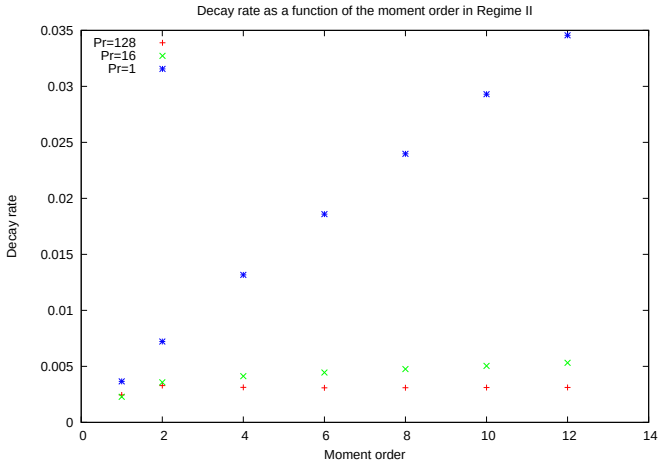

Figure 4–7: Exponential decay of the various moments $\langle|\phi|^n\rangle$ for $1 \leq n \leq 12$ in regime II for the initial condition INIT_HEAVI. As in figure 4–2, we show $Pr = 1; 16; 128$.

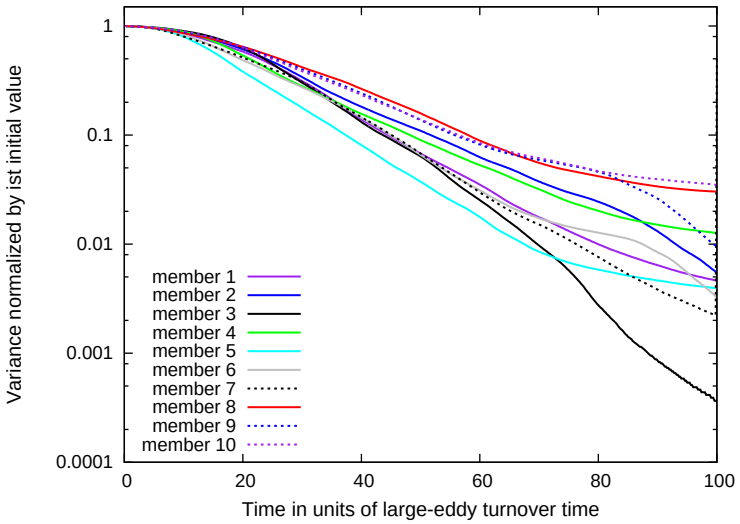

Figure 4–8: Variance decay for individual members, for INIT_HEAVI. The Prandtl number is equal to 128. The scale is logarithmic in the abscissa.

trapped in vortices can be seen on the two bottom panels of figure 4–6, and they correspond to member 8 on figure 4–8. The two panels of the middle correspond to a member where the decay is very fast (the fastest on figure 4–8, member 3). We also noted that some members can have a slow decay before the decay becomes faster, as for member 9 on figure 4–8. For member 9, a vortex is destabilized at $t \approx 80T$ and the tracer that was trapped is suddenly released in parts of the flow where the strain dominates, which explains a fast variance cascade to smaller scales. Whether the decay is slow or fast in regime II is very sensitive to the initial condition: one gets the initial condition on member 10 letting evolving the flow used to initialize member 9 over only half a large-eddy turnover time. The variance are indeed very close up to $t \approx 80T$ and then diverge abruptly.

The core of the pdf is close to being self-similar in time when ϕ is normalized by the square root of the ensemble mean variance (figure 4–3, right panels). This might suggest that outside of where the tracer is trapped, the tracer field has a strange eigenmode behavior, this strange eigenmode filling the whole domain for members where the trapping does not occur. The packed filament structure is visible on figure 4–6 (4 bottom panels). However, because of the tracer trapped in vortices, it is not clear how to normalize ϕ in order to verify if the core of the pdf is self-similar in time, and this might explain why the self-similarity is not perfectly seen on figure 4–3 (it is better achieved when members without trapped tracer are selected, not shown). In addition, the tracer pdf in regime II, for values of $x \equiv \frac{|\phi|}{\langle\overline{\phi^2}\rangle^{\frac{1}{2}}}$ between 1 and 5, scales like x^{-p}, with $p \approx 3$ (not shown). This scaling is consistent with the findings of *Fereday and Haynes* (2004) for a globally controlled decay, like in a strange eigenmode. We note that this form of the pdf is different from regime I (figure 4–3), where the core of the pdf is constituted by stretched exponentials,

away from the spikes, as predicted with LLST arguments by *Pierrehumbert* (2000); *Sukhatme and Pierrehumbert* (2002).

4.4 Conclusion

We have examined the decay of a passive tracer in a dynamically consistent flow with chaotic trajectories that is a solution of the barotropic two-dimensional Navier-Stokes equation. We have adopted an ensemble analysis, each member being defined by the initial condition on the vorticity field taken within the long-term run of a statistically stationary flow. Examining the variance decay, we have observed two consecutive regimes for the decay of variance characterized by different mixing rates: regime I and regime II.

In regime I, whether the control is local or global is not clear, in particular because some tracer is trapped in coherent vortices. However it seems that local theories can explain the shape of the variance spectrum and of the tracer pdf, away from spikes that are the manifestation of the trapped tracer. It could be interesting to do the same experiments but with a tracer initiated at smaller scales and check if the decay is locally controlled, like it would be in simple prescribed kinematics flows with chaotic trajectories (*Antonsen et al.*, 1996; *Fereday and Haynes*, 2004; *Haynes and Vanneste*, 2005).

In regime II, the mixing rate is very sensitive to the initial condition and varies significantly from one member to another, some tracer being possibly trapped inside coherent vortices. The ensemble mean variance decay is probably neither explained by a local mechanism nor a global mechanism in the sense of *Fereday and Haynes* (2004); *Haynes and Vanneste* (2005). The decay is controlled differently from one member to an other. When no tracer is trapped in vortices, a strange eigenmode, and thus a global control, is likely to occur. When some tracer is trapped, the decay is probably controlled by how vorticity filaments, and with them tracer, are ejected

from the vortices. In addition, on a given realization of the flow, the nature of the control of the decay can change, for example if a coherent vortex is destabilized.

Some of our conclusions are speculative and more work is needed to verify and clarify them. However, the phenomenology developed for the decay of a passive tracer in simple ergodic chaotic flow is clearly not sufficient to describe it in dynamically consistent flows essentially because of coherent structures. In particular, the fact that after 100 large-eddy turnover times, the variance having decayed by a factor of 10^2 to 10^3, the initial conditions are not forgotten is particularly striking.

CHAPTER 5
Conclusions

5.1 Results

The subject of this thesis is the study of a chemical reaction in an incompressible flow solution of the barotropic two-dimensional Navier-Stokes equation. This flow is chosen large scale in order to represent stirring by large scale stratospheric flows on isentropes. We study the instantaneous bimolecular chemical reaction $A + B \longrightarrow C$. The motivation is to understand the dependence of the chemistry on horizontal resolution in Climate-Chemistry models. Following previous approaches (*Tan et al.*, 1998; *Wonhas and Vassilicos*, 2002, 2003), we represent a varying resolution by a varying chemical tracer diffusion.

In chapter 2 and chapter 3, we focused on the case where the contact line between the reactants is material, one-dimensional and only dependent on the dynamical properties of the flow. This corresponds in our numerical setting to the initial stage of the reaction, on a time scale smaller than about 5 to 10 large-eddy turnover times. We use a Lagrangian stretching theory approach on the contact zone where the reactants mix under the action of diffusion and react. We show that the ensemble mean of the derivative of the total domain product quantity can be factorized as the product of the ensemble mean contact line length, the ensemble mean gradient along this line and the diffusion κ of the chemicals. It follows that the dependence of the total product concentration on the diffusion is algebraic: it scales like $\kappa^{1/2}$ if the chemicals are initialized with sharp gradients at their interface, because gradients are determined by diffusive processes and scale like $\kappa^{-1/2}$, and like κ if the gradient are initially smooth enough to allow the dynamical properties of the

flow to determine alone the gradient evolution on time scales corresponding to our initial regime. Estimating that current Chemistry-Climate models have a resolution two orders of magnitude smaller than the resolution needed to resolve accurately stratospheric tracer filaments, this scaling means a chemistry 10^2 times too fast in the sharp gradient case and 10^4 times too fast in the smooth gradient case, on time scales of a couple of weeks. Of course, the resolution induced errors decrease for larger time scales (e.g. *Tan et al.* (1998); *Wonhas and Vassilicos* (2002, 2003), see also figure 1–9). However short time scales are relevant for some important stratospheric processes, like ozone depletion in the wintertime surf zone or the formation of the seasonal ozone hole. Also, we have stressed the importance of rare events characterized by high Lagrangian stretching rates in determining the product concentration, rarer events becoming more important as the reactant gradients in the contact zone are smoother. Intuitively, this is because the contact line develop exponentially fast, Lagrangian trajectories being chaotic, such that exponentially rare events determine alone its total length. In the smooth gradient case the chemical production is determined by even rarer events because gradients are also developing exponentially fast: if diffusion is neglected and the flow incompressible, an exponential increase of a contact line element goes with an exponential decrease at the same rate of a line element transverse to it.

We have also shown, in the sharp gradient case, that the probability distribution function of the reactants concentration was independent of diffusion when divided by $\kappa^{1/2}$, for values of the concentration not too close to their initial concentration in their respective domain. The probability density function of the gradients along the contact line multiplied by $\kappa^{1/2}$ was shown to be independent of diffusion and determined by the Lagrangian stretching properties of the flow. Beside improving our understanding of a fast bimolecular reaction in two-dimensional flows with

chaotic trajectories, these results confirm the relevance of LLST to study it and pave the way toward the development of subgrid parametrization for chemical processes in the stratosphere. A previous attempt of slowing down the chemistry in stratospheric Climate-Chemistry models was proposed by *Thuburn and Tan* (1997) but was not really successful. We note that they did not consider the whole distribution of stretching rates in their approach, which is crucial, as shown in the present study.

For longer times, some studies have used LLST results dealing with the passive problem to study fast chemical reaction (*Tsang*, 2009), exploiting the fact that the passive tracer defined as the difference between the reactants contains all the information about both fields (chapter 2). However, the theories developed for simple ergodic chaotic flows do not seem fully applicable to dynamically consistent flows essentially because of coherent transient structures like vortices that can trap some of the reactants (chapter 4).

5.2 Future work

5.2.1 Chemistry at intermediate time scales

We have looked in detail at the initial stage of the reaction (chapters 2 and 3). In this regime, reactants are increasing exponentially fast. In the long-term decay, they are expected to decrease exponentially fast (chapter 4, see also *Tsang* (2009)). It follows that there is a maximum of chemical production at intermediate time scales. Our simulations, not shown in the present thesis, suggest that the time where this maximum occurs scales like the logarithm of κ, or equivalently like the logarithm of the resolution. We think that a LLST approach could be relevant to understand this maximum by relating it to the gradient evolution along the contact line. We would also need the evolution of the contact line length and its dependence on diffusion. Previous work have related the total product concentration to the box counting fractal dimension of the contact line (*Wonhas and Vassilicos*, 2002,

2003). It might be possible to use this dimension to determine the dependence of the contact line on the diffusion, assuming a fractal geometric structure down to the diffusive cutoff. However the physical meaning of a time dependent fractal dimension is not clear (*Tél et al.*, 2005; *Karolyi and Tél*, 2007). Some works have shown the multifractal structure in two-dimensional chaotic flows of passive tracers (*Antonsen and Ott*, 1991; *Antonsen et al.*, 1996) and chemically active tracers (*Neufeld et al.*, 1999, 2000; *Hernandez-Garcia et al.*, 2002). The dimension spectrum relates to the Cramèr function determining the FTLE pdf (e.g. *Ott* (2002) in the general framework of chaotic dynamical systems). This suggests that it might be possible to relate the fractal dimension of the contact line to the FTLE pdf. However, this might necessitate an understanding of the time evolution of the pdf of the FTLE, before its convergence to the form predicted by the large deviation theory.

The same approach could be used in order to have a deeper insight into the very long-term decay, where the fractal dimension is expected to be stationary. A rigorous study of this regime would need to determine more accurately the Cramèr function associated with the FTLE pdf. This could be done using the Monte Carlo method or alternate methods described in *Vanneste* (2010). However, especially in the very long-term decay, the importance of tracer trapped in vortices could jeopardize the use of LLST, as seen in chapter 4.

5.2.2 More realistic chemistries

We have discussed the case of an infinitely fast chemical reaction. The use of LLST can be extended to a smaller first Damkhöler number, the adimensional number measuring the ratio between chemical and advective time scales. Some of our results, not shown in the present thesis, suggest that, for first Damkhöler numbers as small as 0.01, the product's concentration can be accurately predicted using the correlations between the reactants fields from the passive problem. The

reason for it appears unclear, and a LLST approach on the contact zone might be helpful to tackle this problem, at least for second Damkhöler numbers small enough. The second Damkhöler measures the ratio between the chemical time scale and the diffusive time scale on length scales corresponding to the domain.

Also, our theoretical framework could be useful to study other chemical reactions relevant to ozone chemistry, like chemical equilibria, autocatalytic or catalytic reactions.

5.2.3 More realistic flows

A more realistic representation of mixing in the stratosphere could include the modeling of critical layers, like in the numerical model developed in *Brunet and Haynes* (1995) and whose implementation in our pseudospectral code should not be difficult. The dynamics of the critical layer is indeed different from that of the vortices of the flow we used.

Also, two-dimensional mixing is only a partial view of mixing in the stratosphere, tracer filaments being actually sheets that intersect isentropes. Our work could be extended to a more realistic setup using the quasi-geostrophic or the primitive equations for a stratified fluid. A theoretical approach for this problem, extending the LLST approach, can be performed introducing a random shear between two-dimensional layers, as in *Haynes and Anglade* (1997); *Haynes and Vanneste* (2004).

Recently, the extent of the applicability of LLST to the passive problem has been extended to three dimensional flows (*Ngan and Vanneste*, 2011). This leaves the prospect of using LLST for chemical reaction in fully developed three dimensional flows open. In atmospheric science, this can have applications to the advection-reaction of pollutants in the lower troposphere below the synoptic scale.

5.2.4 Dependence of the flow on the resolution

We have only considered the dependence of the chemical tracers on resolution, using the fact the large scale-stirring is responsible for small-scale passive tracer structures in atmospheric flows (Chapter 1). However, it might be interesting to look at how the probability distribution of the the finite time Lyapunov exponents and of other Lagrangian diagnostics like τ and $\widetilde{\tau}$ (equation 2.30) depend on the resolution.

5.3 Discussion

5.3.1 On the relevance of LLST

Local Lagrangian stretching theories are thought to be valid only at intermediate time scales and when the scalar field is small-scale compared to the flow (*Haynes*, 2005). It seems that they are performing well in our problem because we have considered time scales smaller that $T \ln Pe$, with T the large-eddy turnover time and $Pe \equiv \frac{L_{flow}^2}{\kappa T}$ the Peclet number, which is precisely the time scale where LLST are thought to be valid (*Fereday and Haynes*, 2004). The second reason for this good performance is that the transverse length scale of the contact zone is small compared to the flow. This would be no longer true if the chemical reaction was slow, for example as slow as diffusive processes on length scales corresponding to the domain. Our approach might be relevant for reactions that are fast enough, even in the long-term decay, the length of the contact line being controlled globally and constant at a fixed diffusion[1] and the gradient along the contact line being controlled locally. This last assertion has to be checked carefully. An important limitation of this approach,

[1] Determining the dependence of this length with diffusion could make the use of fractal dimensions, as mentioned in 5.1.2

only in dynamically consistent flows, would be the barriers of transport at the edge of coherent vortices that can trap reactants, as mentioned in chapter 4.

5.3.2 On the distribution of the Lagrangian stretching properties

A central assumption of LLST to predict the fluctuation decay of a passive tracer in a large-scale flow with chaotic trajectories is the independence between the FTLE λ and the equivalent time τ (discussion below equation (1.31)) for long enough times. However it seems that this is not true in our flow, the correlation between λ and τ being striking for orbits characterized by a small stretching (figure 2–7), even at times larger than 20 large-eddy turnover times. Indeed, we have observed that the distribution of the Lagrangian correlation time, the typical time scale for the strain to decorrelate on a trajectory, was wide (not shown): low stretching corresponds to correlation times several times longer than the large-eddy turnover time. As a consequence, it appears natural that, on these trajectories, the Lagrangian stretching rate in the recent past τ, i.e on a time scale corresponding to the last correlation time on the orbit, is close to twice the finite-time Lyapunov exponent (the factor two comes from the definition chosen for τ). However we were not able to relate this observation to any feature of the Eulerian field. In particular, these orbits do not correspond to fluid parcels trapped in vortices, as can be conjectured intuitively. It would be interesting to understand the reasons for this dependence and the implications for the theoretical results provided by LLST.

In addition, we do not understand the time evolution of the FTLE pdf before it converges toward the form predicted by the large deviation theory. The FTLE pdf evolves from the strain pdf to a function proportional to $\exp -tG(\lambda)$, where $G(\lambda)$ is the Cramèr function. The ensemble mean Lyapunov exponent is significantly smaller than the mean strain. This is due to the reorientation of the strain axes along chaotic orbits and to the effect of vorticity. However, other phenomena, specific to

dynamically consistent flows, could have an importance here, like the trapping of fluid parcels inside vortices. Moreover, our method to compute the Cramèr function is not accurate enough to determine the validity of the large deviation theory in our Navier-Stokes flow on a time scale of a few tens of turnover times. The observation that correlation times on low-stretching Lagrangian trajectories can be several times larger than the large-eddy turnover time is not consistent with the applicability of the large deviation theory and could explain why the determination of the Cramèr function for small FTLE was so imprecise (figure 2–3).

References

Abraham, E., and M. Bowen (2002), Chaotic stirring by a mesoscale surface-ocean flow, *Chaos*, *12*, 373–381.

Adrover, A., S. Cerbelli, and M. Giona (2002), Quantitative analysis of mixing structures in chaotic flows generated by infinitely fast reactions in the presence of diffusion, *Journal of Physical Chemistry A*, *106*, 5722–5736.

Ait-Chaalal, F. (2008), Nonlinear chemistry in twodimensional turbulence, phd thesis proposal.

Ait-Chaalal, F., M. Bourqui, and P. Bartello (under review), Fast chemical reaction in a two-dimensional navier-stokes flow: Initial regime, *Physical Review E*.

Andrews, D., J. Holton, and C. Leovy (1987), *Middle atmosphere dynamics*, Academic Press.

Antonsen, T., and E. Ott (1991), Multifractal power spectra of passive scalars convected by chaotic fluid flows, *Physical Review A*, *44*(2), 851.

Antonsen, T., Z. Fan, E. Ott, and E. Garcia Lopez (1996), The role of chaotic orbits in the determination of power spectra passive scalars, *Physics of Fluids*, *8*, 3094–3104.

Aref, H. (1984), Stirring by chaotic advection, *Journal of Fluid Mechanics*, *143*, 1–21.

Arnóld, V. (1966), Sur la géométrie différentielle des groupes de lie de dimension infinie et ses applications l'hydrodynamique des fluides parfaits, *Ann. Inst. Fourier*, *16*(1), 319–361.

Bacmeister, J., S. Eckermann, P. Newman, L. Lait, K. Chan, M. Loewenstein, M. Proffitt, and B. Gary (1996), Stratospheric horizontal wavenumber spectra of

winds, potential temperature, and atmospheric tracers observed by high-altitude aircraft, *J. Geophys. Res*, *101*, 9441–9470.

Balkovsky, E., and A. Fouxon (1999), Universal long-time properties of lagrangian statistics in the batchelor regime and their application to the passive scalar problem, *Physical Review E*, *60*, 4164–4174.

Balluch, M., and P. Haynes (1997), Quantification of lower stratospheric mixing processes using aircraft data, *Journal of Geophysical Research-Atmospheres*, *102*, 23,487–23,504.

Bartello, P. (2000), Using low-resolution winds to deduce fine structure in tracers, *Atmosphere-Ocean*, *38*, 303–320.

Bartello, P. (2010), Quasigeostrophic and stratified turbulence in the atmosphere, in *IUTAM Symposium on Turbulence in the Atmosphere and Oceans*, pp. 117–130, Springer.

Batchelor, G. (1959), Small-scale variation of convected quantities like temperature in turbulent fluid .1. general discussion and the case of small conductivity, *Journal of Fluid Mechanics*, *5*(1), 113–133.

Boer, G., and T. Shepherd (1983), Large-scale two-dimensional turbulence in the atmosphere, *Journal of the Atmospheric Sciences*, *40*(1), 164–184.

Brown, M., and R. Samelson (1994), Particle motion in vorticity-conserving, two-dimensional incompressible flows, *Physics of Fluids*, *6*(9), 2875–2876.

Brunet, G., and P. Haynes (1995), The nonlinear evolution of disturbances to a parabolic jet, *Journal of the Atmospheric Sciences*, *52*(4), 464–477.

Charney, J. (1971), Geostrophic turbulence., *Journal of Atmospheric Sciences*, *28*, 1087–1094.

Charney, J., P. Drazin, et al. (1961), Propagation of planetary-scale disturbances from the lower into the upper atmosphere, *J. geophys. Res*, *66*(1), 83–109.

Chen, P. (1996), The influences of zonal flow on wave breaking and tropical-extratropical interaction in the lower stratosphere, *Journal of the atmospheric sciences*, *53*(16), 2379–2392.

Chertkov, M., G. Falkovich, I. Kolokolov, and V. Lebedev (1995), Statistics of a passive scalar advected by a large-scale 2-dimensional velocity-field - analytic solution, *Physical Review E*, *51*, 5609–5627.

Chien, W., H. Rising, and J. Ottino (1986), Laminar mixing and chaotic mixing in several cavity flows, *Journal of Fluid Mechanics*, *170*, 355–377.

Childress, S., and A. Gilbert (1995), Stretch, twist, fold, *The Fast Dynamo, XI, 406 pp.. Springer-Verlag Berlin Heidelberg New York. Also Lecture Notes in Physics, volume 37*, *1*.

Corrsin, S. (1958), Statistical behavior of a reacting mixture in isotropic turbulence, *The Physics of Fluids*, *1*, 42.

Crisanti, A., G. Paladin, and A. Vulpiani (1994), Products of random matrices in statistical physics, *Springer Series in Solid State Sciences (Springer-Verlag, Berlin, to be published)*.

del Castillo-Negrete, D., and P. Morrison (1993), Chaotic transport by rossby waves in shear flow, *Physics of Fluids A Fluid Dynamics*, *5*, 948.

Eckart, C. (1948), An analysis of the stirring and mixing processes in incompressible fluids, *Journal of marine research*, *7*(3), 265–275.

Eckmann, J., and D. Ruelle (1985), Ergodic theory of chaos and strange attractors, *Reviews of modern physics*, *57*(3), 617.

Edouard, S., B. Legras, F. Lefevre, and R. Eymard (1996), The effect of small-scale inhomogeneities on ozone depletion in the arctic, *Nature*, *384*, 444–447.

Falkovich, G., K. Gawdzki, and M. Vergassola (2001), Particles and fields in fluid turbulence, *Reviews of Modern Physics*, *73*(4), 913.

Farman, J., B. Gardiner, and J. Shanklin (1985), Large losses of total ozone in antarctica reveal seasonal ClO_x/NO_x interaction, *Nature*, *315*(6016), 207–210.

Fereday, D., and P. Haynes (2004), Scalar decay in two-dimensional chaotic advection and batchelor-regime turbulence, *Physics of Fluids*, *60*, 4359–4370.

Fereday, D., P. Haynes, A. Wonhas, and J. Vassilicos (), Scalar variance decay in chaotic advection and batchelor-regime turbulence, *Physical Review E*, *65*, 035,301.

Frigo, M., and S. Johnson (2005), The design and implementation of fftw3, *Proceedings of the IEEE*, *93 (2)*, 216–231.

Frisch, U. (1996), *Turbulence*, Cambridge University Press.

Goldhirsch, I., P. Sulem, and S. Orszag (1987), Stability and lyapunov stability of dynamic-systems - a differential approach and a numerical-method, *Physica D*, *27*(3), 311.

Haynes, P. (1985), Nonlinear instability of a rossby-wavecritical layer, *Journal of Fluid Mechanics*, *161*(1), 493–511.

Haynes, P. (2005), Stratospheric dynamics, *Annu. Rev. Fluid Mech.*, *37*, 263–293.

Haynes, P., and J. Anglade (1997), The vertical-scale cascade in atmospheric tracers due to large-scale differential advection, *Journal of the Atmospheric Sciences*, *54*, 1121–1136.

Haynes, P., and E. Shuckburgh (2000), Effective diffusivity as a diagnostic of atmospheric transport. i. stratosphere, *Journal of geophysical research*, *105*, 22.

Haynes, P., and J. Vanneste (2004), Stratospheric tracer spectra, *Journal of the Atmospheric Sciences*, *61*, 161–177.

Haynes, P., and J. Vanneste (2005), What controls the decay of passive scalars in smooth flows?, *Physics of Fluids*, *17*, 097,103.

Haynes, P., D. Poet, and E. Shuckburgh (2007), Transport and mixing in kinematic and dynamically consistent flows, *Journal of the Atmospheric Sciences*, *64*(10),

3640–3651.

Hénon, M. (1966), Sur la topologie des lignes de courant dans un cas particulier, *CR Acad. Sci. Paris*, *262*, 312–314.

Hernandez-Garcia, E., C. Lopez, Z. Neufeld, et al. (2002), Small-scale structure of nonlinearly interacting species advected by chaotic flows., *Chaos*, *12*(2), 470.

Hoskins, B., M. McIntyre, and A. Robertson (1985), On the use and significance of isentropic potential vorticity maps, *Quarterly Journal of the Royal Meteorological Society*, *111*(470), 877–946.

Juckes, M. (1989), A shallow water model of the winter stratosphere., *Journal of Atmospheric Sciences*, *46*, 2934–2956.

Juckes, M., and M. McIntyre (1987), A high-resolution one-layer model of breaking planetary waves in the stratosphere, *Nature*, *328*(6131), 590–596.

Karolyi, G., and T. Tél (2005), Chemical transients in closed chaotic flows: The role of effective dimensions, *Physical Review Letters*, *95*, 264,501.

Karolyi, G., and T. Tél (2007), Effective dimensions and chemical reactions in fluid flows, *Physical Review E*, *76*, 046,315.

Katō, T. (1995), *Perturbation theory for linear operators*, vol. 132, Springer Verlag.

Killworth, P., and M. McIntyre (1985), Do rossby-wave critical layers absorb, reflect, or over-reflect?, *Journal of Fluid Mechanics*, *161*(01).

Knobloch, E., and J. Weiss (1987), Chaotic advection by modulated traveling waves, *Physical Review A*, *36*(3), 1522–1524.

Koshyk, J., and K. Hamilton (2001), The horizontal kinetic energy spectrum and spectral budget simulated by a high-resolution troposphere-stratosphere-mesosphere gcm, *Journal of the Atmospheric Sciences*, *58*, 329–348.

Koshyk, J., B. Boville, K. Hamilton, E. Manzini, and K. Shibata (1999), Kinetic energy spectrum of horizontal motions in middle-atmosphere models, *Journal of*

geophysical research, *104*, 27.

Kraichnan, R. (1967), Inertial ranges in twodimensional turbulence, *Physics of Fluids*, *10*, 1417–1423.

Kraichnan, R. (1974), Convection of a passive scalar by a quasi-uniform random straining field, *Journal of Fluid Mechanics*, *64*(4), 737.

Lapeyre, G. (2002), Characterization of finite-time lyapunov exponents and vectors in two-dimensional turbulence, *Chaos*, *12*, 688–698.

Legras, B., D. Dritschel, and P. Caillol (2001), The erosion of a distributed two-dimensional vortex in a background straining flow, *Journal of Fluid Mechanics*, *441*, 369–398.

Legras, B., I. Pisso, G. Berthet, F. Lefèvre, et al. (2005), Variability of the lagrangian turbulent diffusion in the lower stratosphere, *Atmospheric Chemistry and Physics*, *5*(6), 1622.

Lesieur, M., and J. Herring (1985), Diffusion of a passive scalar in two-dimensional turbulence, *Journal of Fluid Mechanics*, *161*, 77–95.

Majda, A., and P. Kramer (1999), Simplified models for turbulent diffusion: Theory, numerical modelling, and physical phenomena, *Physics reports-review section of physics letters*, *314*(4-5), 238–574.

Martinand, D., and J. Vassilicos (2007), Fast chemical reaction and multiple-scale concentration fields in singular vortices, *Physical Review E*, *75*, 036,315.

McIntyre, M., and T. Palmer (1983), Breaking planetary waves in the stratosphere, *Nature*, *305*(5935), 593–600.

McIntyre, M., and T. Palmer (1984), The 'surf zone' in the stratosphere, *Journal of atmospheric and terrestrial physics*, *46*(9), 825–849.

McWilliams, J. (1984), The emergence of isolated coherent vortices in turbulent-flow, *Journal of Fluid Mechanics*, *146*, 21–43.

Michels, H. (2010), Dislin home page, http://www.mps.mpg.de/dislin/, accessed May 2010.

Molina, L., and M. Molina (1987), Production of chlorine oxide Cl_2O_2 from the self-reaction of the chlorine oxide ClO radical, *Journal of Physical Chemistry*, *91*(2), 433–436.

Monin, A., and A. Yaglom (1975), *Statistical Fluid Mechanics, Volume II*, MIT Press.

Nakamura, N. (1996), Two-dimensional mixing, edge formation, and permeability diagnosed in an area coordinate, *Journal of the atmospheric sciences*, *53*(11), 1524–1537.

Neufeld, Z., C. López, and P. Haynes (1999), Smooth-filamental transition of active tracer fields stirred by chaotic advection, *Physical review letters*, *82*(12), 2606–2609.

Neufeld, Z., C. López, E. Hernández-García, and T. Tél (2000), Multifractal structure of chaotically advected chemical fields, *Physical Review E*, *61*(4), 3857.

Ngan, K., and T. Shepherd (1997a), Chaotic mixing and transport in rossby-wave critical layers, *Journal of Fluid Mechanics*, *334*, 315–351.

Ngan, K., and T. Shepherd (1997b), Comments on some recent measurements of anomalously steep n2o and o3 tracer spectra in the stratospheric surf zone, *Journal of geophysical research*, *102*(D20), 24,001–24.

Ngan, K., and T. Shepherd (1999a), A closer look at chaotic advection in the stratosphere. part 1: Geometric structure, *Journal of the Atmospheric Sciences*, *56*, 4134–4152.

Ngan, K., and T. Shepherd (1999b), A closer look at chaotic advection in the stratosphere. part ii: Statistical diagnostics, *Journal of the Atmospheric Sciences*, *56*, 4153–4166.

Ngan, K., and J. Vanneste (2011), Scalar decay in a three-dimensional chaotic flow, *Physical Review E*, *83*(5), 056,306.

NOAA (2011), National oceanic and atmospheric administration, jetstream - online school for weather, http://forecast.weather.gov/jetstream/atmos/atmprofile.htm, accessed November 2011.

Norton, W. (1994), Breaking rossby waves in a model stratosphere diagnosed by a vortex-following coordinate system and a technique for advecting material contours, *Journal of the atmospheric sciences*, *51*(4), 654–654.

Orszag, S. (1971), Numerical simulation of incompressible flows within simple boundaries: accuracy, *Journal of Fluid Mechanics*, *49*(Part 1), 75–112.

Oseledec, V. (1968), A multiplicative theorem: Lyapunov characteristics numbers for dynamical systems, *Trans. Moscow Math Soc.*, *19*, 197.

Ott, E. (2002), *Chaos in Dynamical Systems*, Cambridge, England.

Ottino, J. (1989), *The kinematics of mixing: stretching, chaos, and transport*, Cambridge University Press.

Ottino, J., C. Leong, H. Rising, and P. Swanson (1988), Morphological structures produced by mixing in chaotic flows, *Nature*, *333*, 419–425.

Peyret, R. (2002), *Spectral methods for incompressible viscous flow*, vol. 148, Springer Verlag.

Pierrehumbert, R. (1991a), Chaotic mixing of tracer and vorticity by modulated traveling rossby waves, *Geophysical and astrophysical fluid dynamics*, p. 285.

Pierrehumbert, R. (1991b), Large-scale horizontal mixing in planetary-atmospheres, *Physics of fluids a-fluid dynamics*, pp. 1250–1260.

Pierrehumbert, R. (1994), Tracer microstructure in the large-eddy dominated regime, *Chaos solitons and fractals*, pp. 1091–1110.

Pierrehumbert, R. (2000), Lattice models of advection-diffusion, *Chaos*, pp. 61–74.

Pierrehumbert, R., and H. Yang (1993), Global chaotic mixing on isentropic surfaces, *Journal of the atmospheric sciences*, pp. 2462–2480.

Pikovsky, A., and O. Popovych (2003), Persistent patterns in deterministic mixing flows, *EPL (Europhysics Letters)*, *61*, 625.

Polvani, L., and R. Plumb (1992), Rossby wave breaking, microbreaking, filamentation, and secondary vortex formation: The dynamics of a perturbed vortex, *Journal of the atmospheric sciences*, *49*(6).

Polvani, L., and R. Saravanan (2000), The three-dimensional structure of breaking rossby waves in the polar wintertime stratosphere, *Journal of the atmospheric sciences*, *57*(21), 3663–3685.

Polvani, L., D. Waugh, and R. Plumb (1995), On the subtropical edge of the stratospheric surf zone, *Journal of Atmospheric Sciences*, *52*(9), 1288–1309.

Rhines, P. (1975), Waves and turbulence on a beta-plane, *Journal of Fluid Mechanics*, *69*(03), 417–443.

Rhines, P. (1979), Geostrophic turbulence, *Annual Review of Fluid Mechanics*, *11*(1), 401–441.

Rossby, C. (1938), Aerological evidence of large scale mixing in the atmosphere, *Trans. Am. Geophys. Union*, pp. 130–136.

Rothstein, D., E. Henry, and J. Gollub (1999), Persistent patterns in transient chaotic fluid mixing, *Nature*, *401*(6755), 770–772.

Salawitch, R., D. Weisenstein, L. Kovalenko, C. Sioris, P. Wennberg, K. Chance, M. Ko, and C. McLinden (2005), Sensitivity of ozone to bromine in the lower stratosphere, *Geophysical research letters*, *32*, L05,811.

Schneider, T. (2004), The tropopause and the thermal stratification in the extratropics of a dry atmosphere, *Journal of the atmospheric sciences*, *61*(12), 1317–1340.

Schneider, T., and C. Walker (2006), Self-organization of atmospheric macroturbulence into critical states of weak nonlinear eddy-eddy interactions, *Journal of the atmospheric sciences*, *63*(6), 1569–1586.

Searle, K., M. Chipperfield, S. Bekki, and J. Pyle (1998a), The impact of spatial averaging on calculated polar ozone loss - 1. model experiments, *Journal of Geophysical Research-Atmospheres*, *103*, 25,397–25,408.

Searle, K., M. Chipperfield, S. Bekki, and J. Pyle (1998b), The impact of spatial averaging on calculated polar ozone loss - 2. theoretical analysis, *Journal of Geophysical Research-Atmospheres*, *103*, 25,409–25,416.

Shepherd, T. (2000), The middle atmosphere, *Journal of Atmospheric and Solar-Terrestrial Physics*, *62*(17-18), 1587–1601.

Shepherd, T. (2007), Transport in the middle atmosphere, *Journal of the Meteorological Society of Japan*, *85B*(0), 165–191.

Shepherd, T., J. Koshyk, and K. Ngan (2000), On the nature of large-scale mixing in the stratosphere and mesosphere, *Journal of Geophysical Research*, *105*(D10), 12,433–12.

Shuckburgh, E., and P. Haynes (2003), Diagnosing transport and mixing using a tracer-based coordinate system, *Physics of Fluids*, *15*, 3342.

Sokolov, I., and A. Blumen (1991), Mixing effects in the $a + b \rightarrow 0$ reaction-diffusion scheme, *Physical Review Letters*, *66*, 1942.

Solomon, S. (1999), Stratospheric ozone depletion: A review of concepts and history, *Reviews of Geophysics*, *37*, 275–316.

Son, D. (1999), Turbulent decay of a passive scalar in the batchelor limit: Exact results from a quantum-mechanical approach, *Physical Review E*, *59*(4), 3811–3814.

Son, S., L. Polvani, D. Waugh, H. Akiyoshi, R. Garcia, D. Kinnison, S. Pawson, E. Rozanov, T. Shepherd, and K. Shibata (2008), The impact of stratospheric ozone recovery on the southern hemisphere westerly jet, *Science*, *320*(5882), 1486.

Stewartson, K. (1977), The evolution of the critical layer of a rossby wave, *Geophysical & Astrophysical Fluid Dynamics*, *9*(1), 185–200.

Strahan, S., and J. Mahlman (1994), Evaluation of the skyhi general circulation model using aircraft N_2O measurements, 1, polar winter stratospheric meteorology and tracer morphology, *Hournal of geophysical research*, *99*, 10–10.

Sukhatme, J., and R. Pierrehumbert (2002), Decay of passive scalars under the action of single scale smooth velocity fields in bounded two-dimensional domains: From non-self-similar probability distribution functions to self-similar eigenmodes, *Physical Review E*, *66*, 056,302.

Tan, D., P. Haynes, A. MacKenzie, and J. Pyle (1998), Effects of fluid-dynamical stirring and mixing on the deactivation of stratospheric chlorine, *Journal of Geophysical Research-Atmospheres*, *103*, 1585–1605.

Tang, X., and A. Boozer (1996), Finite time lyapunov exponent and advection-diffusion equation, *Physica D*, *95*, 283–305.

Tél, T., A. de Mourab, C. Grebogib, and G. Károlyid (2005), Chemical and biological activity in open flows: A dynamical system approach, *Physics Reports*, *413*, 91–196.

Thiffeault, J. (2003), Advection-diffusion in lagrangian coordinates, *Physics Letters A*, *309*(5-6), 415–422.

Thiffeault, J. (2008), Scalar decay in chaotic mixing, in *Transport and Mixing in Geophysical Flows*, vol. 744, pp. 3–540.

Thuburn, J., and D. Tan (1997), A parameterization of mixdown time for atmospheric chemicals, *Journal of Geophysical Research-Atmospheres*, *102*, 13,037–13,049.

Tsang, Y. (2009), Predicting the evolution of fast chemical reactions in chaotic flows, *Physical Review E*, *80*, 026,305.

Tsang, Y., T. Antonsen, and E. Ott (2005), Exponential decay of chaotically advected passive scalars in the zero diffusivity limit, *Physical Review E*, *71*, 066,301.

Tzella, A., and P. Haynes (2009), The role of a delay time on the spatial structure of chaotically advected reactive scalars, *Physics of Fluids*, *21*, 087,101.

Vallis, G. (2006), *Atmospheric and oceanic fluid dynamics: fundamentals and large-scale circulation*, Cambridge University Press.

Vanneste, J. (2010), Estimating generalized lyapunov exponents for products of random matrices., *Physical Review E*, *81*, 036,701.

Vassilicos, J., and J. Hunt (1991), Fractal dimensions and spectra of interfaces with application to turbulence, *Proceedings of the Royal Society of London. Series A: Mathematical and Physical Sciences*, *435*(1895), 505–534.

Voth, G., T. Saint, G. Dobler, and J. Gollub (2003), Mixing rates and symmetry breaking in two-dimensional chaotic flow, *Physics of Fluids*, *15*, 2560.

Warn, T., and H. Warn (1978), The evolution of a nonlinear critical level, *Aplikace Matematiky, Applied Mathematics*, *59*, 37–71.

Waugh, D., and D. Dritschel (1999), Dependence of rossby wave breaking on the vertical structure of the polar vortex, *Journal of the Atmospheric Sciences*, *56*(14), 2359–2375.

Waugh, D., and R. Plumb (1994), Contour advection with surgery: A technique for investigating finescale structure in tracer transport., *Journal of Atmospheric Sciences*, *51*, 530–540.

Waugh, D., and L. Polvani (2010), Stratospheric polar vortices, *Geophysical Monograph Series, American Geophysical Union: Washington, DC*, *190*, 196.

Waugh, D., R. Plumb, R. Atkinson, M. Schoeberl, L. Lait, P. Newman, M. Loewenstein, D. Toohey, L. Avallone, C. Wester, and R. May (1994), Transport of material out of the stratospheric arctic vortex by rossby wave breaking., *Journal of Geophysical Research*, *99*, 1071–1088.

Waugh, D., T. Hall, W. Randel, P. Rasch, B. Boville, K. Boering, S. Wofsy, B. Daube, J. Elkins, D. Fahey, et al. (1997a), Three-dimensional simulations of long-lived tracers using winds from maccm2, *Journal of geophysical research-all series*, *102*, 21–21.

Waugh, D., R. Plumb, J. Elkins, D. Fahey, K. Boering, G. Dutton, C. Volk, E. Keim, R. Gao, B. Daube, et al. (1997b), Mixing of polar vortex air into middle latitudes as revealed by tracer-tracer scatterplots, *Journal of geophysical research*, *102*(D11), 13,119.

Waugh, D., E. Abraham, and M. Bowen (2006), Spatial variations of stirring in the surface ocean: A case study of the tasman sea, *Journal of Physical Oceanography*, *36*, 526–542.

Waugh, D., L. Oman, P. Newman, R. Stolarski, S. Pawson, J. Nielsen, and J. Perlwitz (2009), Effect of zonal asymmetries in stratospheric ozone on simulated southern hemisphere climate trends, *Geophys. Res. Lett*, *36*, L18,701.

Waugh, D. W., and E. R. Abraham (2008), Stirring in the global surface ocean, *Geophysical Research Letters*, *35*, L20,605.

Weiss, J., and E. Knobloch (1989), Mass transport and mixing by modulated traveling waves, *Physical Review A*, *40*(5), 2579.

Welander, P. (1955), Studies on the general development of motion in a two-dimensional, ideal fluid, *Tellus*, *7*(2), 141–156.

Wiggins, S. (1988), Stirred but not mixed, *Nature*, *333*(6172), 395–396.

Wiggins, S., and J. Ottino (2004), Foundations of chaotic mixing, *Philosophical Transactions of the Royal Society of London. Series A: Mathematical, Physical and Engineering Sciences*, *362*(1818), 937–970.

Winter, B., and M. Bourqui (2010), Wave forcing in the stratosphere under doubled-CO_2 conditions in a 100-year coupled chemistry-climate model study, *J. Geophys. Res*, *115*, D12,126.

Wonhas, A., and J. Vassilicos (2002), Diffusivity dependence of ozone depletion over the midnorthern latitudes, *Physical Review E*, *65*, 051,111.

Wonhas, A., and J. Vassilicos (2003), Mixing and geometry of advected, chemically reactive scalar fields: Application to chlorine deactivation over the midnorthern latitudes, *J. Geophys. Res*, *108*, 4325.

Yuan, G., K. Nam, T. Antonsen Jr, E. Ott, and P. Guzdar (2000), Power spectrum of passive scalars in two-dimensional chaotic flows, *Chaos*, *10*, 39–49.